IEEE Access
Multidisciplinary | Rapid Review | Open Access Journal

Received November 21, 2019, accepted December 4, 2019, date of publication December 13, 2019, date of current version January 6, 2020.

Digital Object Identifier 10.1109/ACCESS.2019.2959235

A Novel Estimator for TDOA and FDOA Positioning of Multiple Disjoint Sources in the Presence of Calibration Emitters

DING WANG[1,2], PEICHANG ZHANG[3], ZEYU YANG[1,2], FUSHAN WEI[1,4], AND CHENG WANG[1,2]

[1]College of Information System Engineering, PLA Strategic Support Force Information Engineering University, Zhengzhou 450001, China
[2]National Digital Switching System Engineering and Technological Research Center, Zhengzhou 450002, China
[3]College of Electronics and Information Engineering, Shenzhen University, Shenzhen 518000, China
[4]State Key Laboratory of Mathematical Engineering and Advanced Computing, Zhengzhou 450001, China

Corresponding authors: Ding Wang (wang_ding814@aliyun.com) and Peichang Zhang (pzhang@szu.edu.cn)

This work was supported in part by the National Natural Science Foundation of China under Grant 61601304, Grant 61772548, Grant 61401513, and Grant 61201381, in part by the China Postdoctoral Science Foundation under Grant 2016M592989, in part by the Key Scientific and Technological Research Project in Henan Province under Grant 192102210092 and Grant 192102210117, in part by the Weapons and Equipment Preresearch Project under Grant a3119, in part by the Key Technology of Signal Analysis Project under Grant b3103, in part by the Compound Fight of Network and Electronic Project under Grant b3105, and in part by the Foundation of Science and Technology on Information Assurance Laboratory under Grant KJ-17-001.

ABSTRACT Multiple-target localization is extensively applied in wireless connected networks. However, sensor location uncertainty is known to degrade significantly the target localization accuracy. Fortunately, calibration emitters such as unmanned aerial vehicles (UAV) with known location can be used to reduce the loss in localization accuracy due to sensor location errors. This paper is devoted to the use of UAV calibration emitters for time differences of arrival (TDOA) and frequency differences of arrival (FDOA) positioning of multiple targets. The study starts with deriving the Cramér–Rao bound (CRB) for TDOA/FDOA-based target location estimate when several UAV calibration signals are available. Subsequently, the paper presents an iterative constrained weighted least squares (ICWLS) estimator for multiple-target joint localization using TDOA/FDOA measurements from both target sources and UAV calibration emitters. The newly proposed method consists of two stages. In the first phase, the sensor locations are refined based on the calibration measurements as well as the prior knowledge of sensor locations. The second step provides the estimate of multiple-target locations by combining the measurements of target signals as well as the estimated values in the first phase. An efficient ICWLS algorithm is presented at each stage. Both the two algorithms are implemented by using matrix singular value decomposition (SVD), which is able to provide a closed-form solution and update the weighting matrix at every iteration. Finally, the convergence behavior and estimation mean-square-error (MSE) of the new estimator are deduced. Both theoretical analysis and simulation results show that the developed method can improve the TDOA/FDOA localization accuracy obviously with the help of UAV calibration emitters.

INDEX TERMS Target localization, unmanned aerial vehicle (UAV), time difference of arrival (TDOA), frequency difference of arrival (FDOA), multiple targets, calibration emitters, constrained weighted least squares (CWLS), Cramér–Rao bound (CRB), singular value decomposition (SVD).

I. INTRODUCTION

Determining the target locations from source signal measurements collected by a wireless connected network (or an array) of sensors at a time instance has become a fundamental issue during the past few decades [1]–[15]. It has inspired numerous applications in wireless communications, unmanned system, wireless connected robot swarms, object tracking and many other areas. Unfortunately, target localization is a non-trivial problem, mainly because the target positions and the

The associate editor coordinating the review of this manuscript and approving it for publication was Bo Zhang.

signal measurements are generally nonlinearly related. The localization task is usually accomplished using a two-step approach. In the first step, certain signal parameters are extracted from the radiated signal at the output of an array of spatially distributed sensors. In the second step, the target location is estimated by solving a set of non-linear equations defined by the signal parameters obtained in the first step. In this work, we restrict our attention to the second step.

Typical positioning parameters include time of arrival (TOA) [16], time difference of arrival (TDOA) [17], angle of arrival (AOA) [18], received signal strength (RSS) [19], and a combination of them [20]. When there is relative motion between the target and the sensors, frequency differences of arrival (FDOA) can be exploited not only to further improve the estimation accuracy of the target position, but also to provide an estimate of the target velocity. Besides, combinations of TDOA and FDOA measurements can facilitate localization of the target source in a wide range of bandwidths. As a consequence, FDOA is often combined with TDOA for moving target localization. However, finding the target position and velocity from TDOA and FDOA measurements obtained at a single time instant is not easy to complete as the equations are nonlinear. Another undesirable factor is that there are often random errors in the positions and velocities of the mobile sensors, which will result in obvious losses in estimation accuracy. To limit the scope of this paper, we concentrate on the TDOA/FDOA-based target localization problem.

Over the years, a number of algorithms for TDOA and FDOA positioning have been presented in the literature. Among the existing methods, the two-stage weighted least squares (TSWLS) algorithm [21] is very popular because it has closed-form solution and asymptotic efficiency. However, this classical TSWLS algorithm has poor localization accuracy when the target is located near any coordinate axis of the reference sensor. To remove this shortcoming, an improved version of the popular TSWLS algorithm is proposed in [22]. An alternative approach that can yield explicit solutions for target position and velocity is based on multidimensional scaling (MDS) analysis [23], which has been developed for data analysis in fields such as physics, geography and biology. This method is designed to minimize the cost function dependent on the scalar product matrix in the MDS framework. Theoretical analysis and simulation results demonstrate that this method is more robust against high measurement noise than the classical TSWLS method. Certainly, the closed-form methods have low computational complexity and do not suffer from local minima and divergence problems. However, the accuracy of these estimators can attain Cramér–Rao bound (CRB) only when the noise level is sufficiently low. To improve the estimation performance in the high noise region, iterative localization approaches can be exploited. The most common iterative technique is perhaps the Taylor-series linearization algorithm [24], which can be applied to almost any localization scenario. A point to note is that this method requires a proper initial position and velocity guess close to the true solution, and such a good guess may not be easy to obtain because the pseudo-linear equations are not available in this algorithm. Additionally, the semidefinite relaxation technique has been employed to relax the maximum likelihood (ML) estimator to semidefinite programming (SDP) [25]. The advantage of the SDP-based method lies in the fact that the cost function has no local minima or saddle points and thus the iterative sequence always convergence to the global minimum. However, this kind of method generally has a complex mathematical model and requires high computational complexity for reasonable localization accuracy. An efficient constrained total least squares (CTLS) algorithm for estimating the position and velocity of a moving target is developed in [26], and a constrained weighted least squares (CWLS) algorithm for TDOA and FDOA positioning is presented in [27]. These two estimators show superior performance and can reach CRB accuracy under moderate noise level conditions. However, both methods are implemented based on Newton's iteration. Hence, global convergence cannot be ensured unless the initial guess is close enough to the optimal solution. In [28], a polynomial root-finding-based CWLS algorithm is developed for TDOA/FDOA-based emitter locations. It makes use of the altitude constraint to reduce the localization errors. Unfortunately, the altitude of the emitter may not be accurately known or measured in practice. Recently, an iterative constrained weighted least squares (ICWLS) algorithm has been presented in [29]. It iteratively performs a linearization procedure on the quadratic equality constraints to get approximate programming with linear constraints. As a consequence, a closed-form solution is available at every iteration. Both theoretical analysis and simulation studies reveal that this novel method has better convergence properties and is able to delay the thresholding effect where the performance drops suddenly.

In addition to the estimation errors in TDOA/FDOA measurements, the uncertainties in sensor position and velocity can also cause the location performance to deteriorate dramatically, regardless of the approaches used to determine the solution. Indeed, a slight error in sensor location may lead to a large error in the target location estimate. It must be pointed out that sensor position and velocity errors often occur in real scenarios [30]–[37]. Recently, an emitter localization problem that accounts for uncertainties in sensor location has attracted considerable attention. In [30], [31], the increase in the mean-square error (MSE) in the target location estimate is derived when the sensor positions and velocities are assumed correct, but in fact they are not accurate due to random errors. To obtain the asymptotic optimum performance for this localization scenario, TSWLS and the CWLS estimators are proposed in [30] and [33], respectively. Both methods can achieve CRB accuracy over a small noise region. On the other hand, the problem of locating multiple disjoint sources using TDOAs and FDOAs is also studied in the literature, especially for intelligent robot swarms. Note that the positioning parameters (e.g., TDOA and FDOA) of the disjoint sources can be estimated separately because of the disjointness in time,

frequency or both. An important observation about multiple disjoint sources is that they are subject to the same sensor location displacements. Thus it is possible to reduce the performance loss resulting from sensor location uncertainties by joint localization. This procedure can be interpreted as multiple-target cooperative positioning. In [34], a closed-form solution is proposed to locate multiple disjoint sources in the presence of random sensor location errors. This solution has been proven analytically to reach CRB performance when the amount of noise is small. However, this estimator cannot provide optimum accuracy for sensor positions and velocities. Following the work of [34], an improved closed-form solution for simultaneously locating multiple disjoint sources and refining erroneous sensor positions and velocities is proposed in [35], [36], where the source and the receiver location estimates can asymptotically attain CRB. In addition, an ICWLS estimator for TDOA/FDOA positioning of multiple disjoint sources is developed in [37]. This method can also yield solutions for both target and sensor locations, and moreover, it can tolerate higher noise levels before the thresholding effect starts to happen.

To further optimize the localization performance in the presence of erroneous sensor locations, we can exploit a set of calibration emitters whose positions and/or velocities are known to an estimator in advance. Extensive studies have shown that the use of calibration emitters can significantly reduce the loss in target localization accuracy when the available sensor locations have random errors. In [38], the use of a single calibration emitter with known position is investigated to mitigate the TDOA-based localization errors caused by sensor position uncertainties. The gain in localization accuracy resulting from a calibration signal is evaluated based on the CRB analysis results. Additionally, a closed-form solution is presented for target localization using TDOA measurements from both the target source and the calibration emitter. Reference [39] extends the work in [38] to a more practical scenario where the position of a calibration emitter is not known accurately. An asymptotically efficient solution is developed by incorporating statistical knowledge of the calibration position errors. It can be easily observed that the performance gain from a calibration emitter depends on its position. Consequently, the calibration position is optimized in [40] by improving the Fisher information matrix of the target location estimate. The use and geometric effects of multiple calibration emitters are studied in [41], which presents the analytical conditions under which sensor position errors can be completely eliminated in target localization through the use of multiple calibration emitters. A Taylor-series TDOA localization method with calibration emitters in the presence of synchronization clock bias and sensor location errors is proposed in [42]. Note that the above-mentioned approaches only consider a stationary source location using TDOA measurements. For a moving target localization, some efficient methods with calibration signal are also developed in the literature. Specifically, reference [43] develops an explicit solution for moving target location using TDOA and FDOA from both the target source and the calibration emitter. The work in [44] focuses on the use of calibration sensors for locating a moving target based on TDOA/FDOA measurements. The calibration sensors can broadcast calibration signals to other sensors and can also receive signals from the target source and other calibration sensors. It presents a closed-form estimator with low complexity. It must be emphasized, however, that the solutions in [43], [44] are designed for the localization of a single source only. Moreover, their noise thresholds could be further improved because they directly follow the idea behind the classical TSWLS estimator.

This paper focuses on developing a novel estimator for the TDOA/FDOA multiple-target positioning for wireless connected network in the presence of calibration emitters. In the localization scenario studied here, the calibration emitters are stalled on the cooperative unmanned aerial vehicles (UAVs), whose locations can be known accurately. In addition, the target sources may be placed on any mobile vehicles, such as aircrafts or mobile robots. The study starts by deriving the CRB for the TDOA/FDOA-based target location estimate when some UAV calibration emitters with known locations are available. The insight gained from the CRB illustrates that UAV calibration emitters are very useful in reducing the effects of sensor position and velocity errors. Moreover, the cooperative gain is considerable when the multiple moving targets are located simultaneously in the presence of UAV calibration emitters, even if the target sources are disjoint. To achieve the optimum estimation accuracy, this work proceeds to develop an ICWLS localization approach using TDOA/FDOA measurements from both target sources and calibration emitters. Similar to [29], the estimator presented here also uses a set of linear equality constraints instead of the quadratic constraints to yield an explicit solution in each iteration. The difference lies in the fact that our method has two stages and can utilizes the calibration measurements to locate multiple targets in the presence of sensor position and velocity errors. Specifically, the first stage uses the calibration TDOA/FDOA measurements as well as the statistical characteristics of the noisy sensor locations to refine the sensor locations. The second stage provides estimates of the multiple-target locations by combining the measurements of target signals and the values estimated in the first step. An efficient ICWLS algorithm is designed at each stage. Both algorithms are implemented using matrix singular value decomposition (SVD), which can be achieved through some simple and efficient numerical techniques. Moreover, in the proposed iterative algorithms, a closed-form solution is available at every iteration and the weighting matrix can be updated recursively. The theoretical performance of the proposed ICWLS estimator is also studied. The performance analysis covers convergence property and MSE of the estimation. The results indicate that the proposed method, if it converges, can yield the optimal solution to the formulated non-convex CWLS problem. Besides, its estimation MSE can achieve CRB with UAV calibration emitters at moderate noise levels. Numerical experiments are conducted to confirm the

TABLE 1. Notational conventions.

Notation	Explanation
$\otimes$	Kronecker product
$\odot$	Schur product
$\boldsymbol{I}_n$	$n\times n$ identity matrix
$\boldsymbol{i}_n^{(m)}$	the m th column in matrix $\boldsymbol{I}_n$
$\boldsymbol{O}_{n\times m}$	$n\times m$ matrix of zeros
$\boldsymbol{1}_{n\times m}$	$n\times m$ matrix of ones
blkdiag$[\boldsymbol{A}_1\ \boldsymbol{A}_2\ \cdots \boldsymbol{A}_n]$	a block diagonal matrix with matrices $\{\boldsymbol{A}_k\}_{1\le k\le n}$ on the main diagonal
range$\{\boldsymbol{A}\}$	linear subspace spanned by the column vectors of matrix $\boldsymbol{A}$
$\boldsymbol{A}^{1/2}$	square root of matrix $\boldsymbol{A}$
$\boldsymbol{A}^{\dagger}$	Moore-Penrose inverse of matrix $\boldsymbol{A}$
$\boldsymbol{\Pi}^{\perp}[\boldsymbol{A}]$	orthogonal projection matrix onto the orthogonal subspace of range$\{\boldsymbol{A}\}$
$<\boldsymbol{a}>_m$	the m th element in vector $\boldsymbol{a}$

effectiveness of the theoretical analysis and demonstrate the advantages of the proposed ICWLS method.

The remainder of this paper is organized as follows. In Section II, the localization scenario is described and the measurement model is formulated. The CRB expressions for parameter estimation are derived in Section III. Section IV deduces the pseudo-linear equations. The quadratic equation constraints are presented in Section V. Section VI develops a novel ICWLS localization method by the use of UAV calibration emitters. The theoretical analysis of the proposed estimator is derived in Section VII. Simulation results are reported in Section VIII. The conclusions are drawn in Section IX, and the proofs of the main results are given in the Appendices.

In this paper, lowercase and uppercase boldface letters are used to denote vectors and matrices, respectively. In addition, the notational conventions and matrix identities that are used throughout this paper are listed in Tables 1 and 2, respectively.

II. MEASUREMENT MODEL AND PROBLEM FORMULATION

A. MEASUREMENT MODEL FOR TARGET SOURCE

This paper considers a three-dimension (3D) localization scenario based on wireless connected network as shown in Fig.1. It consists of a total of D moving targets whose positions and velocities are to be determined. The target sources may be stalled on any mobile vehicles, such as aircrafts or mobile robots. The calibration emitters can be placed on the cooperative UAVs, whose locations are obtained accurately. In addition, the sensors are also moving, and their locations can not be known accurately.

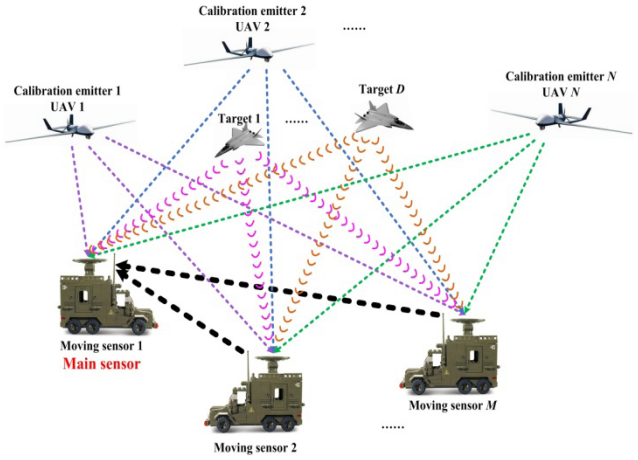

FIGURE 1. Localization scenario based on wireless connected network.

Let $\boldsymbol{u}_d$ and $\dot{\boldsymbol{u}}_d$ be the true position and velocity of the dth target, respectively. Then, the location vector for the dth target source is denoted as $\bar{\boldsymbol{u}}_d = [\boldsymbol{u}_d^{\mathrm{T}}\ \dot{\boldsymbol{u}}_d^{\mathrm{T}}]^{\mathrm{T}}$. In order to implement multiple-target cooperative positioning, we need to define a high-dimensional location vector as $\bar{\boldsymbol{u}} = [\bar{\boldsymbol{u}}_1^{\mathrm{T}}\ \bar{\boldsymbol{u}}_2^{\mathrm{T}}\ \cdots\ \bar{\boldsymbol{u}}_D^{\mathrm{T}}]^{\mathrm{T}}$, which is found through the use of M moving sensors. The actual position and velocity of the mth sensor are denoted by $\boldsymbol{s}_m$ and $\dot{\boldsymbol{s}}_m$, respectively. So, the location vector of the mth sensor is represented as $\bar{\boldsymbol{s}}_m = [\boldsymbol{s}_m^{\mathrm{T}}\ \dot{\boldsymbol{s}}_m^{\mathrm{T}}]^{\mathrm{T}}$, and the composite sensor location vector can be written as $\bar{\boldsymbol{s}} = [\bar{\boldsymbol{s}}_1^{\mathrm{T}}\ \bar{\boldsymbol{s}}_2^{\mathrm{T}}\ \cdots\ \bar{\boldsymbol{s}}_M^{\mathrm{T}}]^{\mathrm{T}}$. The TDOAs and FDOAs are exacted from the received signals to locate the multiple targets simultaneously. Notice that this work focuses on the case where the target sources are disjoint so that for

TABLE 2. Matrix identities.

Serial number	Matrix identity
I	$\begin{bmatrix} \boldsymbol{A} & \boldsymbol{B} \\ \boldsymbol{B}^{\mathrm{T}} & \boldsymbol{C} \end{bmatrix}^{-1} = \left[\begin{array}{c\|c} (\boldsymbol{A}-\boldsymbol{B}\boldsymbol{C}^{-1}\boldsymbol{B}^{\mathrm{T}})^{-1} & -(\boldsymbol{A}-\boldsymbol{B}\boldsymbol{C}^{-1}\boldsymbol{B}^{\mathrm{T}})^{-1}\boldsymbol{B}\boldsymbol{C}^{-1} \\ \hline -\boldsymbol{C}^{-1}\boldsymbol{B}^{\mathrm{T}}(\boldsymbol{A}-\boldsymbol{B}\boldsymbol{C}^{-1}\boldsymbol{B}^{\mathrm{T}})^{-1} & (\boldsymbol{C}-\boldsymbol{B}^{\mathrm{T}}\boldsymbol{A}^{-1}\boldsymbol{B})^{-1} \end{array}\right]$ (where $\boldsymbol{A}$ and $\boldsymbol{C}$ are symmetric matrices)
II	$(\boldsymbol{A}+\boldsymbol{B}\boldsymbol{C}\boldsymbol{D})^{-1} = \boldsymbol{A}^{-1} - \boldsymbol{A}^{-1}\boldsymbol{B}(\boldsymbol{C}^{-1}+\boldsymbol{D}\boldsymbol{A}^{-1}\boldsymbol{B})^{-1}\boldsymbol{D}\boldsymbol{A}^{-1}$
III	$\boldsymbol{\Pi}^{\perp}[\boldsymbol{A}] = \boldsymbol{I} - \boldsymbol{A}(\boldsymbol{A}^{\mathrm{T}}\boldsymbol{A})^{-1}\boldsymbol{A}^{\mathrm{T}}$ (where $\boldsymbol{A}$ is full column rank)

each emitting source, a separate set of TDOA and FDOA measurements can be obtained. The disjointness may be in time, frequency or both.

It is worthy to point out that TDOA and FDOA can be replaced by range difference of arrival (RDOA) and range difference rate of arrival (RDROA), respectively, in a constant-velocity propagation medium. In the sequel, we use RDOA and RDROA to describe the proposed estimator and conduct the performance analysis for easy of presentation. Without loss of generality, let the first sensor be the reference. Then, the RDOA measurement between sensor pair m and 1 from the dth target is given by

$$\hat{r}_{dm} = r_{dm} + \varepsilon_{\mathrm{p},dm} = f_{\mathrm{p},m}(\bar{\boldsymbol{u}}_d, \bar{\boldsymbol{s}}) + \varepsilon_{\mathrm{p},dm} \quad \begin{pmatrix} 2 \le m \le M \\ 1 \le d \le D \end{pmatrix} \tag{1}$$

where $\varepsilon_{\mathrm{p},dm}$ is the RDOA error; r_{dm} is the true RDOA; $f_{\mathrm{p},m}(\bar{\boldsymbol{u}}_d, \bar{\boldsymbol{s}}) = ||\boldsymbol{u}_d - \boldsymbol{s}_m||_2 - ||\boldsymbol{u}_d - \boldsymbol{s}_1||_2$ is a function with respect to $\bar{\boldsymbol{u}}_d$ and $\bar{\boldsymbol{s}}$. The collection of RDOA measurements from the dth target yields

$$\begin{aligned} \hat{\boldsymbol{r}}_d &= [\hat{r}_{d2}\ \hat{r}_{d3}\ \cdots\ \hat{r}_{dM}]^{\mathrm{T}} = \boldsymbol{r}_d + \boldsymbol{\varepsilon}_{\mathrm{p},d} \\ &= \boldsymbol{f}_{\mathrm{p}}(\bar{\boldsymbol{u}}_d, \bar{\boldsymbol{s}}) + \boldsymbol{\varepsilon}_{\mathrm{p},d} \quad (1 \le d \le D) \end{aligned} \tag{2}$$

where

$$\begin{cases} \boldsymbol{r}_d = [r_{d2}\ r_{d3}\ \cdots\ r_{dM}]^{\mathrm{T}}; \\ \boldsymbol{\varepsilon}_{\mathrm{p},d} = [\varepsilon_{\mathrm{p},d2}\ \varepsilon_{\mathrm{p},d3}\ \cdots\ \varepsilon_{\mathrm{p},dM}]^{\mathrm{T}} \\ \boldsymbol{f}_{\mathrm{p}}(\bar{\boldsymbol{u}}_d, \bar{\boldsymbol{s}}) = [f_{\mathrm{p},2}(\bar{\boldsymbol{u}}_d, \bar{\boldsymbol{s}})\, f_{\mathrm{p},3}(\bar{\boldsymbol{u}}_d, \bar{\boldsymbol{s}})\ \cdots\ f_{\mathrm{p},M}(\bar{\boldsymbol{u}}_d, \bar{\boldsymbol{s}})]^{\mathrm{T}} \end{cases} \tag{3}$$

Taking time derivative of (1), the RDROA measurement between sensor pair m and 1 from the dth target can be written as

$$\hat{\dot{r}}_{dm} = \dot{r}_{dm} + \varepsilon_{\mathrm{v},dm} = f_{\mathrm{v},m}(\bar{\boldsymbol{u}}_d, \bar{\boldsymbol{s}}) + \varepsilon_{\mathrm{v},dm} \quad \begin{pmatrix} 2 \le m \le M \\ 1 \le d \le D \end{pmatrix} \tag{4}$$

where $\varepsilon_{\mathrm{v},dm}$ is the RDROA noise; $\dot{r}_{dm}$ is the true RDROA; $f_{\mathrm{v},m}(\bar{\boldsymbol{u}}_d, \bar{\boldsymbol{s}}) = \frac{(\boldsymbol{u}_d - \boldsymbol{s}_m)^{\mathrm{T}}(\dot{\boldsymbol{u}}_d - \dot{\boldsymbol{s}}_m)}{||\boldsymbol{u}_d - \boldsymbol{s}_m||_2} - \frac{(\boldsymbol{u}_d - \boldsymbol{s}_1)^{\mathrm{T}}(\dot{\boldsymbol{u}}_d - \dot{\boldsymbol{s}}_1)}{||\boldsymbol{u}_d - \boldsymbol{s}_1||_2}$ is a function of both $\bar{\boldsymbol{u}}_d$ and. Combining all the RDROA measurements from the dth target produces

$$\begin{aligned} \hat{\dot{\boldsymbol{r}}}_d &= [\hat{\dot{r}}_{d2}\ \hat{\dot{r}}_{d3}\ \cdots\ \hat{\dot{r}}_{dM}]^{\mathrm{T}} = \dot{\boldsymbol{r}}_d + \boldsymbol{\varepsilon}_{\mathrm{v},d} \\ &= \boldsymbol{f}_{\mathrm{v}}(\bar{\boldsymbol{u}}_d, \bar{\boldsymbol{s}}) + \boldsymbol{\varepsilon}_{\mathrm{v},d} \quad (1 \le d \le D) \end{aligned} \tag{5}$$

where

$$\begin{cases} \dot{\boldsymbol{r}}_d = [\dot{r}_{d2}\ \dot{r}_{d3}\ \cdots\ \dot{r}_{dM}]^{\mathrm{T}}; \\ \boldsymbol{\varepsilon}_{\mathrm{v},d} = [\varepsilon_{\mathrm{v},d2}\ \varepsilon_{\mathrm{v},d3}\ \cdots\ \varepsilon_{\mathrm{v},dM}]^{\mathrm{T}} \\ \boldsymbol{f}_{\mathrm{v}}(\bar{\boldsymbol{u}}_d, \bar{\boldsymbol{s}}) = [f_{\mathrm{v},2}(\bar{\boldsymbol{u}}_d, \bar{\boldsymbol{s}})\, f_{\mathrm{v},3}(\bar{\boldsymbol{u}}_d, \bar{\boldsymbol{s}})\ \cdots\ f_{\mathrm{v},M}(\bar{\boldsymbol{u}}_d, \bar{\boldsymbol{s}})]^{\mathrm{T}} \end{cases} \tag{6}$$

Putting (2) and (5) together, we have the total measurement vector for target d as follows:

$$\hat{\bar{\boldsymbol{r}}}_d = [\hat{\boldsymbol{r}}_d^{\mathrm{T}}\ \hat{\dot{\boldsymbol{r}}}_d^{\mathrm{T}}]^{\mathrm{T}} = \bar{\boldsymbol{r}}_d + \boldsymbol{\varepsilon}_d = \boldsymbol{f}(\bar{\boldsymbol{u}}_d, \bar{\boldsymbol{s}}) + \boldsymbol{\varepsilon}_d \quad (1 \le d \le D) \tag{7}$$

where $\bar{\boldsymbol{r}}_d = [\boldsymbol{r}_d^{\mathrm{T}}\ \dot{\boldsymbol{r}}_d^{\mathrm{T}}]^{\mathrm{T}}$; $\boldsymbol{f}(\bar{\boldsymbol{u}}_d, \bar{\boldsymbol{s}}) = [(\boldsymbol{f}_{\mathrm{p}}(\bar{\boldsymbol{u}}_d, \bar{\boldsymbol{s}}))^{\mathrm{T}}\ (\boldsymbol{f}_{\mathrm{v}}(\bar{\boldsymbol{u}}_d, \bar{\boldsymbol{s}}))^{\mathrm{T}}]^{\mathrm{T}}$; $\boldsymbol{\varepsilon}_d = [\boldsymbol{\varepsilon}_{\mathrm{p},d}^{\mathrm{T}}\ \boldsymbol{\varepsilon}_{\mathrm{v},d}^{\mathrm{T}}]^{\mathrm{T}}$ is the composite noise vector that follows zero-mean Gaussian distribution with covariance matrix

$$\boldsymbol{E}_d = \begin{bmatrix} \boldsymbol{E}_{\mathrm{p},d} & \boldsymbol{E}_{\mathrm{pv},d} \\ \boldsymbol{E}_{\mathrm{pv},d}^{\mathrm{T}} & \boldsymbol{E}_{\mathrm{v},d} \end{bmatrix} \quad (1 \le d \le D) \tag{8}$$

It must be emphasized that $\boldsymbol{E}_{\mathrm{pv},d}$ characterizes the cross-correlation between the RDOA and RDROA measurements. Collecting the RDOAs and RDROAs from all the target sources produces

$$\hat{\bar{\boldsymbol{r}}} = [\hat{\bar{\boldsymbol{r}}}_1^{\mathrm{T}}\ \hat{\bar{\boldsymbol{r}}}_2^{\mathrm{T}}\ \cdots\ \hat{\bar{\boldsymbol{r}}}_D^{\mathrm{T}}]^{\mathrm{T}} = \bar{\boldsymbol{r}} + \bar{\boldsymbol{\varepsilon}} = \bar{\boldsymbol{f}}(\bar{\boldsymbol{u}}, \bar{\boldsymbol{s}}) + \bar{\boldsymbol{\varepsilon}} \tag{9}$$

where

$$\begin{cases} \bar{\boldsymbol{r}} = [\bar{\boldsymbol{r}}_1^{\mathrm{T}}\ \bar{\boldsymbol{r}}_2^{\mathrm{T}}\ \cdots\ \bar{\boldsymbol{r}}_D^{\mathrm{T}}]^{\mathrm{T}}; \quad \bar{\boldsymbol{\varepsilon}} = [\boldsymbol{\varepsilon}_1^{\mathrm{T}}\ \boldsymbol{\varepsilon}_2^{\mathrm{T}}\ \cdots\ \boldsymbol{\varepsilon}_D^{\mathrm{T}}]^{\mathrm{T}} \\ \bar{\boldsymbol{f}}(\bar{\boldsymbol{u}}, \bar{\boldsymbol{s}}) = [(\boldsymbol{f}(\bar{\boldsymbol{u}}_1, \bar{\boldsymbol{s}}))^{\mathrm{T}}\ (\boldsymbol{f}(\bar{\boldsymbol{u}}_2, \bar{\boldsymbol{s}}))^{\mathrm{T}}\ \cdots\ (\boldsymbol{f}(\bar{\boldsymbol{u}}_D, \bar{\boldsymbol{s}}))^{\mathrm{T}}]^{\mathrm{T}} \end{cases} \tag{10}$$

It is easy to see that the high-dimensional error $\bar{\boldsymbol{\varepsilon}}$ obeys the Gaussian distribution with zero mean and covariance matrix $\bar{\boldsymbol{E}}_{\mathrm{A}} = \mathrm{blkdiag}[\boldsymbol{E}_1\ \boldsymbol{E}_2\ \cdots\ \boldsymbol{E}_D]$, which is block-diagonal due to the disjointness of the received signals.

On the other hand, the accurate sensor location vectors $\{\bar{\boldsymbol{s}}_m\}_{1 \le m \le M}$ are not known and only noisy versions of them, denoted by $\{\hat{\bar{\boldsymbol{s}}}_m\}_{1 \le m \le M}$, are available. They can be modeled as

$$\hat{\bar{\boldsymbol{s}}}_m = \bar{\boldsymbol{s}}_m + \boldsymbol{\xi}_m \quad (1 \le m \le M) \tag{11}$$

where $\boldsymbol{\xi}_m$ is the error in $\hat{\bar{\boldsymbol{s}}}_m$. For convenience purpose, let us collect $\{\hat{\bar{\boldsymbol{s}}}_m\}_{1 \le m \le M}$ to form the $6M \times 1$ sensor location vector as follows:

$$\hat{\bar{\boldsymbol{s}}} = [\hat{\bar{\boldsymbol{s}}}_1^{\mathrm{T}}\ \hat{\bar{\boldsymbol{s}}}_2^{\mathrm{T}}\ \cdots\ \hat{\bar{\boldsymbol{s}}}_M^{\mathrm{T}}]^{\mathrm{T}} = \bar{\boldsymbol{s}} + \bar{\boldsymbol{\xi}} \tag{12}$$

where $\bar{\boldsymbol{\xi}} = [\boldsymbol{\xi}_1^{\mathrm{T}}\ \boldsymbol{\xi}_2^{\mathrm{T}}\ \cdots\ \boldsymbol{\xi}_M^{\mathrm{T}}]^{\mathrm{T}}$ is the sensor location error vector, which is zero-mean Gaussian distributed with covariance matrix $\bar{\boldsymbol{E}}_{\mathrm{B}}$.

B. MEASUREMENT MODEL FOR CALIBRATION EMITTER

It is well known that sensor location uncertainties can degrade the target localization accuracy considerably. To reduce the effects of sensor location errors, it is desirable to use some UAV calibration emitters, whose locations are known to an estimator in advance. The number of calibration emitters is set to N and the position and velocity of the nth calibration emitter are assumed to be $\boldsymbol{w}_d$ and $\dot{\boldsymbol{w}}_d$, respectively. Moreover, the calibration emitters are also uncorrelated with each other. Similar to (2), the noisy RDOA measurement vector for the nth calibration signal can be written as

$$\hat{\boldsymbol{r}}_n^{(\mathrm{c})} = \boldsymbol{r}_n^{(\mathrm{c})} + \boldsymbol{\varepsilon}_{\mathrm{p},n}^{(\mathrm{c})} = \boldsymbol{f}_{\mathrm{p},n}^{(\mathrm{c})}(\bar{\boldsymbol{s}}) + \boldsymbol{\varepsilon}_{\mathrm{p},n}^{(\mathrm{c})} \quad (1 \le n \le N) \tag{13}$$

where $\boldsymbol{\varepsilon}_{\mathrm{p},n}^{(\mathrm{c})}$ is the error vector; $\boldsymbol{r}_n^{(\mathrm{c})} = [r_{n2}^{(\mathrm{c})}\ r_{n3}^{(\mathrm{c})}\ \cdots\ r_{nM}^{(\mathrm{c})}]^{\mathrm{T}}$ is the noiseless RDOA vector; $\boldsymbol{f}_{\mathrm{p},n}^{(\mathrm{c})}(\bar{\boldsymbol{s}}) = [f_{\mathrm{p},n2}^{(\mathrm{c})}(\bar{\boldsymbol{s}})\, f_{\mathrm{p},n3}^{(\mathrm{c})}(\bar{\boldsymbol{s}})\ \cdots\ f_{\mathrm{p},nM}^{(\mathrm{c})}(\bar{\boldsymbol{s}})]^{\mathrm{T}}$, in which

$$f_{\mathrm{p},nm}^{(\mathrm{c})}(\bar{\boldsymbol{s}}) = ||\boldsymbol{w}_n - \boldsymbol{s}_m|| _2 - ||\boldsymbol{w}_n - \boldsymbol{s}_1|| _2 \quad (2 \le m \le M) \tag{14}$$

Following (5), the RDROA measurement vector for the nth calibration signal is given by

$$\hat{\dot{\boldsymbol{r}}}_n^{(\mathrm{c})} = \dot{\boldsymbol{r}}_n^{(\mathrm{c})} + \boldsymbol{\varepsilon}_{\mathrm{v},n}^{(\mathrm{c})} = \boldsymbol{f}_{\mathrm{v},n}^{(\mathrm{c})}(\bar{\boldsymbol{s}}) + \boldsymbol{\varepsilon}_{\mathrm{v},n}^{(\mathrm{c})} \quad (1 \le n \le N) \tag{15}$$

where $\boldsymbol{\varepsilon}_{\mathrm{v},n}^{(\mathrm{c})}$ is the error vector; $\dot{\boldsymbol{r}}_n^{(\mathrm{c})} = [\dot{r}_{n2}^{(\mathrm{c})}\ \dot{r}_{n3}^{(\mathrm{c})}\ \cdots\ \dot{r}_{nM}^{(\mathrm{c})}]^{\mathrm{T}}$ is the noiseless RDROA vector; $\boldsymbol{f}_{\mathrm{v},n}^{(\mathrm{c})}(\bar{\boldsymbol{s}}) = [f_{\mathrm{v},n2}^{(\mathrm{c})}(\bar{\boldsymbol{s}})\, f_{\mathrm{v},n3}^{(\mathrm{c})}(\bar{\boldsymbol{s}})\ \cdots\ f_{\mathrm{v},nM}^{(\mathrm{c})}(\bar{\boldsymbol{s}})]^{\mathrm{T}}$, in which

$$f_{\mathrm{v},nm}^{(\mathrm{c})}(\bar{\boldsymbol{s}}) = \frac{(\boldsymbol{w}_n - \boldsymbol{s}_m)^{\mathrm{T}}(\dot{\boldsymbol{w}}_n - \dot{\boldsymbol{s}}_m)}{||\boldsymbol{w}_n - \boldsymbol{s}_m|| _2} - \frac{(\boldsymbol{w}_n - \boldsymbol{s}_1)^{\mathrm{T}}(\dot{\boldsymbol{w}}_n - \dot{\boldsymbol{s}}_1)}{||\boldsymbol{w}_n - \boldsymbol{s}_1|| _2} \quad (2 \le m \le M) \tag{16}$$

Combining (13) and (15) produces

$$\begin{aligned}\hat{\bar{\boldsymbol{r}}}_n^{(\mathrm{c})} &= [\hat{\boldsymbol{r}}_n^{(\mathrm{c})\mathrm{T}}\ \hat{\dot{\boldsymbol{r}}}_n^{(\mathrm{c})\mathrm{T}}]^{\mathrm{T}} = \bar{\boldsymbol{r}}_n^{(\mathrm{c})} + \boldsymbol{\varepsilon}_n^{(\mathrm{c})} \\ &= \boldsymbol{f}_n^{(\mathrm{c})}(\bar{\boldsymbol{s}}) + \boldsymbol{\varepsilon}_n^{(\mathrm{c})} \quad (1 \le n \le N)\end{aligned} \tag{17}$$

where $\bar{\boldsymbol{r}}_n^{(\mathrm{c})} = [\boldsymbol{r}_n^{(\mathrm{c})\mathrm{T}}\ \dot{\boldsymbol{r}}_n^{(\mathrm{c})\mathrm{T}}]^{\mathrm{T}}$; $\boldsymbol{f}_n^{(\mathrm{c})}(\bar{\boldsymbol{s}}) = [(\boldsymbol{f}_{\mathrm{p},n}^{(\mathrm{c})}(\bar{\boldsymbol{s}}))^{\mathrm{T}}\ (\boldsymbol{f}_{\mathrm{v},n}^{(\mathrm{c})}(\bar{\boldsymbol{s}}))^{\mathrm{T}}]^{\mathrm{T}}$; $\boldsymbol{\varepsilon}_n^{(\mathrm{c})} = [\boldsymbol{\varepsilon}_{\mathrm{p},n}^{(\mathrm{c})\mathrm{T}}\ \boldsymbol{\varepsilon}_{\mathrm{v},n}^{(\mathrm{c})\mathrm{T}}]^{\mathrm{T}}$, which is modeled as a zero-mean Gaussian random vector with covariance matrix

$$\boldsymbol{E}_n^{(\mathrm{c})} = \begin{bmatrix} \boldsymbol{E}_{\mathrm{p},n}^{(\mathrm{c})} & \boldsymbol{E}_{\mathrm{pv},n}^{(\mathrm{c})} \\ \boldsymbol{E}_{\mathrm{pv},n}^{(\mathrm{c})\mathrm{T}} & \boldsymbol{E}_{\mathrm{v},n}^{(\mathrm{c})} \end{bmatrix} \quad (1 \le n \le N) \tag{18}$$

Putting all the N equations in (17) together yields

$$\begin{aligned}\hat{\bar{\boldsymbol{r}}}^{(\mathrm{c})} &= [\hat{\bar{\boldsymbol{r}}}_1^{(\mathrm{c})\mathrm{T}}\ \hat{\bar{\boldsymbol{r}}}_2^{(\mathrm{c})\mathrm{T}}\ \cdots\ \hat{\bar{\boldsymbol{r}}}_N^{(\mathrm{c})\mathrm{T}}]^{\mathrm{T}} = \bar{\boldsymbol{r}}^{(\mathrm{c})} + \bar{\boldsymbol{\varepsilon}}^{(\mathrm{c})} \\ &= \bar{\boldsymbol{f}}^{(\mathrm{c})}(\bar{\boldsymbol{s}}) + \bar{\boldsymbol{\varepsilon}}^{(\mathrm{c})}\end{aligned} \tag{19}$$

where

$$\begin{cases} \bar{\boldsymbol{r}}^{(\mathrm{c})} = [\bar{\boldsymbol{r}}_1^{(\mathrm{c})\mathrm{T}}\ \bar{\boldsymbol{r}}_2^{(\mathrm{c})\mathrm{T}}\ \cdots\ \bar{\boldsymbol{r}}_N^{(\mathrm{c})\mathrm{T}}]^{\mathrm{T}} \\ \bar{\boldsymbol{\varepsilon}}^{(\mathrm{c})} = [\boldsymbol{\varepsilon}_1^{(\mathrm{c})\mathrm{T}}\ \boldsymbol{\varepsilon}_2^{(\mathrm{c})\mathrm{T}}\ \cdots\ \boldsymbol{\varepsilon}_N^{(\mathrm{c})\mathrm{T}}]^{\mathrm{T}} \\ \bar{\boldsymbol{f}}^{(\mathrm{c})}(\bar{\boldsymbol{s}}) = [(\boldsymbol{f}_1^{(\mathrm{c})}(\bar{\boldsymbol{s}}))^{\mathrm{T}}\ (\boldsymbol{f}_2^{(\mathrm{c})}(\bar{\boldsymbol{s}}))^{\mathrm{T}}\ \cdots\ (\boldsymbol{f}_N^{(\mathrm{c})}(\bar{\boldsymbol{s}}))^{\mathrm{T}}]^{\mathrm{T}} \end{cases} \tag{20}$$

Clearly, $\bar{\boldsymbol{\varepsilon}}^{(\mathrm{c})}$ is a zero-mean Gaussian random vector with covariance matrix $\bar{\boldsymbol{E}}_{\mathrm{A}}^{(\mathrm{c})} = \mathrm{blkdiag}[\boldsymbol{E}_1^{(\mathrm{c})}\ \boldsymbol{E}_2^{(\mathrm{c})}\ \cdots\ \boldsymbol{E}_N^{(\mathrm{c})}]$.

C. PROBLEM FORMULATION

The multiple-target cooperative localization problem in this work can be stated as follows: Given the available erroneous sensor locations and the RDOA/RDROA measurements from both target sources and UAV calibration emitters, identify the composite location vector of the multiple targets as accurately as possible.

III. CRB DERIVATION AND ANALYSIS

This section is devoted to the derivation of the CRB on the estimation of the parameters of interest. The obtained results can provide some valuable insights into the performance gain for target localization through the use of UAV calibration emitters. In addition, we also compare the obtained CRB with the one when the target locations are identified separately. The comparison of these two CRBs can indicate the improvement in localization accuracy resulted from multiple-target cooperative positioning.

A. CRB DERIVATION AND ANALYSIS BASED ON ALL THE TDOA/FDOA MEASUREMENTS

In this subsection, the CRB on the covariance matrix of parameter estimation are deduced based on the TDOA/FDOA measurements from both target sources and calibration emitters. In this situation, the observations consist of $\hat{\bar{\boldsymbol{r}}}$, $\hat{\bar{\boldsymbol{r}}}^{(\mathrm{c})}$ and $\hat{\bar{\boldsymbol{s}}}$, and the unknowns include $\bar{\boldsymbol{u}}$ and $\bar{\boldsymbol{s}}$. Applying the result in [38], the CRB matrix for joint estimation of $\bar{\boldsymbol{u}}$ and $\bar{\boldsymbol{s}}$ is given in (21), as shown at the bottom of the next page, where $\bar{\boldsymbol{F}}_1(\bar{\boldsymbol{u}}, \bar{\boldsymbol{s}}) = \frac{\partial \bar{\boldsymbol{f}}(\bar{\boldsymbol{u}}, \bar{\boldsymbol{s}})}{\partial \bar{\boldsymbol{u}}^{\mathrm{T}}}$, $\bar{\boldsymbol{F}}_2(\bar{\boldsymbol{u}}, \bar{\boldsymbol{s}}) = \frac{\partial \bar{\boldsymbol{f}}(\bar{\boldsymbol{u}}, \bar{\boldsymbol{s}})}{\partial \bar{\boldsymbol{s}}^{\mathrm{T}}}$ and $\bar{\boldsymbol{F}}^{(\mathrm{c})}(\bar{\boldsymbol{s}}) = \frac{\partial \bar{\boldsymbol{f}}^{(\mathrm{c})}(\bar{\boldsymbol{s}})}{\partial \bar{\boldsymbol{s}}^{\mathrm{T}}}$. Then, using matrix identities (I)-(III) in Table 2 yields

$$\begin{aligned}\mathbf{CRB}(\bar{\boldsymbol{u}}) = {} & ((\bar{\boldsymbol{F}}_1(\bar{\boldsymbol{u}}, \bar{\boldsymbol{s}}))^{\mathrm{T}}(\bar{\boldsymbol{E}}_{\mathrm{A}} + \bar{\boldsymbol{F}}_2(\bar{\boldsymbol{u}}, \bar{\boldsymbol{s}})(\bar{\boldsymbol{E}}_{\mathrm{B}}^{-1} \\ & + (\bar{\boldsymbol{F}}^{(\mathrm{c})}(\bar{\boldsymbol{s}}))^{\mathrm{T}}(\bar{\boldsymbol{E}}_{\mathrm{A}}^{(\mathrm{c})})^{-1}\bar{\boldsymbol{F}}^{(\mathrm{c})}(\bar{\boldsymbol{s}}))^{-1}(\bar{\boldsymbol{F}}_2(\bar{\boldsymbol{u}}, \bar{\boldsymbol{s}}))^{\mathrm{T}})^{-1} \\ & \times \bar{\boldsymbol{F}}_1(\bar{\boldsymbol{u}}, \bar{\boldsymbol{s}}))^{-1}\end{aligned} \tag{22}$$

$$\begin{aligned}\mathbf{CRB}(\bar{\boldsymbol{s}}) = {} & (\bar{\boldsymbol{E}}_{\mathrm{B}}^{-1} + (\bar{\boldsymbol{F}}^{(\mathrm{c})}(\bar{\boldsymbol{s}}))^{\mathrm{T}}(\bar{\boldsymbol{E}}_{\mathrm{A}}^{(\mathrm{c})})^{-1}\bar{\boldsymbol{F}}^{(\mathrm{c})}(\bar{\boldsymbol{s}}) \\ & + (\bar{\boldsymbol{F}}_2(\bar{\boldsymbol{u}}, \bar{\boldsymbol{s}}))^{\mathrm{T}}\bar{\boldsymbol{E}}_{\mathrm{A}}^{-1/2}\boldsymbol{\Pi}^{\perp}[\bar{\boldsymbol{E}}_{\mathrm{A}}^{-1/2}\bar{\boldsymbol{F}}_1(\bar{\boldsymbol{u}}, \bar{\boldsymbol{s}})]\bar{\boldsymbol{E}}_{\mathrm{A}}^{-1/2} \\ & \times \bar{\boldsymbol{F}}_2(\bar{\boldsymbol{u}}, \bar{\boldsymbol{s}}))^{-1}\end{aligned} \tag{23}$$

Before proceeding, three remarks are made.

Remark 1: According to the result in [34], the CRB of $\bar{\boldsymbol{u}}$ without calibration emitters can be written as

$$\begin{aligned}&\mathbf{CRB}_{\mathrm{n}}(\bar{\boldsymbol{u}}) \\ &= \left((\bar{\boldsymbol{F}}_1(\bar{\boldsymbol{u}}, \bar{\boldsymbol{s}}))^{\mathrm{T}}\begin{pmatrix} \bar{\boldsymbol{E}}_{\mathrm{A}} + \bar{\boldsymbol{F}}_2(\bar{\boldsymbol{u}}, \bar{\boldsymbol{s}}) \\ \times \bar{\boldsymbol{E}}_{\mathrm{B}}(\bar{\boldsymbol{F}}_2(\bar{\boldsymbol{u}}, \bar{\boldsymbol{s}}))^{\mathrm{T}} \end{pmatrix}^{-1}\bar{\boldsymbol{F}}_1(\bar{\boldsymbol{u}}, \bar{\boldsymbol{s}})\right)^{-1}\end{aligned} \tag{24}$$

where the subscript "n" is used to indicate that this CRB corresponds to the case of no calibration signals. Since $(\bar{\boldsymbol{E}}_{\mathrm{B}}^{-1} + (\bar{\boldsymbol{F}}^{(\mathrm{c})}(\bar{\boldsymbol{s}}))^{\mathrm{T}}(\bar{\boldsymbol{E}}_{\mathrm{A}}^{(\mathrm{c})})^{-1}\bar{\boldsymbol{F}}^{(\mathrm{c})}(\bar{\boldsymbol{s}}))^{-1} \le \bar{\boldsymbol{E}}_{\mathrm{B}}$, it can be seen from (22) and (24) that $\mathbf{CRB}(\bar{\boldsymbol{u}}) \le \mathbf{CRB}_{\mathrm{n}}(\bar{\boldsymbol{u}})$, which means that improving the best localization accuracy is possible by the use of calibration emitters. In fact, the improvement could be significant at typical measurement noise level, as is illustrated in simulation section.

Remark 2: Applying the result of [35], the CRB for the estimate of $\bar{\boldsymbol{s}}$ in the absence of calibration emitters is given by

$$\mathbf{CRB}_{\mathrm{n}}(\bar{\boldsymbol{s}}) = \begin{pmatrix} \bar{\boldsymbol{E}}_{\mathrm{B}}^{-1} + (\bar{\boldsymbol{F}}_2(\bar{\boldsymbol{u}},\bar{\boldsymbol{s}}))^{\mathrm{T}}\bar{\boldsymbol{E}}_{\mathrm{A}}^{-1/2} \\ \times \boldsymbol{\Pi}^{\perp}[\bar{\boldsymbol{E}}_{\mathrm{A}}^{-1/2}\bar{\boldsymbol{F}}_1(\bar{\boldsymbol{u}},\bar{\boldsymbol{s}})]\bar{\boldsymbol{E}}_{\mathrm{A}}^{-1/2}\bar{\boldsymbol{F}}_2(\bar{\boldsymbol{u}},\bar{\boldsymbol{s}}) \end{pmatrix}^{-1} \tag{25}$$

Since $(\bar{\boldsymbol{F}}^{(\mathrm{c})}(\bar{\boldsymbol{s}}))^{\mathrm{T}}(\bar{\boldsymbol{E}}_{\mathrm{A}}^{(\mathrm{c})})^{-1}\bar{\boldsymbol{F}}^{(\mathrm{c})}(\bar{\boldsymbol{s}}) \geq \boldsymbol{O}$, comparing (23) with (25) immediately results in $\mathbf{CRB}(\bar{\boldsymbol{s}}) \leq \mathbf{CRB}_{\mathrm{n}}(\bar{\boldsymbol{s}})$. Therefore, the best achievable estimation accuracy for sensor locations can also be improved with the help of calibration emitters.

Remark 3: It can be readily seen from (22) that the CRB for the estimate of the dth target location is given in (26), as shown at the bottom of this page. It is noteworthy that this CRB corresponds to the scenario of multiple-target cooperative localization. If each target source is located separately, the CRB of $\boldsymbol{u}_d$ becomes

$$\begin{aligned} \mathbf{CRB}_{\mathrm{i}}(\bar{\boldsymbol{u}}_d) = {} & ((\boldsymbol{F}_1(\bar{\boldsymbol{u}}_d,\bar{\boldsymbol{s}}))^{\mathrm{T}}(\boldsymbol{E}_d + \boldsymbol{F}_2(\bar{\boldsymbol{u}}_d,\bar{\boldsymbol{s}})(\bar{\boldsymbol{E}}_{\mathrm{B}}^{-1} \\ & + (\bar{\boldsymbol{F}}^{(\mathrm{c})}(\bar{\boldsymbol{s}}))^{\mathrm{T}}(\bar{\boldsymbol{E}}_{\mathrm{A}}^{(\mathrm{c})})^{-1}\bar{\boldsymbol{F}}^{(\mathrm{c})}(\bar{\boldsymbol{s}}))^{-1}(\boldsymbol{F}_2(\bar{\boldsymbol{u}}_d,\bar{\boldsymbol{s}}))^{\mathrm{T}})^{-1} \\ & \times \boldsymbol{F}_1(\bar{\boldsymbol{u}}_d,\bar{\boldsymbol{s}}))^{-1} \quad (1 \leq d \leq D) \end{aligned} \tag{27}$$

where $\boldsymbol{F}_1(\bar{\boldsymbol{u}}_d,\bar{\boldsymbol{s}}) = \frac{\partial \boldsymbol{f}(\bar{\boldsymbol{u}}_d,\bar{\boldsymbol{s}})}{\partial \bar{\boldsymbol{u}}_d^{\mathrm{T}}}$ and $\boldsymbol{F}_2(\bar{\boldsymbol{u}}_d,\bar{\boldsymbol{s}}) = \frac{\partial \boldsymbol{f}(\bar{\boldsymbol{u}}_d,\bar{\boldsymbol{s}})}{\partial \bar{\boldsymbol{s}}^{\mathrm{T}}}$. The subscript "i" is used to indicate that these CRB matrices are obtained for the case of non-cooperative localization. Appendix A proves that $\mathbf{CRB}(\bar{\boldsymbol{u}}_d) \leq \mathbf{CRB}_{\mathrm{i}}(\bar{\boldsymbol{u}}_d)$ $(1 \leq d \leq D)$. This result reveals that, compared with the non-cooperative positioning, the joint localization of multiple targets can achieve higher estimation accuracy.

B. CRB DERIVATION AND ANALYSIS BASED ON THE TDOA/FDOA MEASUREMENTS FORM CALIBRATION EMITTERS ONLY

The subsection presents the CRB on the estimation of parameter $\bar{\boldsymbol{s}}$ based on the TDOA/FDOA measurements from the calibration emitters only. In this case, the observations are composed of $\hat{\bar{\boldsymbol{r}}}^{(\mathrm{c})}$ and $\hat{\bar{\boldsymbol{s}}}$, and the unknown is $\bar{\boldsymbol{s}}$. The CRB matrix for $\bar{\boldsymbol{s}}$ is denoted as $\mathbf{CRB}_{\mathrm{o}}(\bar{\boldsymbol{s}})$. Then, the CRB matrix is given by

$$\mathbf{CRB}_{\mathrm{o}}(\bar{\boldsymbol{s}}) = (\bar{\boldsymbol{E}}_{\mathrm{B}}^{-1} + (\bar{\boldsymbol{F}}^{(\mathrm{c})}(\bar{\boldsymbol{s}}))^{\mathrm{T}}(\bar{\boldsymbol{E}}_{\mathrm{A}}^{(\mathrm{c})})^{-1}\bar{\boldsymbol{F}}^{(\mathrm{c})}(\bar{\boldsymbol{s}}))^{-1} \tag{28}$$

Remark 4: Since $(\bar{\boldsymbol{F}}_2(\bar{\boldsymbol{u}},\bar{\boldsymbol{s}}))^{\mathrm{T}}\bar{\boldsymbol{E}}_{\mathrm{A}}^{-1/2}\boldsymbol{\Pi}^{\perp}[\bar{\boldsymbol{E}}_{\mathrm{A}}^{-1/2}\bar{\boldsymbol{F}}_1(\bar{\boldsymbol{u}},\bar{\boldsymbol{s}})]\bar{\boldsymbol{E}}_{\mathrm{A}}^{-1/2}\bar{\boldsymbol{F}}_2(\bar{\boldsymbol{u}},\bar{\boldsymbol{s}}) \geq \boldsymbol{O}$, it follows from (23) and (28) that $\mathbf{CRB}_{\mathrm{o}}(\bar{\boldsymbol{s}}) \geq \mathbf{CRB}(\bar{\boldsymbol{s}})$. Hence, the TDOA/FDOA measurements from target sources can be exploited to improve the optimum accuracy of sensor location estimates.

IV. PSEUDO-LINEAR EQUATIONS FOR TDOA/FDOA MEASUREMENTS

The aim of this section is to derive the pseudo-linear equations for TDOA/FDOA measurements from both target sources and UAV calibration emitters.

A. PSEUDO-LINEAR EQUATIONS ASSOCIATED WITH TARGET SOURCES

From (1), the RDOA equation of the dth target source can be transformed into

$$\begin{aligned} & 2(\boldsymbol{s}_1 - \boldsymbol{s}_m)^{\mathrm{T}}(\boldsymbol{u}_d - \boldsymbol{s}_1) - 2r_{dm}||\boldsymbol{u}_d - \boldsymbol{s}_1||_2 \\ & \qquad = r_{dm}^2 - ||\boldsymbol{s}_1 - \boldsymbol{s}_m||_2^2 \quad \begin{pmatrix} 2 \leq m \leq M \\ 1 \leq d \leq D \end{pmatrix} \end{aligned} \tag{29}$$

The matrix form of (29) can be described as

$$\boldsymbol{A}_{\mathrm{p}}(\bar{\boldsymbol{r}}_d,\bar{\boldsymbol{s}})\boldsymbol{t}_d = \boldsymbol{A}_{\mathrm{p}}(\bar{\boldsymbol{r}}_d,\bar{\boldsymbol{s}})\boldsymbol{h}(\bar{\boldsymbol{u}}_d,\bar{\boldsymbol{s}}) = \boldsymbol{b}_{\mathrm{p}}(\bar{\boldsymbol{r}}_d,\bar{\boldsymbol{s}}) \quad (1 \leq d \leq D) \tag{30}$$

where

$$\begin{cases} \boldsymbol{A}_{\mathrm{p}}(\bar{\boldsymbol{r}}_d,\bar{\boldsymbol{s}}) = \begin{bmatrix} 2(\boldsymbol{s}_1 - \boldsymbol{s}_2)^{\mathrm{T}} & \boldsymbol{O}_{1\times 3} & -2r_{d2} & 0 \\ 2(\boldsymbol{s}_1 - \boldsymbol{s}_3)^{\mathrm{T}} & \boldsymbol{O}_{1\times 3} & -2r_{d3} & 0 \\ \vdots & \vdots & \vdots & \vdots \\ 2(\boldsymbol{s}_1 - \boldsymbol{s}_M)^{\mathrm{T}} & \boldsymbol{O}_{1\times 3} & -2r_{dM} & 0 \end{bmatrix} \\ \boldsymbol{b}_{\mathrm{p}}(\bar{\boldsymbol{r}}_d,\bar{\boldsymbol{s}}) = \begin{bmatrix} r_{d2}^2 - ||\boldsymbol{s}_1 - \boldsymbol{s}_2||_2^2 \\ r_{d3}^2 - ||\boldsymbol{s}_1 - \boldsymbol{s}_3||_2^2 \\ \vdots \\ r_{dM}^2 - ||\boldsymbol{s}_1 - \boldsymbol{s}_M||_2^2 \end{bmatrix}; \\ \boldsymbol{h}(\bar{\boldsymbol{u}}_d,\bar{\boldsymbol{s}}) = \begin{bmatrix} \bar{\boldsymbol{u}}_d - \boldsymbol{\Xi}\bar{\boldsymbol{s}} \\ \beta_1(\bar{\boldsymbol{u}}_d,\bar{\boldsymbol{s}}) \\ \beta_2(\bar{\boldsymbol{u}}_d,\bar{\boldsymbol{s}}) \end{bmatrix} \end{cases} \tag{31}$$

$$\mathbf{CRB}\left(\begin{bmatrix} \bar{\boldsymbol{u}} \\ \bar{\boldsymbol{s}} \end{bmatrix}\right) = \left[\begin{array}{c|c} (\bar{\boldsymbol{F}}_1(\bar{\boldsymbol{u}},\bar{\boldsymbol{s}}))^{\mathrm{T}}\bar{\boldsymbol{E}}_{\mathrm{A}}^{-1}\bar{\boldsymbol{F}}_1(\bar{\boldsymbol{u}},\bar{\boldsymbol{s}}) & (\bar{\boldsymbol{F}}_1(\bar{\boldsymbol{u}},\bar{\boldsymbol{s}}))^{\mathrm{T}}\bar{\boldsymbol{E}}_{\mathrm{A}}^{-1}\bar{\boldsymbol{F}}_2(\bar{\boldsymbol{u}},\bar{\boldsymbol{s}}) \\ \hline (\bar{\boldsymbol{F}}_2(\bar{\boldsymbol{u}},\bar{\boldsymbol{s}}))^{\mathrm{T}}\bar{\boldsymbol{E}}_{\mathrm{A}}^{-1}\bar{\boldsymbol{F}}_1(\bar{\boldsymbol{u}},\bar{\boldsymbol{s}}) & \begin{array}{c} \bar{\boldsymbol{E}}_{\mathrm{B}}^{-1} + (\bar{\boldsymbol{F}}_2(\bar{\boldsymbol{u}},\bar{\boldsymbol{s}}))^{\mathrm{T}}\bar{\boldsymbol{E}}_{\mathrm{A}}^{-1}\bar{\boldsymbol{F}}_2(\bar{\boldsymbol{u}},\bar{\boldsymbol{s}}) \\ +(\bar{\boldsymbol{F}}^{(\mathrm{c})}(\bar{\boldsymbol{s}}))^{\mathrm{T}}(\bar{\boldsymbol{E}}_{\mathrm{A}}^{(\mathrm{c})})^{-1}\bar{\boldsymbol{F}}^{(\mathrm{c})}(\bar{\boldsymbol{s}}) \end{array} \end{array}\right]^{-1} \tag{21}$$

$$\begin{aligned} \mathbf{CRB}(\bar{\boldsymbol{u}}_d) &= (\boldsymbol{i}_D^{(d)\mathrm{T}} \otimes \boldsymbol{I}_6)\mathbf{CRB}(\bar{\boldsymbol{u}})(\boldsymbol{i}_D^{(d)} \otimes \boldsymbol{I}_6) \\ &= (\boldsymbol{i}_D^{(d)\mathrm{T}} \otimes \boldsymbol{I}_6)\left((\bar{\boldsymbol{F}}_1(\bar{\boldsymbol{u}},\bar{\boldsymbol{s}}))^{\mathrm{T}}\left(\bar{\boldsymbol{E}}_{\mathrm{A}} + \bar{\boldsymbol{F}}_2(\bar{\boldsymbol{u}},\bar{\boldsymbol{s}})\left(\bar{\boldsymbol{E}}_{\mathrm{B}}^{-1} + (\bar{\boldsymbol{F}}^{(\mathrm{c})}(\bar{\boldsymbol{s}}))^{\mathrm{T}}\right.\right.\right. \\ &\quad \left.\left.\left.\times(\bar{\boldsymbol{E}}_{\mathrm{A}}^{(\mathrm{c})})^{-1}\bar{\boldsymbol{F}}^{(\mathrm{c})}(\bar{\boldsymbol{s}})\right)^{-1}(\bar{\boldsymbol{F}}_2(\bar{\boldsymbol{u}},\bar{\boldsymbol{s}}))^{\mathrm{T}}\right)^{-1}\bar{\boldsymbol{F}}_1(\bar{\boldsymbol{u}},\bar{\boldsymbol{s}})\right)^{-1}(\boldsymbol{i}_D^{(d)} \otimes \boldsymbol{I}_6) \\ &\quad (1 \leq d \leq D) \end{aligned} \tag{26}$$

in which

$$\begin{cases} \boldsymbol{\Xi} = [\boldsymbol{I}_6\ \boldsymbol{O}_{6\times 6(M-1)}]\ ; \quad \beta_1(\bar{\boldsymbol{u}}_d, \bar{\boldsymbol{s}}) = ||\boldsymbol{u}_d - \boldsymbol{s}_1||_2 \\ \beta_2(\bar{\boldsymbol{u}}_d, \bar{\boldsymbol{s}}) = \dfrac{(\boldsymbol{u}_d - \boldsymbol{s}_1)^{\mathrm{T}}(\dot{\boldsymbol{u}}_d - \dot{\boldsymbol{s}}_1)}{||\boldsymbol{u}_d - \boldsymbol{s}_1||_2} \end{cases} \tag{32}$$

Here, $\beta_1(\bar{\boldsymbol{u}}_d, \bar{\boldsymbol{s}})$ and $\beta_2(\bar{\boldsymbol{u}}_d, \bar{\boldsymbol{s}})$ should be considered as auxiliary variables, which plays a very crucial role in ensuing the equations are linear. Subsequently, to get the pseudo-linear equations with respect to the RDROA measurements, we take the time derivative of (29), leading to

$$\begin{aligned} &(\dot{\boldsymbol{s}}_1 - \dot{\boldsymbol{s}}_m)^{\mathrm{T}}(\boldsymbol{u}_d - \boldsymbol{s}_1) + (\boldsymbol{s}_1 - \boldsymbol{s}_m)^{\mathrm{T}}(\dot{\boldsymbol{u}}_d - \dot{\boldsymbol{s}}_1) \\ &\quad - \dot{r}_{dm}||\boldsymbol{u}_d - \boldsymbol{s}_1||_2 - r_{dm}\frac{(\boldsymbol{u}_d - \boldsymbol{s}_1)^{\mathrm{T}}(\dot{\boldsymbol{u}}_d - \dot{\boldsymbol{s}}_1)}{||\boldsymbol{u}_d - \boldsymbol{s}_1||_2} \\ &= r_{dm}\dot{r}_{dm} - (\boldsymbol{s}_1 - \boldsymbol{s}_m)^{\mathrm{T}}(\dot{\boldsymbol{s}}_1 - \dot{\boldsymbol{s}}_m) \quad \begin{pmatrix} 2 \le m \le M \\ 1 \le d \le D \end{pmatrix} \end{aligned} \tag{33}$$

Similarly, the matrix form of (33) can be expressed as

$$\boldsymbol{A}_{\mathrm{v}}(\bar{\boldsymbol{r}}_d, \bar{\boldsymbol{s}})\boldsymbol{t}_d = \boldsymbol{A}_{\mathrm{v}}(\bar{\boldsymbol{r}}_d, \bar{\boldsymbol{s}})\boldsymbol{h}(\bar{\boldsymbol{u}}_d, \bar{\boldsymbol{s}}) = \boldsymbol{b}_{\mathrm{v}}(\bar{\boldsymbol{r}}_d, \bar{\boldsymbol{s}}) \quad (1 \le d \le D) \tag{34}$$

where

$$\begin{cases} \boldsymbol{A}_{\mathrm{v}}(\bar{\boldsymbol{r}}_d, \bar{\boldsymbol{s}}) = \begin{bmatrix} (\dot{\boldsymbol{s}}_1 - \dot{\boldsymbol{s}}_2)^{\mathrm{T}} & (\boldsymbol{s}_1 - \boldsymbol{s}_2)^{\mathrm{T}} & -\dot{r}_{d2} & -r_{d2} \\ (\dot{\boldsymbol{s}}_1 - \dot{\boldsymbol{s}}_3)^{\mathrm{T}} & (\boldsymbol{s}_1 - \boldsymbol{s}_3)^{\mathrm{T}} & -\dot{r}_{d3} & -r_{d3} \\ \vdots & \vdots & \vdots & \vdots \\ (\dot{\boldsymbol{s}}_1 - \dot{\boldsymbol{s}}_M)^{\mathrm{T}} & (\boldsymbol{s}_1 - \boldsymbol{s}_M)^{\mathrm{T}} & -\dot{r}_{dM} & -r_{dM} \end{bmatrix} \\ \boldsymbol{b}_{\mathrm{v}}(\bar{\boldsymbol{r}}_d, \bar{\boldsymbol{s}}) = \begin{bmatrix} r_{d2}\dot{r}_{d2} - (\boldsymbol{s}_1 - \boldsymbol{s}_2)^{\mathrm{T}}(\dot{\boldsymbol{s}}_1 - \dot{\boldsymbol{s}}_2) \\ r_{d3}\dot{r}_{d3} - (\boldsymbol{s}_1 - \boldsymbol{s}_3)^{\mathrm{T}}(\dot{\boldsymbol{s}}_1 - \dot{\boldsymbol{s}}_3) \\ \vdots \\ r_{dM}\dot{r}_{dM} - (\boldsymbol{s}_1 - \boldsymbol{s}_M)^{\mathrm{T}}(\dot{\boldsymbol{s}}_1 - \dot{\boldsymbol{s}}_M) \end{bmatrix} \end{cases} \tag{35}$$

Stacking (30) and (34) yields the following composite matrix equation for the dth target from both RDOA and RDROA measurements

$$\boldsymbol{A}(\bar{\boldsymbol{r}}_d, \bar{\boldsymbol{s}})\boldsymbol{t}_d = \boldsymbol{A}(\bar{\boldsymbol{r}}_d, \bar{\boldsymbol{s}})\boldsymbol{h}(\bar{\boldsymbol{u}}_d, \bar{\boldsymbol{s}}) = \boldsymbol{b}(\bar{\boldsymbol{r}}_d, \bar{\boldsymbol{s}}) \quad (1 \le d \le D) \tag{36}$$

where

$$\boldsymbol{A}(\bar{\boldsymbol{r}}_d, \bar{\boldsymbol{s}}) = \begin{bmatrix} \boldsymbol{A}_{\mathrm{p}}(\bar{\boldsymbol{r}}_d, \bar{\boldsymbol{s}}) \\ \boldsymbol{A}_{\mathrm{v}}(\bar{\boldsymbol{r}}_d, \bar{\boldsymbol{s}}) \end{bmatrix}; \quad \boldsymbol{b}(\bar{\boldsymbol{r}}_d, \bar{\boldsymbol{s}}) = \begin{bmatrix} \boldsymbol{b}_{\mathrm{p}}(\bar{\boldsymbol{r}}_d, \bar{\boldsymbol{s}}) \\ \boldsymbol{b}_{\mathrm{v}}(\bar{\boldsymbol{r}}_d, \bar{\boldsymbol{s}}) \end{bmatrix} \tag{37}$$

To achieve multiple-target cooperative localization, we need to collect all the D equations in (36) together to form the high-dimensional pseudo-linear equation:

$$\bar{\boldsymbol{A}}(\bar{\boldsymbol{r}}, \bar{\boldsymbol{s}})\bar{\boldsymbol{t}} = \bar{\boldsymbol{A}}(\bar{\boldsymbol{r}}, \bar{\boldsymbol{s}})\bar{\boldsymbol{h}}(\bar{\boldsymbol{u}}, \bar{\boldsymbol{s}}) = \bar{\boldsymbol{b}}(\bar{\boldsymbol{r}}, \bar{\boldsymbol{s}}) \tag{38}$$

where

$$\begin{cases} \bar{\boldsymbol{A}}(\bar{\boldsymbol{r}}, \bar{\boldsymbol{s}}) = \mathrm{blkdiag}[\boldsymbol{A}(\bar{\boldsymbol{r}}_1, \bar{\boldsymbol{s}})\ \boldsymbol{A}(\bar{\boldsymbol{r}}_2, \bar{\boldsymbol{s}})\ \cdots\ \boldsymbol{A}(\bar{\boldsymbol{r}}_D, \bar{\boldsymbol{s}})] \\ \bar{\boldsymbol{b}}(\bar{\boldsymbol{r}}, \bar{\boldsymbol{s}}) = [(\boldsymbol{b}(\bar{\boldsymbol{r}}_1, \bar{\boldsymbol{s}}))^{\mathrm{T}}\ (\boldsymbol{b}(\bar{\boldsymbol{r}}_2, \bar{\boldsymbol{s}}))^{\mathrm{T}}\ \cdots\ (\boldsymbol{b}(\bar{\boldsymbol{r}}_D, \bar{\boldsymbol{s}}))^{\mathrm{T}}]^{\mathrm{T}} \\ \bar{\boldsymbol{t}} = \bar{\boldsymbol{h}}(\bar{\boldsymbol{u}}, \bar{\boldsymbol{s}}) = [\boldsymbol{t}_1^{\mathrm{T}}\ \boldsymbol{t}_2^{\mathrm{T}}\ \cdots\ \boldsymbol{t}_D^{\mathrm{T}}]^{\mathrm{T}} \\ = [(\boldsymbol{h}(\bar{\boldsymbol{u}}_1, \bar{\boldsymbol{s}}))^{\mathrm{T}}\ (\boldsymbol{h}(\bar{\boldsymbol{u}}_2, \bar{\boldsymbol{s}}))^{\mathrm{T}}\ \cdots\ (\boldsymbol{h}(\bar{\boldsymbol{u}}_D, \bar{\boldsymbol{s}}))^{\mathrm{T}}]^{\mathrm{T}} \end{cases} \tag{39}$$

B. PSEUDO-LINEAR EQUATIONS ASSOCIATED WITH CALIBRATION EMITTERS

Using (14), we can transform the RDOA equation of the nth calibration emitter into

$$\begin{aligned} &2\boldsymbol{w}_n^{\mathrm{T}}\boldsymbol{s}_1 - 2\boldsymbol{w}_n^{\mathrm{T}}\boldsymbol{s}_m - ||\boldsymbol{s}_1||_2^2 + ||\boldsymbol{s}_m||_2^2 \\ &\quad - 2r_{nm}^{(\mathrm{c})}||\boldsymbol{s}_1 - \boldsymbol{w}_n||_2 = (r_{nm}^{(\mathrm{c})})^2 \quad \begin{pmatrix} 2 \le m \le M \\ 1 \le n \le N \end{pmatrix} \end{aligned} \tag{40}$$

Eq.(40) can be restated in a matrix form as (41) [see (42), as shown at the bottom of the next page].

$$\boldsymbol{A}_{\mathrm{p},n}^{(\mathrm{c})}(\bar{\boldsymbol{r}}_n^{(\mathrm{c})})\boldsymbol{\eta} = \boldsymbol{A}_{\mathrm{p},n}^{(\mathrm{c})}(\bar{\boldsymbol{r}}_n^{(\mathrm{c})})\boldsymbol{\psi}(\bar{\boldsymbol{s}}) = \boldsymbol{b}_{\mathrm{p}}^{(\mathrm{c})}(\bar{\boldsymbol{r}}_n^{(\mathrm{c})}) \quad (1 \le n \le N) \tag{41}$$

in which

$$\begin{cases} \boldsymbol{\psi}_1(\bar{\boldsymbol{s}}) = \begin{bmatrix} ||\boldsymbol{s}_1||_2^2 \\ ||\boldsymbol{s}_2||_2^2 \\ \vdots \\ ||\boldsymbol{s}_M||_2^2 \end{bmatrix}; \quad \boldsymbol{\psi}_2(\bar{\boldsymbol{s}}) = \begin{bmatrix} \boldsymbol{s}_1^{\mathrm{T}}\dot{\boldsymbol{s}}_1 \\ \boldsymbol{s}_2^{\mathrm{T}}\dot{\boldsymbol{s}}_2 \\ \vdots \\ \boldsymbol{s}_M^{\mathrm{T}}\dot{\boldsymbol{s}}_M \end{bmatrix} \\ \boldsymbol{\psi}_3(\bar{\boldsymbol{s}}) = \begin{bmatrix} ||\boldsymbol{s}_1 - \boldsymbol{w}_1||_2 \\ ||\boldsymbol{s}_1 - \boldsymbol{w}_2||_2 \\ \vdots \\ ||\boldsymbol{s}_1 - \boldsymbol{w}_N||_2 \end{bmatrix}; \\ \boldsymbol{\psi}_4(\bar{\boldsymbol{s}}) = \begin{bmatrix} \dfrac{(\boldsymbol{s}_1 - \boldsymbol{w}_1)^{\mathrm{T}}(\dot{\boldsymbol{s}}_1 - \dot{\boldsymbol{w}}_1)}{||\boldsymbol{s}_1 - \boldsymbol{w}_1||_2} \\ \dfrac{(\boldsymbol{s}_1 - \boldsymbol{w}_2)^{\mathrm{T}}(\dot{\boldsymbol{s}}_1 - \dot{\boldsymbol{w}}_2)}{||\boldsymbol{s}_1 - \boldsymbol{w}_2||_2} \\ \vdots \\ \dfrac{(\boldsymbol{s}_1 - \boldsymbol{w}_N)^{\mathrm{T}}(\dot{\boldsymbol{s}}_1 - \dot{\boldsymbol{w}}_N)}{||\boldsymbol{s}_1 - \boldsymbol{w}_N||_2} \end{bmatrix} \end{cases} \tag{43}$$

Taking the time derivative of (40) leads to the following equations related to the RDROA measurements

$$\begin{aligned} &\dot{\boldsymbol{w}}_n^{\mathrm{T}}\boldsymbol{s}_1 + \boldsymbol{w}_n^{\mathrm{T}}\dot{\boldsymbol{s}}_1 - \dot{\boldsymbol{w}}_n^{\mathrm{T}}\boldsymbol{s}_m - \boldsymbol{w}_n^{\mathrm{T}}\dot{\boldsymbol{s}}_m - \boldsymbol{s}_1^{\mathrm{T}}\dot{\boldsymbol{s}}_1 + \boldsymbol{s}_m^{\mathrm{T}}\dot{\boldsymbol{s}}_m \\ &\quad - \dot{r}_{nm}^{(\mathrm{c})}||\boldsymbol{s}_1 - \boldsymbol{w}_n||_2 - r_{nm}^{(\mathrm{c})}\frac{(\boldsymbol{s}_1 - \boldsymbol{w}_n)^{\mathrm{T}}(\dot{\boldsymbol{s}}_1 - \dot{\boldsymbol{w}}_n)}{||\boldsymbol{s}_1 - \boldsymbol{w}_n||_2} \\ &= r_{nm}^{(\mathrm{c})}\dot{r}_{nm}^{(\mathrm{c})} \quad \begin{pmatrix} 2 \le m \le M \\ 1 \le n \le N \end{pmatrix} \end{aligned} \tag{44}$$

whose matrix form is given in (45) and (46), as shown at the bottom of the next page.

$$\boldsymbol{A}_{\mathrm{v},n}^{(\mathrm{c})}(\bar{\boldsymbol{r}}_n^{(\mathrm{c})})\boldsymbol{\eta} = \boldsymbol{A}_{\mathrm{v},n}^{(\mathrm{c})}(\bar{\boldsymbol{r}}_n^{(\mathrm{c})})\boldsymbol{\psi}(\bar{\boldsymbol{s}}) = \boldsymbol{b}_{\mathrm{v}}^{(\mathrm{c})}(\bar{\boldsymbol{r}}_n^{(\mathrm{c})}) \quad (1 \le n \le N) \tag{45}$$

Combining (41) and (45), we get the following composite matrix equation for the nth calibration emitter

$$\boldsymbol{A}_n^{(\mathrm{c})}(\bar{\boldsymbol{r}}_n^{(\mathrm{c})})\boldsymbol{\eta} = \boldsymbol{A}_n^{(\mathrm{c})}(\bar{\boldsymbol{r}}_n^{(\mathrm{c})})\boldsymbol{\psi}(\bar{\boldsymbol{s}}) = \boldsymbol{b}^{(\mathrm{c})}(\bar{\boldsymbol{r}}_n^{(\mathrm{c})}) \quad (1 \le n \le N) \tag{47}$$

where

$$\boldsymbol{A}_n^{(\mathrm{c})}(\bar{\boldsymbol{r}}_n^{(\mathrm{c})}) = \begin{bmatrix} \boldsymbol{A}_{\mathrm{p},n}^{(\mathrm{c})}(\bar{\boldsymbol{r}}_n^{(\mathrm{c})}) \\ \boldsymbol{A}_{\mathrm{v},n}^{(\mathrm{c})}(\bar{\boldsymbol{r}}_n^{(\mathrm{c})}) \end{bmatrix}; \quad \boldsymbol{b}^{(\mathrm{c})}(\bar{\boldsymbol{r}}_n^{(\mathrm{c})}) = \begin{bmatrix} \boldsymbol{b}_{\mathrm{p}}^{(\mathrm{c})}(\bar{\boldsymbol{r}}_n^{(\mathrm{c})}) \\ \boldsymbol{b}_{\mathrm{v}}^{(\mathrm{c})}(\bar{\boldsymbol{r}}_n^{(\mathrm{c})}) \end{bmatrix} \tag{48}$$

Stacking (47) for $n = 1, 2, \cdots, N$ yields the entire matrix equation with respect to the composite unknown vector as follows:

$$\bar{\boldsymbol{A}}^{(\mathrm{c})}(\bar{\boldsymbol{r}}^{(\mathrm{c})})\boldsymbol{\eta} = \bar{\boldsymbol{A}}^{(\mathrm{c})}(\bar{\boldsymbol{r}}^{(\mathrm{c})})\boldsymbol{\psi}(\bar{\boldsymbol{s}}) = \bar{\boldsymbol{b}}^{(\mathrm{c})}(\bar{\boldsymbol{r}}^{(\mathrm{c})}) \tag{49}$$

where $\bar{\boldsymbol{b}}^{(\mathrm{c})}(\bar{\boldsymbol{r}}^{(\mathrm{c})}) = [(\boldsymbol{b}^{(\mathrm{c})}(\bar{\boldsymbol{r}}_1^{(\mathrm{c})}))^{\mathrm{T}}(\boldsymbol{b}^{(\mathrm{c})}(\bar{\boldsymbol{r}}_2^{(\mathrm{c})}))^{\mathrm{T}}\cdots(\boldsymbol{b}^{(\mathrm{c})}(\bar{\boldsymbol{r}}_N^{(\mathrm{c})}))^{\mathrm{T}}]^{\mathrm{T}}$ and $\bar{\boldsymbol{A}}^{(\mathrm{c})}(\bar{\boldsymbol{r}}^{(\mathrm{c})}) = [(\boldsymbol{A}_1^{(\mathrm{c})}(\bar{\boldsymbol{r}}_1^{(\mathrm{c})}))^{\mathrm{T}}(\boldsymbol{A}_2^{(\mathrm{c})}(\bar{\boldsymbol{r}}_2^{(\mathrm{c})}))^{\mathrm{T}}\cdots(\boldsymbol{A}_N^{(\mathrm{c})}(\bar{\boldsymbol{r}}_N^{(\mathrm{c})}))^{\mathrm{T}}]^{\mathrm{T}}$.

V. QUADRATIC EQUATION CONSTRAINTS FOR TDOA/FDOA LOCALIZATION

This section is devoted to presenting the quadratic equation constraints on vectors $\bar{\boldsymbol{t}}$ and $\boldsymbol{\eta}$. They play important role in the development of the proposed estimator.

A. QUADRATIC EQUATION CONSTRAINTS ON VECTOR $\bar{\boldsymbol{t}}$

In this subsection, a set of quadratic equation constraints on vector $\bar{\boldsymbol{t}}$ is given. To this end, we first need to deduce the quadratic equations that vectors $\boldsymbol{t}_d = \boldsymbol{h}(\bar{\boldsymbol{u}}_d, \bar{\boldsymbol{s}})\quad (1 \le d \le D)$ satisfy. Since vector $\boldsymbol{t}_d$ includes two intermediate variables, namely, $\beta_1(\bar{\boldsymbol{u}}_d, \bar{\boldsymbol{s}})$ and $\beta_2(\bar{\boldsymbol{u}}_d, \bar{\boldsymbol{s}})$, there exist two constraints related to $\boldsymbol{t}_d$. It follows from the functional forms of $\beta_1(\bar{\boldsymbol{u}}_d, \bar{\boldsymbol{s}})$ and $\beta_2(\bar{\boldsymbol{u}}_d, \bar{\boldsymbol{s}})$ that

$$\begin{cases} \boldsymbol{t}_d^{\mathrm{T}}\begin{bmatrix} \boldsymbol{I}_3 & \boldsymbol{O}_{3\times3} & \boldsymbol{O}_{3\times1} & \boldsymbol{O}_{3\times1} \\ \boldsymbol{O}_{3\times3} & \boldsymbol{O}_{3\times3} & \boldsymbol{O}_{3\times1} & \boldsymbol{O}_{3\times1} \\ \boldsymbol{O}_{1\times3} & \boldsymbol{O}_{1\times3} & -1 & 0 \\ \boldsymbol{O}_{1\times3} & \boldsymbol{O}_{1\times3} & 0 & 0 \end{bmatrix}\boldsymbol{t}_d = \boldsymbol{t}_d^{\mathrm{T}}\boldsymbol{\Gamma}_1\boldsymbol{t}_d = 0 \\ \boldsymbol{t}_d^{\mathrm{T}}\begin{bmatrix} \boldsymbol{O}_{3\times3} & \boldsymbol{I}_3 & \boldsymbol{O}_{3\times1} & \boldsymbol{O}_{3\times1} \\ \boldsymbol{I}_3 & \boldsymbol{O}_{3\times3} & \boldsymbol{O}_{3\times1} & \boldsymbol{O}_{3\times1} \\ \boldsymbol{O}_{1\times3} & \boldsymbol{O}_{1\times3} & 0 & -1 \\ \boldsymbol{O}_{1\times3} & \boldsymbol{O}_{1\times3} & -1 & 0 \end{bmatrix}\boldsymbol{t}_d = \boldsymbol{t}_d^{\mathrm{T}}\boldsymbol{\Gamma}_2\boldsymbol{t}_d = 0 \end{cases} \tag{50}$$

Obviously, the element in $\boldsymbol{\Gamma}_1$ and $\boldsymbol{\Gamma}_2$ is either one or zero. Both matrices are symmetric. From (50), we arrive at

$$\begin{cases} \bar{\boldsymbol{t}}^{\mathrm{T}}((\boldsymbol{i}_D^{(d)}\boldsymbol{i}_D^{(d)\mathrm{T}}) \otimes \boldsymbol{\Gamma}_1)\bar{\boldsymbol{t}} = \bar{\boldsymbol{t}}^{\mathrm{T}}\bar{\boldsymbol{\Gamma}}_{1d}\bar{\boldsymbol{t}} = 0 \\ \bar{\boldsymbol{t}}^{\mathrm{T}}((\boldsymbol{i}_D^{(d)}\boldsymbol{i}_D^{(d)\mathrm{T}}) \otimes \boldsymbol{\Gamma}_2)\bar{\boldsymbol{t}} = \bar{\boldsymbol{t}}^{\mathrm{T}}\bar{\boldsymbol{\Gamma}}_{2d}\bar{\boldsymbol{t}} = 0 \end{cases} \quad (1 \le d \le D) \tag{51}$$

where $\bar{\boldsymbol{\Gamma}}_{1d} = (\boldsymbol{i}_D^{(d)}\boldsymbol{i}_D^{(d)\mathrm{T}}) \otimes \boldsymbol{\Gamma}_1$ and $\bar{\boldsymbol{\Gamma}}_{2d} = (\boldsymbol{i}_D^{(d)}\boldsymbol{i}_D^{(d)\mathrm{T}}) \otimes \boldsymbol{\Gamma}_2$. It is noteworthy that (51) describes the final quadratic equation constraints on $\bar{\boldsymbol{t}}$. The number of constraints is equal to $2D$, which is also the number of nuisance variables in $\bar{\boldsymbol{t}}$.

On the other hand, differentiating both sides of the first equality in (51) with respect to $\bar{\boldsymbol{u}}$ yields

$$(\bar{\boldsymbol{H}}_1(\bar{\boldsymbol{u}}, \bar{\boldsymbol{s}}))^{\mathrm{T}}\bar{\boldsymbol{\Gamma}}_{1d}\bar{\boldsymbol{t}} = \boldsymbol{O}_{6D\times1} \quad (1 \le d \le D) \tag{52}$$

where

$$\begin{aligned} \bar{\boldsymbol{H}}_1(\bar{\boldsymbol{u}}, \bar{\boldsymbol{s}}) &= \frac{\partial \bar{\boldsymbol{h}}(\bar{\boldsymbol{u}}, \bar{\boldsymbol{s}})}{\partial \bar{\boldsymbol{u}}^{\mathrm{T}}} \\ &= \mathrm{blkdiag}\left[\begin{bmatrix} \boldsymbol{I}_6 \\ \frac{\partial\beta_1(\bar{\boldsymbol{u}}_1,\bar{\boldsymbol{s}})}{\partial\bar{\boldsymbol{u}}_1^{\mathrm{T}}} \\ \frac{\partial\beta_2(\bar{\boldsymbol{u}}_1,\bar{\boldsymbol{s}})}{\partial\bar{\boldsymbol{u}}_1^{\mathrm{T}}} \end{bmatrix}\begin{bmatrix} \boldsymbol{I}_6 \\ \frac{\partial\beta_1(\bar{\boldsymbol{u}}_2,\bar{\boldsymbol{s}})}{\partial\bar{\boldsymbol{u}}_2^{\mathrm{T}}} \\ \frac{\partial\beta_2(\bar{\boldsymbol{u}}_2,\bar{\boldsymbol{s}})}{\partial\bar{\boldsymbol{u}}_2^{\mathrm{T}}} \end{bmatrix}\cdots\begin{bmatrix} \boldsymbol{I}_6 \\ \frac{\partial\beta_1(\bar{\boldsymbol{u}}_D,\bar{\boldsymbol{s}})}{\partial\bar{\boldsymbol{u}}_D^{\mathrm{T}}} \\ \frac{\partial\beta_2(\bar{\boldsymbol{u}}_D,\bar{\boldsymbol{s}})}{\partial\bar{\boldsymbol{u}}_D^{\mathrm{T}}} \end{bmatrix}\right] \end{aligned} \tag{53}$$

Following an analogous derivation, we get form the second equality in (51) the relation

$$(\bar{\boldsymbol{H}}_1(\bar{\boldsymbol{u}}, \bar{\boldsymbol{s}}))^{\mathrm{T}}\bar{\boldsymbol{\Gamma}}_{2d}\bar{\boldsymbol{t}} = \boldsymbol{O}_{6D\times1} \quad (1 \le d \le D) \tag{54}$$

Notice that (52) and (54) are both crucial for the performance analysis in Section VII.

B. QUADRATIC EQUATION CONSTRAINTS ON VECTOR $\boldsymbol{\eta}$

This subsection shows the quadratic equation constraints on vector $\boldsymbol{\eta}$. It can be observed from the definition of $\boldsymbol{\eta}$ that there exist four kinds of instrumental variables in $\boldsymbol{\eta}$ and the number of these variables equals to $2(M+N)$. So, we can form $2(M+N)$ quadratic equation constraints with respect to $\boldsymbol{\eta}$.

According to the definitions of $\boldsymbol{\psi}_1(\bar{\boldsymbol{s}})$, $\boldsymbol{\psi}_2(\bar{\boldsymbol{s}})$, $\boldsymbol{\psi}_3(\bar{\boldsymbol{s}})$ and $\boldsymbol{\psi}_4(\bar{\boldsymbol{s}})$, it can be verified that

$$\boldsymbol{\eta}^{\mathrm{T}}\begin{bmatrix} (\boldsymbol{i}_M^{(m)}\boldsymbol{i}_M^{(m)\mathrm{T}}) \otimes \begin{bmatrix} \boldsymbol{I}_3 & \boldsymbol{O}_{3\times3} \\ \boldsymbol{O}_{3\times3} & \boldsymbol{I}_3 \end{bmatrix} & \boldsymbol{O}_{6M\times(2M+2N)} \\ \boldsymbol{O}_{(2M+2N)\times6M} & \boldsymbol{O}_{(2M+2N)\times(2M+2N)} \end{bmatrix}\boldsymbol{\eta} \tag{55}$$

$$-\boldsymbol{i}_{8M+2N}^{(6M+m)\mathrm{T}}\boldsymbol{\eta} = \boldsymbol{\eta}^{\mathrm{T}}\boldsymbol{\Omega}_{1m}\boldsymbol{\eta} + \boldsymbol{\rho}_{1m}^{\mathrm{T}}\boldsymbol{\eta} = 0 \quad (1 \le m \le M)$$

$$\boldsymbol{\eta}^{\mathrm{T}}\begin{bmatrix} (\boldsymbol{i}_M^{(m)}\boldsymbol{i}_M^{(m)\mathrm{T}}) \otimes \begin{bmatrix} \boldsymbol{O}_{3\times3} & \boldsymbol{I}_3 \\ \boldsymbol{I}_3 & \boldsymbol{O}_{3\times3} \end{bmatrix} & \boldsymbol{O}_{6M\times(2M+2N)} \\ \boldsymbol{O}_{(2M+2N)\times6M} & \boldsymbol{O}_{(2M+2N)\times(2M+2N)} \end{bmatrix}\boldsymbol{\eta} \tag{56}$$

$$-2\boldsymbol{i}_{8M+2N}^{(7M+m)\mathrm{T}}\boldsymbol{\eta} = \boldsymbol{\eta}^{\mathrm{T}}\boldsymbol{\Omega}_{2m}\boldsymbol{\eta} + \boldsymbol{\rho}_{2m}^{\mathrm{T}}\boldsymbol{\eta} = 0 \quad (1 \le m \le M)$$

$$\boldsymbol{\eta}^{\mathrm{T}}\begin{bmatrix} \boldsymbol{O}_{8M\times8M} & \boldsymbol{O}_{8M\times N} & \boldsymbol{O}_{8M\times N} \\ \boldsymbol{O}_{N\times8M} & \boldsymbol{i}_N^{(n)}\boldsymbol{i}_N^{(n)\mathrm{T}} & \boldsymbol{O}_{N\times N} \\ \boldsymbol{O}_{N\times8M} & \boldsymbol{O}_{N\times N} & \boldsymbol{O}_{N\times N} \end{bmatrix}\boldsymbol{\eta} + \left(\begin{bmatrix} 2\boldsymbol{w}_n \\ \boldsymbol{O}_{(8M+2N-3)\times1} \end{bmatrix} - \boldsymbol{i}_{8M+2N}^{(6M+1)}\right)^{\mathrm{T}}\boldsymbol{\eta} \tag{57}$$

$$\begin{cases} \boldsymbol{A}_{\mathrm{p},n}^{(\mathrm{c})}(\bar{\boldsymbol{r}}_n^{(\mathrm{c})}) = [\,[\boldsymbol{I}_{M-1} \;\; -\boldsymbol{I}_{M-1}] \otimes [2\boldsymbol{w}_n^{\mathrm{T}} \;\; \boldsymbol{O}_{1\times3}] \;\vdots\; [-\boldsymbol{I}_{M-1} \;\; \boldsymbol{I}_{M-1}] \;\vdots\; \boldsymbol{O}_{(M-1)\times M} \;\vdots\; -2\boldsymbol{r}_n^{(\mathrm{c})}\boldsymbol{i}_N^{(n)\mathrm{T}} \;\vdots\; \boldsymbol{O}_{(M-1)\times N}\,] \\ \boldsymbol{b}_{\mathrm{p}}^{(\mathrm{c})}(\bar{\boldsymbol{r}}_n^{(\mathrm{c})}) = ([\boldsymbol{I}_{M-1} \;\; \boldsymbol{O}_{(M-1)\times(M-1)}]\bar{\boldsymbol{r}}_n^{(\mathrm{c})}) \odot ([\boldsymbol{I}_{M-1} \;\; \boldsymbol{O}_{(M-1)\times(M-1)}]\bar{\boldsymbol{r}}_n^{(\mathrm{c})}) \\ \boldsymbol{\eta} = \boldsymbol{\psi}(\bar{\boldsymbol{s}}) = [\bar{\boldsymbol{s}}^{\mathrm{T}} \;(\boldsymbol{\psi}_1(\bar{\boldsymbol{s}}))^{\mathrm{T}} \;(\boldsymbol{\psi}_2(\bar{\boldsymbol{s}}))^{\mathrm{T}} \;(\boldsymbol{\psi}_3(\bar{\boldsymbol{s}}))^{\mathrm{T}} \;(\boldsymbol{\psi}_4(\bar{\boldsymbol{s}}))^{\mathrm{T}}]^{\mathrm{T}} \end{cases} \tag{42}$$

$$\begin{cases} \boldsymbol{A}_{\mathrm{v},n}^{(\mathrm{c})}(\bar{\boldsymbol{r}}_n^{(\mathrm{c})}) = [\,[\boldsymbol{I}_{M-1} \;\; -\boldsymbol{I}_{M-1}] \otimes [\dot{\boldsymbol{w}}_n^{\mathrm{T}} \;\; \boldsymbol{w}_n^{\mathrm{T}}] \;\vdots\; \boldsymbol{O}_{(M-1)\times M} \;\vdots\; [-\boldsymbol{I}_{M-1} \;\; \boldsymbol{I}_{M-1}] \;\vdots\; -\dot{\boldsymbol{r}}_n^{(\mathrm{c})}\boldsymbol{i}_N^{(n)\mathrm{T}} \;\vdots\; -\boldsymbol{r}_n^{(\mathrm{c})}\boldsymbol{i}_N^{(n)\mathrm{T}}\,] \\ \boldsymbol{b}_{\mathrm{v}}^{(\mathrm{c})}(\bar{\boldsymbol{r}}_n^{(\mathrm{c})}) = ([\boldsymbol{I}_{M-1} \;\; \boldsymbol{O}_{(M-1)\times(M-1)}]\bar{\boldsymbol{r}}_n^{(\mathrm{c})}) \odot ([\boldsymbol{O}_{(M-1)\times(M-1)} \;\; \boldsymbol{I}_{M-1}]\bar{\boldsymbol{r}}_n^{(\mathrm{c})}) \end{cases} \tag{46}$$

$$= \boldsymbol{\eta}^{\mathrm{T}}\boldsymbol{\Omega}_{3n}\boldsymbol{\eta} + \boldsymbol{\rho}_{3n}^{\mathrm{T}}\boldsymbol{\eta} = ||\boldsymbol{w}_n||_2^2 \quad (1 \le n \le N)$$

$$\boldsymbol{\eta}^{\mathrm{T}}\begin{bmatrix} \boldsymbol{O}_{8M\times 8M} & \boldsymbol{O}_{8M\times N} & \boldsymbol{O}_{8M\times N} \\ \boldsymbol{O}_{N\times 8M} & \boldsymbol{O}_{N\times N} & \boldsymbol{i}_N^{(n)}\boldsymbol{i}_N^{(n)\mathrm{T}} \\ \boldsymbol{O}_{N\times 8M} & \boldsymbol{i}_N^{(n)}\boldsymbol{i}_N^{(n)\mathrm{T}} & \boldsymbol{O}_{N\times N} \end{bmatrix}\boldsymbol{\eta} + \left(\begin{bmatrix} 2\dot{\boldsymbol{w}}_n \\ 2\boldsymbol{w}_n \\ \boldsymbol{O}_{(8M+2N-6)\times 1} \end{bmatrix} - 2\boldsymbol{i}_{8M+2N}^{(7M+1)}\right)^{\mathrm{T}}\boldsymbol{\eta} \quad (58)$$

$$= \boldsymbol{\eta}^{\mathrm{T}}\boldsymbol{\Omega}_{4n}\boldsymbol{\eta} + \boldsymbol{\rho}_{4n}^{\mathrm{T}}\boldsymbol{\eta} = 2\boldsymbol{w}_n^{\mathrm{T}}\dot{\boldsymbol{w}}_n \quad (1 \le n \le N)$$

The elements in $\boldsymbol{\Omega}_{1m}$, $\boldsymbol{\Omega}_{2m}$, $\boldsymbol{\Omega}_{3n}$, $\boldsymbol{\Omega}_{4n}$, $\boldsymbol{\rho}_{1m}$, $\boldsymbol{\rho}_{2m}$, $\boldsymbol{\rho}_{3n}$ and $\boldsymbol{\rho}_{4n}$ can be found from (55)-(58).

Differentiating both sides of (55)-(58) with respect to $\bar{\boldsymbol{s}}$ leads to

$$(\boldsymbol{\Psi}(\bar{\boldsymbol{s}}))^{\mathrm{T}}\left(\boldsymbol{\Omega}_{1m}\boldsymbol{\eta} + \frac{1}{2}\boldsymbol{\rho}_{1m}\right) = \boldsymbol{O}_{6M\times 1} \quad (1 \le m \le M) \quad (59)$$

$$(\boldsymbol{\Psi}(\bar{\boldsymbol{s}}))^{\mathrm{T}}\left(\boldsymbol{\Omega}_{2m}\boldsymbol{\eta} + \frac{1}{2}\boldsymbol{\rho}_{2m}\right) = \boldsymbol{O}_{6M\times 1} \quad (1 \le m \le M) \quad (60)$$

$$(\boldsymbol{\Psi}(\bar{\boldsymbol{s}}))^{\mathrm{T}}\left(\boldsymbol{\Omega}_{3n}\boldsymbol{\eta} + \frac{1}{2}\boldsymbol{\rho}_{3n}\right) = \boldsymbol{O}_{6M\times 1} \quad (1 \le n \le N) \quad (61)$$

$$(\boldsymbol{\Psi}(\bar{\boldsymbol{s}}))^{\mathrm{T}}\left(\boldsymbol{\Omega}_{4n}\boldsymbol{\eta} + \frac{1}{2}\boldsymbol{\rho}_{4n}\right) = \boldsymbol{O}_{6M\times 1} \quad (1 \le n \le N) \quad (62)$$

where

$$\boldsymbol{\Psi}(\bar{\boldsymbol{s}}) = \frac{\partial \boldsymbol{\psi}(\bar{\boldsymbol{s}})}{\partial \bar{\boldsymbol{s}}^{\mathrm{T}}} = [\boldsymbol{I}_{6M}\ (\boldsymbol{\Psi}_1(\bar{\boldsymbol{s}}))^{\mathrm{T}}\ (\boldsymbol{\Psi}_2(\bar{\boldsymbol{s}}))^{\mathrm{T}}\ (\boldsymbol{\Psi}_3(\bar{\boldsymbol{s}}))^{\mathrm{T}}\ (\boldsymbol{\Psi}_4(\bar{\boldsymbol{s}}))^{\mathrm{T}}]^{\mathrm{T}} \quad (63)$$

in which $\boldsymbol{\Psi}_j(\bar{\boldsymbol{s}}) = \frac{\partial \boldsymbol{\psi}_j(\bar{\boldsymbol{s}})}{\partial \bar{\boldsymbol{s}}^{\mathrm{T}}}$ $(1 \le j \le 4)$. We stress that (59)-(62) are useful for the performance analysis in Subsection VI.B.

VI. PROPOSED ICWLS ESTIMATOR BASED ON TDOA/FDOA MEASUREMENTS

The objective of this section is to present a novel TDOA/FDOA localization approach for multiple targets when a set of UAV calibration emitters with known locations are available. The proposed estimator is based on the pseudo-linear equations derived in Section IV as well as the quadratic equation constraints given in Section V. The new method has two stages. In the first stage, the sensor locations are refined based on the UAV calibration measurements as well as the prior knowledge of sensor locations. In the second stage, the multiple-target cooperative localization is performed by combining the measurements form the target signals with the estimated values in the first phase. It is noteworthy that in each stage a novel ICWLS algorithm is developed. The algorithms are implemented by using matrix SVD, which has robust numerical performance. Moreover, the algorithm can provide closed-form solutions and update the weighting matrices accurately in every iteration.

A. STAGE-1 OF THE PROPOSED METHOD

In the first stage, the measurement vectors $\hat{\bar{\boldsymbol{r}}}^{(\mathrm{c})}$ and $\hat{\bar{\boldsymbol{s}}}$ are combined to estimate $\bar{\boldsymbol{s}}$. For this purpose, a novel ICWLS estimator is formulated by using the weighted least squares (WLS) criterion, which is asymptotically efficient under Gaussian noise assumption.

1) OPTIMIZATION MODEL FOR ESTIMATION OF SENSOR LOCATIONS

Notice that the functional forms of $\bar{\boldsymbol{A}}^{(\mathrm{c})}(\cdot)$ and $\bar{\boldsymbol{b}}^{(\mathrm{c})}(\cdot)$ in (49) are known, but vector $\bar{\boldsymbol{r}}^{(\mathrm{c})}$ is not exactly known and only its noisy value (i.e., $\hat{\bar{\boldsymbol{r}}}^{(\mathrm{c})}$) is available. To construct the cost function, we introduce an error vector as

$$\bar{\boldsymbol{\delta}}^{(\mathrm{c})} = \bar{\boldsymbol{b}}^{(\mathrm{c})}(\hat{\bar{\boldsymbol{r}}}^{(\mathrm{c})}) - \bar{\boldsymbol{A}}^{(\mathrm{c})}(\hat{\bar{\boldsymbol{r}}}^{(\mathrm{c})})\boldsymbol{\eta} \quad (64)$$

Applying a first-order Taylor series expansion of $\bar{\boldsymbol{b}}^{(\mathrm{c})}(\hat{\bar{\boldsymbol{r}}}^{(\mathrm{c})})$ and $\bar{\boldsymbol{A}}^{(\mathrm{c})}(\hat{\bar{\boldsymbol{r}}}^{(\mathrm{c})})$ around $\bar{\boldsymbol{r}}^{(\mathrm{c})}$ produces

$$\begin{cases} \bar{\boldsymbol{b}}^{(\mathrm{c})}(\hat{\bar{\boldsymbol{r}}}^{(\mathrm{c})}) \approx \bar{\boldsymbol{b}}^{(\mathrm{c})}(\bar{\boldsymbol{r}}^{(\mathrm{c})}) + \bar{\boldsymbol{B}}^{(\mathrm{c})}(\bar{\boldsymbol{r}}^{(\mathrm{c})})\bar{\boldsymbol{\varepsilon}}^{(\mathrm{c})} \\ \bar{\boldsymbol{A}}^{(\mathrm{c})}(\hat{\bar{\boldsymbol{r}}}^{(\mathrm{c})}) \approx \bar{\boldsymbol{A}}^{(\mathrm{c})}(\bar{\boldsymbol{r}}^{(\mathrm{c})}) + \sum_{j=1}^{2N(M-1)} \langle\bar{\boldsymbol{\varepsilon}}^{(\mathrm{c})}\rangle_j \dot{\bar{\boldsymbol{A}}}_j^{(\mathrm{c})}(\bar{\boldsymbol{r}}^{(\mathrm{c})}) \end{cases} \quad (65)$$

where

$$\begin{cases} \bar{\boldsymbol{B}}^{(\mathrm{c})}(\bar{\boldsymbol{r}}^{(\mathrm{c})}) = \dfrac{\partial \bar{\boldsymbol{b}}^{(\mathrm{c})}(\bar{\boldsymbol{r}}^{(\mathrm{c})})}{\partial \bar{\boldsymbol{r}}^{(\mathrm{c})\mathrm{T}}} \\ = \mathrm{blkdiag}[\boldsymbol{B}^{(\mathrm{c})}(\bar{\boldsymbol{r}}_1^{(\mathrm{c})})\ \boldsymbol{B}^{(\mathrm{c})}(\bar{\boldsymbol{r}}_2^{(\mathrm{c})})\ \cdots\ \boldsymbol{B}^{(\mathrm{c})}(\bar{\boldsymbol{r}}_N^{(\mathrm{c})})] \\ \dot{\bar{\boldsymbol{A}}}_j^{(\mathrm{c})}(\bar{\boldsymbol{r}}^{(\mathrm{c})}) = \dfrac{\partial \bar{\boldsymbol{A}}^{(\mathrm{c})}(\bar{\boldsymbol{r}}^{(\mathrm{c})})}{\partial \langle\bar{\boldsymbol{r}}^{(\mathrm{c})}\rangle_j} \\ = \boldsymbol{i}_N^{(n_j)} \otimes \dfrac{\partial \boldsymbol{A}_{n_j}^{(\mathrm{c})}(\bar{\boldsymbol{r}}_{n_j}^{(\mathrm{c})})}{\partial \langle\bar{\boldsymbol{r}}_{n_j}^{(\mathrm{c})}\rangle_{j-2(n_j-1)(M-1)}} \quad (1 \le j \le 2N(M-1)) \end{cases} \quad (66)$$

in which $\boldsymbol{B}^{(\mathrm{c})}(\bar{\boldsymbol{r}}_n^{(\mathrm{c})}) = \frac{\partial \boldsymbol{b}^{(\mathrm{c})}(\bar{\boldsymbol{r}}_n^{(\mathrm{c})})}{\partial \bar{\boldsymbol{r}}_n^{(\mathrm{c})\mathrm{T}}}$ $(1 \le n \le N)$ and $n_j = \left\lceil \frac{j}{2(M-1)} \right\rceil$. Substituting (65) into (64) yields

$$\bar{\boldsymbol{\delta}}^{(\mathrm{c})} \approx \bar{\boldsymbol{B}}^{(\mathrm{c})}(\bar{\boldsymbol{r}}^{(\mathrm{c})})\bar{\boldsymbol{\varepsilon}}^{(\mathrm{c})} - \sum_{j=1}^{2N(M-1)} \langle\bar{\boldsymbol{\varepsilon}}^{(\mathrm{c})}\rangle_j \dot{\bar{\boldsymbol{A}}}_j^{(\mathrm{c})}(\bar{\boldsymbol{r}}^{(\mathrm{c})})\boldsymbol{\eta} = \bar{\boldsymbol{C}}^{(\mathrm{c})}(\boldsymbol{\eta}, \bar{\boldsymbol{r}}^{(\mathrm{c})})\bar{\boldsymbol{\varepsilon}}^{(\mathrm{c})} \quad (67)$$

where

$$\bar{\boldsymbol{C}}^{(\mathrm{c})}(\boldsymbol{\eta}, \bar{\boldsymbol{r}}^{(\mathrm{c})}) = \bar{\boldsymbol{B}}^{(\mathrm{c})}(\bar{\boldsymbol{r}}^{(\mathrm{c})}) - [\dot{\bar{\boldsymbol{A}}}_1^{(\mathrm{c})}(\bar{\boldsymbol{r}}^{(\mathrm{c})})\boldsymbol{\eta}\ \dot{\bar{\boldsymbol{A}}}_2^{(\mathrm{c})}(\bar{\boldsymbol{r}}^{(\mathrm{c})})\boldsymbol{\eta}\ \cdots\ \dot{\bar{\boldsymbol{A}}}_{2N(M-1)}^{(\mathrm{c})}(\bar{\boldsymbol{r}}^{(\mathrm{c})})\boldsymbol{\eta}] \quad (68)$$

It follows from (67) that $\bar{\boldsymbol{\delta}}^{(\mathrm{c})}$ is approximately Gaussian distributed with zero mean and covariance matrix

$$\bar{\boldsymbol{\Phi}}^{(\mathrm{c})} = \mathrm{E}[\bar{\boldsymbol{\delta}}^{(\mathrm{c})}\bar{\boldsymbol{\delta}}^{(\mathrm{c})\mathrm{T}}] = \bar{\boldsymbol{C}}^{(\mathrm{c})}(\boldsymbol{\eta}, \bar{\boldsymbol{r}}^{(\mathrm{c})})\bar{\boldsymbol{E}}_{\mathrm{A}}^{(\mathrm{c})}(\bar{\boldsymbol{C}}^{(\mathrm{c})}(\boldsymbol{\eta}, \bar{\boldsymbol{r}}^{(\mathrm{c})}))^{\mathrm{T}} \quad (69)$$

For the purpose of exploiting the noisy measurements of sensor locations, we should introduce an augmented error vector as

$$\tilde{\boldsymbol{\delta}}^{(\mathrm{c})} = \begin{bmatrix} \bar{\boldsymbol{\delta}}^{(\mathrm{c})} \\ \bar{\boldsymbol{\xi}} \end{bmatrix} = \tilde{\boldsymbol{b}}^{(\mathrm{c})}(\hat{\bar{\boldsymbol{r}}}^{(\mathrm{c})}, \hat{\bar{\boldsymbol{s}}}) - \tilde{\boldsymbol{A}}^{(\mathrm{c})}(\hat{\bar{\boldsymbol{r}}}^{(\mathrm{c})})\boldsymbol{\eta} \quad (70)$$

where

$$\begin{cases} \tilde{\boldsymbol{b}}^{(\mathrm{c})}(\hat{\bar{\boldsymbol{r}}}^{(\mathrm{c})}, \hat{\tilde{\boldsymbol{s}}}) = \begin{bmatrix} \bar{\boldsymbol{b}}^{(\mathrm{c})}(\hat{\bar{\boldsymbol{r}}}^{(\mathrm{c})}) \\ \hat{\tilde{\boldsymbol{s}}} \end{bmatrix}; \ \tilde{\boldsymbol{A}}^{(\mathrm{c})}(\hat{\bar{\boldsymbol{r}}}^{(\mathrm{c})}) = \begin{bmatrix} \bar{\boldsymbol{A}}^{(\mathrm{c})}(\hat{\bar{\boldsymbol{r}}}^{(\mathrm{c})}) \\ \bar{\boldsymbol{I}}_{6M\times(8M+2N)} \end{bmatrix} \\ \bar{\boldsymbol{I}}_{6M\times(8M+2N)} = [\boldsymbol{I}_{6M} \ \boldsymbol{O}_{6M\times(2M+2N)}] \end{cases} \tag{71}$$

Inserting (67) into (70) leads to

$$\tilde{\boldsymbol{\delta}}^{(\mathrm{c})} \approx \tilde{\boldsymbol{C}}^{(\mathrm{c})}(\boldsymbol{\eta}, \bar{\boldsymbol{r}}^{(\mathrm{c})}) \begin{bmatrix} \bar{\boldsymbol{\varepsilon}}^{(\mathrm{c})} \\ \bar{\boldsymbol{\xi}} \end{bmatrix} \tag{72}$$

where $\tilde{\boldsymbol{C}}^{(\mathrm{c})}(\boldsymbol{\eta}, \bar{\boldsymbol{r}}^{(\mathrm{c})}) = \mathrm{blkdiag}[\bar{\boldsymbol{C}}^{(\mathrm{c})}(\boldsymbol{\eta}, \bar{\boldsymbol{r}}^{(\mathrm{c})}) \ \ \boldsymbol{I}_{6M}]$. From (70), it can be seen that $\tilde{\boldsymbol{\delta}}^{(\mathrm{c})}$ approximately obeys a zero-mean Gaussian distribution with covariance matrix

$$\begin{aligned} \tilde{\boldsymbol{\Phi}}^{(\mathrm{c})} &= \mathrm{E}[\tilde{\boldsymbol{\delta}}^{(\mathrm{c})}\tilde{\boldsymbol{\delta}}^{(\mathrm{c})\mathrm{T}}] \\ &= \mathrm{blkdiag}[\bar{\boldsymbol{C}}^{(\mathrm{c})}(\boldsymbol{\eta}, \bar{\boldsymbol{r}}^{(\mathrm{c})})\bar{\boldsymbol{E}}_{\mathrm{A}}^{(\mathrm{c})}(\bar{\boldsymbol{C}}^{(\mathrm{c})}(\boldsymbol{\eta}, \bar{\boldsymbol{r}}^{(\mathrm{c})}))^{\mathrm{T}} \ \ \bar{\boldsymbol{E}}_{\mathrm{B}}] \end{aligned} \tag{73}$$

Putting (55)-(58), (70) and (73) together, we can formulate the following constrained minimization problem in (74), as shown at the bottom of this page.

Problem (74) is certainly a quadratic programming with $2M + 2N$ quadratic indefinite equality constraints, which are nonconvex. Hence, (74) can be viewed as a CWLS problem. It does not seem possible to solve (74) in closed form because of its nonlinearity. Therefore, we have to develop an iterative algorithm to obtain the solution of (74). Besides, it is important to point out that the weighting matrix $\tilde{\boldsymbol{\Phi}}^{(\mathrm{c})}$ is dependent on the unknown vector $\boldsymbol{\eta}$ so that, strictly speaking, it should be denoted as $\tilde{\boldsymbol{\Phi}}^{(\mathrm{c})}(\boldsymbol{\eta})$. However, since the weighting matrix is updated recursively in the proposed iterative algorithm, we denote it as $\tilde{\boldsymbol{\Phi}}^{(\mathrm{c})}$ for the sake of brevity.

2) PROPOSED ITERATION ALGORITHM

The aim of this subsection is to present an iterative algorithm to solve the quadratic programming in (74).

In optimization problem (74), the Hessian matrix of the quadratic objective function is positive semidefinite; thus the cost function is convex. But, all the equality constraints in (74) are homogenous, indefinite and non-convex, so the key difficulty focuses on the constraints. Inspired by the work of [29], we would like to make the non-convex constraints become a set of linear equality constraints. As a result, a new convex programming can be obtained as an approximation of (74).

For each homogenous quadratic equality constraint in (74), if one of the variable $\boldsymbol{\eta}$ is replaced with its last iteration's value, then the non-convex quadratic constraints become linear and convex. The resulted programming is a convex approximation of (74). To be more specific, in the $k+1$th iteration we can formulate a convex optimization problem in (75), as shown at the bottom of this page.

where $\hat{\boldsymbol{\eta}}(k)$ is the estimated result in the kth iteration. An important advantage of the problem (75) lies in that its optimal solution can be analytically expressed. We are now ready to state the main result.

Proposition 1: Define the vector $\boldsymbol{g}^{(\mathrm{c})}(\hat{\boldsymbol{\eta}}(k))$ and matrix $\boldsymbol{G}^{(\mathrm{c})}(\hat{\boldsymbol{\eta}}(k))$ as follows in (76), (77), and (78), as shown at the bottom of the next page.

$$\begin{cases} \boldsymbol{g}^{(\mathrm{c})}(\hat{\boldsymbol{\eta}}(k)) \\ = [(\boldsymbol{g}_1^{(\mathrm{c})}(\hat{\boldsymbol{\eta}}(k)))^{\mathrm{T}} \ (\boldsymbol{g}_2^{(\mathrm{c})}(\hat{\boldsymbol{\eta}}(k)))^{\mathrm{T}} \ \cdots \ (\boldsymbol{g}_4^{(\mathrm{c})}(\hat{\boldsymbol{\eta}}(k)))^{\mathrm{T}}]^{\mathrm{T}} \\ \boldsymbol{G}^{(\mathrm{c})}(\hat{\boldsymbol{\eta}}(k)) \\ = [\boldsymbol{G}_1^{(\mathrm{c})}(\hat{\boldsymbol{\eta}}(k)) \ \boldsymbol{G}_2^{(\mathrm{c})}(\hat{\boldsymbol{\eta}}(k)) \ \cdots \ \boldsymbol{G}_4^{(\mathrm{c})}(\hat{\boldsymbol{\eta}}(k))] \end{cases} \tag{76}$$

If $\tilde{\boldsymbol{A}}^{(\mathrm{c})}(\hat{\bar{\boldsymbol{r}}}^{(\mathrm{c})})$ has full column rank and $(\boldsymbol{G}^{(\mathrm{c})}(\hat{\boldsymbol{\eta}}(k)))^{\mathrm{T}}$ is of full row rank, then the optimal solution of (75) can be expressed as

$$\begin{aligned} &\hat{\boldsymbol{\eta}}_{\mathrm{opt}}(k+1) \\ &= \hat{\boldsymbol{\eta}}'_{\mathrm{opt}}(k+1) - ((\tilde{\boldsymbol{A}}^{(\mathrm{c})}(\hat{\bar{\boldsymbol{r}}}^{(\mathrm{c})}))^{\mathrm{T}}(\tilde{\boldsymbol{\Phi}}^{(\mathrm{c})})^{-1}\tilde{\boldsymbol{A}}^{(\mathrm{c})}(\hat{\bar{\boldsymbol{r}}}^{(\mathrm{c})}))^{-1}\boldsymbol{G}^{(\mathrm{c})}(\hat{\boldsymbol{\eta}}(k)) \\ &\quad \times ((\boldsymbol{G}^{(\mathrm{c})}(\hat{\boldsymbol{\eta}}(k)))^{\mathrm{T}}((\tilde{\boldsymbol{A}}^{(\mathrm{c})}(\hat{\bar{\boldsymbol{r}}}^{(\mathrm{c})}))^{\mathrm{T}}(\tilde{\boldsymbol{\Phi}}^{(\mathrm{c})})^{-1}\tilde{\boldsymbol{A}}^{(\mathrm{c})}(\hat{\bar{\boldsymbol{r}}}^{(\mathrm{c})}))^{-1} \\ &\quad \times \boldsymbol{G}^{(\mathrm{c})}(\hat{\boldsymbol{\eta}}(k)))^{-1}((\boldsymbol{G}^{(\mathrm{c})}(\hat{\boldsymbol{\eta}}(k)))^{\mathrm{T}}\hat{\boldsymbol{\eta}}'_{\mathrm{opt}}(k+1) - \boldsymbol{g}^{(\mathrm{c})}(\hat{\boldsymbol{\eta}}(k))) \end{aligned} \tag{79}$$

$$\begin{cases} \min\limits_{\boldsymbol{\eta}\in R^{(8M+2N)\times 1}} J^{(\mathrm{c})}(\boldsymbol{\eta}) = \min\limits_{\boldsymbol{\eta}\in R^{(8M+2N)\times 1}} (\tilde{\boldsymbol{A}}^{(\mathrm{c})}(\hat{\bar{\boldsymbol{r}}}^{(\mathrm{c})})\boldsymbol{\eta} - \tilde{\boldsymbol{b}}^{(\mathrm{c})}(\hat{\bar{\boldsymbol{r}}}^{(\mathrm{c})}, \hat{\tilde{\boldsymbol{s}}}))^{\mathrm{T}}(\tilde{\boldsymbol{\Phi}}^{(\mathrm{c})})^{-1}(\tilde{\boldsymbol{A}}^{(\mathrm{c})}(\hat{\bar{\boldsymbol{r}}}^{(\mathrm{c})})\boldsymbol{\eta} - \tilde{\boldsymbol{b}}^{(\mathrm{c})}(\hat{\bar{\boldsymbol{r}}}^{(\mathrm{c})}, \hat{\tilde{\boldsymbol{s}}})) \\ \text{s.t. } \boldsymbol{\eta}^{\mathrm{T}}\boldsymbol{\Omega}_{1m}\boldsymbol{\eta} + \boldsymbol{\rho}_{1m}^{\mathrm{T}}\boldsymbol{\eta} = 0 \ ; \ \boldsymbol{\eta}^{\mathrm{T}}\boldsymbol{\Omega}_{2m}\boldsymbol{\eta} + \boldsymbol{\rho}_{2m}^{\mathrm{T}}\boldsymbol{\eta} = 0 \quad (1 \le m \le M) \\ \quad \boldsymbol{\eta}^{\mathrm{T}}\boldsymbol{\Omega}_{3n}\boldsymbol{\eta} + \boldsymbol{\rho}_{3n}^{\mathrm{T}}\boldsymbol{\eta} = ||\boldsymbol{w}_n||_2^2 \ ; \ \boldsymbol{\eta}^{\mathrm{T}}\boldsymbol{\Omega}_{4n}\boldsymbol{\eta} + \boldsymbol{\rho}_{4n}^{\mathrm{T}}\boldsymbol{\eta} = 2\boldsymbol{w}_n^{\mathrm{T}}\dot{\boldsymbol{w}}_n \quad (1 \le n \le N) \end{cases} \tag{74}$$

$$\begin{cases} \min\limits_{\boldsymbol{\eta}\in R^{(8M+2N)\times 1}} J^{(\mathrm{c})}(\boldsymbol{\eta}) = \min\limits_{\boldsymbol{\eta}\in R^{(8M+2N)\times 1}} (\tilde{\boldsymbol{A}}^{(\mathrm{c})}(\hat{\bar{\boldsymbol{r}}}^{(\mathrm{c})})\boldsymbol{\eta} - \tilde{\boldsymbol{b}}^{(\mathrm{c})}(\hat{\bar{\boldsymbol{r}}}^{(\mathrm{c})}, \hat{\tilde{\boldsymbol{s}}}))^{\mathrm{T}}(\tilde{\boldsymbol{\Phi}}^{(\mathrm{c})})^{-1}(\tilde{\boldsymbol{A}}^{(\mathrm{c})}(\hat{\bar{\boldsymbol{r}}}^{(\mathrm{c})})\boldsymbol{\eta} - \tilde{\boldsymbol{b}}^{(\mathrm{c})}(\hat{\bar{\boldsymbol{r}}}^{(\mathrm{c})}, \hat{\tilde{\boldsymbol{s}}})) \\ \text{s.t. } (\hat{\boldsymbol{\eta}}(k))^{\mathrm{T}}\boldsymbol{\Omega}_{1m}\boldsymbol{\eta} + \frac{1}{2}\boldsymbol{\rho}_{1m}^{\mathrm{T}}\boldsymbol{\eta} = -\frac{1}{2}\boldsymbol{\rho}_{1m}^{\mathrm{T}}\hat{\boldsymbol{\eta}}(k) \quad (1 \le m \le M) \\ \quad (\hat{\boldsymbol{\eta}}(k))^{\mathrm{T}}\boldsymbol{\Omega}_{2m}\boldsymbol{\eta} + \frac{1}{2}\boldsymbol{\rho}_{2m}^{\mathrm{T}}\boldsymbol{\eta} = -\frac{1}{2}\boldsymbol{\rho}_{2m}^{\mathrm{T}}\hat{\boldsymbol{\eta}}(k) \quad (1 \le m \le M) \\ \quad (\hat{\boldsymbol{\eta}}(k))^{\mathrm{T}}\boldsymbol{\Omega}_{3n}\boldsymbol{\eta} + \frac{1}{2}\boldsymbol{\rho}_{3n}^{\mathrm{T}}\boldsymbol{\eta} = ||\boldsymbol{w}_n||_2^2 - \frac{1}{2}\boldsymbol{\rho}_{3n}^{\mathrm{T}}\hat{\boldsymbol{\eta}}(k) \quad (1 \le n \le N) \\ \quad (\hat{\boldsymbol{\eta}}(k))^{\mathrm{T}}\boldsymbol{\Omega}_{4n}\boldsymbol{\eta} + \frac{1}{2}\boldsymbol{\rho}_{4n}^{\mathrm{T}}\boldsymbol{\eta} = 2\boldsymbol{w}_n^{\mathrm{T}}\dot{\boldsymbol{w}}_n - \frac{1}{2}\boldsymbol{\rho}_{4n}^{\mathrm{T}}\hat{\boldsymbol{\eta}}(k) \quad (1 \le n \le N) \end{cases} \tag{75}$$

where $\hat{\boldsymbol{\eta}}'_{\text{opt}}(k+1) = ((\tilde{\boldsymbol{A}}^{(\text{c})}(\hat{\tilde{\boldsymbol{r}}}^{(\text{c})}))^{\text{T}}(\tilde{\boldsymbol{\Phi}}^{(\text{c})})^{-1}\tilde{\boldsymbol{A}}^{(\text{c})}(\hat{\tilde{\boldsymbol{r}}}^{(\text{c})}))^{-1} \times (\tilde{\boldsymbol{A}}^{(\text{c})}(\hat{\tilde{\boldsymbol{r}}}^{(\text{c})}))^{\text{T}}(\tilde{\boldsymbol{\Phi}}^{(\text{c})})^{-1}\tilde{\boldsymbol{b}}^{(\text{c})}(\hat{\tilde{\boldsymbol{r}}}^{(\text{c})}, \hat{\tilde{\boldsymbol{s}}})$.

Proposition 1 can be proved by applying Lagrange multiplier method in a direct manner, so it is omitted due to limited space. It should be emphasized that Proposition 1 holds only when matrix $\tilde{\boldsymbol{A}}^{(\text{c})}(\hat{\tilde{\boldsymbol{r}}}^{(\text{c})})$ is of full column rank, which means that there are at least two calibration emitters that must be used for target localization. Next, we want to present an alternative solution of (75) by using matrix SVD technique, with no requirement on the number of calibration emitters. Moreover, it requires less computation and has better numerical stability compared with the solution in Proposition 1, due to the advantage of matrix SVD.

Proposition 2: Performing matrix SVD on $\boldsymbol{G}^{(\text{c})}(\hat{\boldsymbol{\eta}}(k))$ leads to

$$\begin{aligned}&\boldsymbol{G}^{(\text{c})}(\hat{\boldsymbol{\eta}}(k))\\&= [\boldsymbol{Q}_{11}^{(\text{c})}(k+1)\ \boldsymbol{Q}_{12}^{(\text{c})}(k+1)]\begin{bmatrix}\boldsymbol{\Sigma}_1^{(\text{c})}(k+1)\\ \boldsymbol{O}_{6M\times(2M+2N)}\end{bmatrix}(\boldsymbol{R}_1^{(\text{c})}(k+1))^{\text{T}}\\&= \boldsymbol{Q}_{11}^{(\text{c})}(k+1)\boldsymbol{\Sigma}_1^{(\text{c})}(k+1)(\boldsymbol{R}_1^{(\text{c})}(k+1))^{\text{T}}\end{aligned} \tag{80}$$

where $[\boldsymbol{Q}_{11}^{(\text{c})}(k+1)\ \ \boldsymbol{Q}_{12}^{(\text{c})}(k+1)]$ is an orthogonal matrix; $\boldsymbol{R}_1^{(\text{c})}(k+1)$ is an orthogonal matrix; $\boldsymbol{\Sigma}_1^{(\text{c})}(k+1)$ is a diagonal matrix, whose diagonal elements are the singular values of $\boldsymbol{G}^{(\text{c})}(\hat{\boldsymbol{\eta}}(k))$. Subsequently, performing matrix SVD on $(\tilde{\boldsymbol{\Phi}}^{(\text{c})})^{-1/2}\tilde{\boldsymbol{A}}^{(\text{c})}(\hat{\tilde{\boldsymbol{r}}}^{(\text{c})})\boldsymbol{Q}_{12}^{(\text{c})}(k+1)$ yields

$$\begin{aligned}&(\tilde{\boldsymbol{\Phi}}^{(\text{c})})^{-1/2}\tilde{\boldsymbol{A}}^{(\text{c})}(\hat{\tilde{\boldsymbol{r}}}^{(\text{c})})\boldsymbol{Q}_{12}^{(\text{c})}(k+1)\\&= [\boldsymbol{Q}_{21}^{(\text{c})}(k+1)\ \boldsymbol{Q}_{22}^{(\text{c})}(k+1)]\begin{bmatrix}\boldsymbol{\Sigma}_2^{(\text{c})}(k+1)\\ \boldsymbol{O}_{2N(M-1)\times 6M}\end{bmatrix}(\boldsymbol{R}_2^{(\text{c})}(k+1))^{\text{T}}\\&= \boldsymbol{Q}_{21}^{(\text{c})}(k+1)\boldsymbol{\Sigma}_2^{(\text{c})}(k+1)(\boldsymbol{R}_2^{(\text{c})}(k+1))^{\text{T}}\end{aligned} \tag{81}$$

where $[\boldsymbol{Q}_{21}^{(\text{c})}(k+1)\ \ \boldsymbol{Q}_{22}^{(\text{c})}(k+1)]$ is an orthogonal matrix; $\boldsymbol{R}_2^{(\text{c})}(k+1)$ is an orthogonal matrix; $\boldsymbol{\Sigma}_2^{(\text{c})}(k+1)$ is a diagonal matrix, whose diagonal entries are the singular values of $(\tilde{\boldsymbol{\Phi}}^{(\text{c})})^{-1/2}\tilde{\boldsymbol{A}}^{(\text{c})}(\hat{\tilde{\boldsymbol{r}}}^{(\text{c})})\boldsymbol{Q}_{12}^{(\text{c})}(k+1)$. Further, let us define a vector $\boldsymbol{x}_1(k+1)$ that satisfies a set of linear equations:

$$\boldsymbol{R}_1^{(\text{c})}(k+1)\boldsymbol{\Sigma}_1^{(\text{c})}(k+1)\boldsymbol{x}_1(k+1) = \boldsymbol{g}^{(\text{c})}(\hat{\boldsymbol{\eta}}(k)), \tag{82}$$

and define a vector $\boldsymbol{x}_2(k+1)$ that satisfies the linear relationship:

$$\begin{aligned}&\boldsymbol{\Sigma}_2^{(\text{c})}(k+1)(\boldsymbol{R}_2^{(\text{c})}(k+1))^{\text{T}}\boldsymbol{x}_2(k+1)\\&\quad= (\boldsymbol{Q}_{21}^{(\text{c})}(k+1))^{\text{T}}(\tilde{\boldsymbol{\Phi}}^{(\text{c})})^{-1/2}\begin{pmatrix}\tilde{\boldsymbol{b}}^{(\text{c})}(\hat{\tilde{\boldsymbol{r}}}^{(\text{c})}, \hat{\tilde{\boldsymbol{s}}}) - \tilde{\boldsymbol{A}}^{(\text{c})}(\hat{\tilde{\boldsymbol{r}}}^{(\text{c})})\\ \times\boldsymbol{Q}_{11}^{(\text{c})}(k+1)\boldsymbol{x}_1(k+1)\end{pmatrix}\end{aligned} \tag{83}$$

Then, the optimal solution of (75) is given by

$$\hat{\boldsymbol{\eta}}_{\text{opt}}(k+1) = \boldsymbol{Q}_{11}^{(\text{c})}(k+1)\boldsymbol{x}_1(k+1) + \boldsymbol{Q}_{12}^{(\text{c})}(k+1)\boldsymbol{x}_2(k+1) \tag{84}$$

The proof of Proposition 2 is shown in Appendix B. Certainly, when $\tilde{\boldsymbol{A}}^{(\text{c})}(\hat{\tilde{\boldsymbol{r}}}^{(\text{c})})$ has full column rank, the solution in Proposition 2 is consistent with that in Proposition 1. However, if this condition is not satisfied, for example, only a single calibration emitter is present, then only the solution in Proposition 2 can be applied.

Although the solution to problem (75) is an approximation of the optimal solution of the original problem (74), it incorporates $2M + 2N$ approximate linear equality constraints to improve the estimation performance. An intuitive update strategy is to choose the optimal solution (84) to be the $k+1$th iteration's value. However, this update strategy requires minor modification to avoid possible divergence problem. We would like to adopt the update procedure introduced in [29], which determines the current iteration's value using the linear combination of the solution to problem (75) and the estimation result in the last iteration. Besides, since the weighting matrix $\tilde{\boldsymbol{\Phi}}^{(\text{c})}$ is dependent on $\boldsymbol{\eta}$, it should also be updated at each iteration step.

The first stage of the proposed ICWLS method is formally summarized in Table 3.

The following remarks concern the presented algorithm described above.

Remark 5: If the optimization problem is non-convex, it is very crucial to choose a reasonable proper starting point to guarantee that the iterative algorithm converges to the global minimum of the optimization problem. For the proposed algorithm, we can exploit the prior measurement $\hat{\tilde{\boldsymbol{s}}}$ to form

$$\begin{cases}\boldsymbol{g}_1^{(\text{c})}(\hat{\boldsymbol{\eta}}(k)) = \left[-\frac{1}{2}\boldsymbol{\rho}_{11}^{\text{T}}\hat{\boldsymbol{\eta}}(k) \quad -\frac{1}{2}\boldsymbol{\rho}_{12}^{\text{T}}\hat{\boldsymbol{\eta}}(k) \quad \cdots \quad -\frac{1}{2}\boldsymbol{\rho}_{1M}^{\text{T}}\hat{\boldsymbol{\eta}}(k)\right]^{\text{T}}\\ \boldsymbol{g}_2^{(\text{c})}(\hat{\boldsymbol{\eta}}(k)) = \left[-\frac{1}{2}\boldsymbol{\rho}_{21}^{\text{T}}\hat{\boldsymbol{\eta}}(k) \quad -\frac{1}{2}\boldsymbol{\rho}_{22}^{\text{T}}\hat{\boldsymbol{\eta}}(k) \quad \cdots \quad -\frac{1}{2}\boldsymbol{\rho}_{2M}^{\text{T}}\hat{\boldsymbol{\eta}}(k)\right]^{\text{T}}\\ \boldsymbol{g}_3^{(\text{c})}(\hat{\boldsymbol{\eta}}(k)) = \left[||\boldsymbol{w}_1||_2^2 - \frac{1}{2}\boldsymbol{\rho}_{31}^{\text{T}}\hat{\boldsymbol{\eta}}(k) \quad ||\boldsymbol{w}_2||_2^2 - \frac{1}{2}\boldsymbol{\rho}_{32}^{\text{T}}\hat{\boldsymbol{\eta}}(k) \quad \cdots \quad ||\boldsymbol{w}_N||_2^2 - \frac{1}{2}\boldsymbol{\rho}_{3N}^{\text{T}}\hat{\boldsymbol{\eta}}(k)\right]^{\text{T}}\\ \boldsymbol{g}_4^{(\text{c})}(\hat{\boldsymbol{\eta}}(k)) = \left[2\boldsymbol{w}_1^{\text{T}}\dot{\boldsymbol{w}}_1 - \frac{1}{2}\boldsymbol{\rho}_{41}^{\text{T}}\hat{\boldsymbol{\eta}}(k) \quad 2\boldsymbol{w}_2^{\text{T}}\dot{\boldsymbol{w}}_2 - \frac{1}{2}\boldsymbol{\rho}_{42}^{\text{T}}\hat{\boldsymbol{\eta}}(k) \quad \cdots \quad 2\boldsymbol{w}_N^{\text{T}}\dot{\boldsymbol{w}}_N - \frac{1}{2}\boldsymbol{\rho}_{4N}^{\text{T}}\hat{\boldsymbol{\eta}}(k)\right]^{\text{T}}\end{cases} \tag{77}$$

$$\begin{cases}\boldsymbol{G}_i^{(\text{c})}(\hat{\boldsymbol{\eta}}(k)) = \left[\boldsymbol{\Omega}_{i1}\hat{\boldsymbol{\eta}}(k) + \frac{1}{2}\boldsymbol{\rho}_{i1} \quad \boldsymbol{\Omega}_{i2}\hat{\boldsymbol{\eta}}(k) + \frac{1}{2}\boldsymbol{\rho}_{i2} \quad \cdots \quad \boldsymbol{\Omega}_{iM}\hat{\boldsymbol{\eta}}(k) + \frac{1}{2}\boldsymbol{\rho}_{iM}\right] \quad (i = 1\ ,\ 2)\\ \boldsymbol{G}_j^{(\text{c})}(\hat{\boldsymbol{\eta}}(k)) = \left[\boldsymbol{\Omega}_{j1}\hat{\boldsymbol{\eta}}(k) + \frac{1}{2}\boldsymbol{\rho}_{j1} \quad \boldsymbol{\Omega}_{j2}\hat{\boldsymbol{\eta}}(k) + \frac{1}{2}\boldsymbol{\rho}_{j2} \quad \cdots \quad \boldsymbol{\Omega}_{jN}\hat{\boldsymbol{\eta}}(k) + \frac{1}{2}\boldsymbol{\rho}_{jN}\right] \quad (j = 3\ ,\ 4)\end{cases} \tag{78}$$

TABLE 3. Procedure of the first stage of the proposed ICWLS method.

Step 1: Define a convergence threshold $\tau > 0$ and find a proper initial guess $\hat{\boldsymbol{\eta}}(0)$.
Step 2: Compute the matrix $\widetilde{\boldsymbol{A}}^{(\mathrm{c})}(\hat{\bar{\boldsymbol{r}}}^{(\mathrm{c})})$ and the vector $\widetilde{\boldsymbol{b}}^{(\mathrm{c})}(\hat{\bar{\boldsymbol{r}}}^{(\mathrm{c})},\hat{\bar{\boldsymbol{s}}})$ from (71).
Step 3: Set the iteration counter $k := 0$ and compute the weighting matrix $\widetilde{\boldsymbol{\Phi}}^{(\mathrm{c})}$ based on (66), (68) and (73).
Step 4: Calculate the matrix $\boldsymbol{G}^{(\mathrm{c})}(\hat{\boldsymbol{\eta}}(k))$ and the vector $\boldsymbol{g}^{(\mathrm{c})}(\hat{\boldsymbol{\eta}}(k))$ according to (76)-(78).
Step 5: Perform the matrix SVD on $\boldsymbol{G}^{(\mathrm{c})}(\hat{\boldsymbol{\eta}}(k))$ to generate $\boldsymbol{Q}_{11}^{(\mathrm{c})}(k+1)$, $\boldsymbol{Q}_{12}^{(\mathrm{c})}(k+1)$, $\boldsymbol{\Sigma}_1^{(\mathrm{c})}(k+1)$ and $\boldsymbol{R}_1^{(\mathrm{c})}(k+1)$.
Step 6: Solve $\boldsymbol{x}_1(k+1)$ from the linear system (82).
Step 7: Conduct the matrix SVD on $(\widetilde{\boldsymbol{\Phi}}^{(\mathrm{c})})^{-1/2}\widetilde{\boldsymbol{A}}^{(\mathrm{c})}(\hat{\bar{\boldsymbol{r}}}^{(\mathrm{c})})\boldsymbol{Q}_{12}^{(\mathrm{c})}(k+1)$ to produce $\boldsymbol{Q}_{21}^{(\mathrm{c})}(k+1)$, $\boldsymbol{\Sigma}_2^{(\mathrm{c})}(k+1)$ and $\boldsymbol{R}_2^{(\mathrm{c})}(k+1)$.
Step 8: Solve the linear system (83) to get $\boldsymbol{x}_2(k+1)$.
Step 9: Compute the vector $\hat{\boldsymbol{\eta}}_{\mathrm{opt}}(k+1)$ using (84).
Step 10: Calculate $\hat{\boldsymbol{\eta}}(k+1) = w_1\hat{\boldsymbol{\eta}}(k) + w_2\hat{\boldsymbol{\eta}}_{\mathrm{opt}}(k+1)$, where $w_1 > 0$, $w_2 > 0$ and $w_1 + w_2 = 1$. If $\|\hat{\boldsymbol{\eta}}(k+1) - \hat{\boldsymbol{\eta}}(k)\|_2 \le \tau$, let $\hat{\boldsymbol{\eta}}_{\mathrm{f}} = \hat{\boldsymbol{\eta}}(k+1)$ and go to Step 12; otherwise go to Step 11.
Step 11: Increment the iteration counter $k := k+1$ and create the weighting matrix $\widetilde{\boldsymbol{\Phi}}^{(\mathrm{c})}$ by using (66), (68) and (73) and go to Step 4.
Step 12: Determine the final result by $\hat{\bar{\boldsymbol{s}}}_{\mathrm{f}} = [\boldsymbol{I}_{6M}\ \boldsymbol{O}_{6M\times(2M+2N)}]\hat{\boldsymbol{\eta}}_{\mathrm{f}}$ and stop the procedure.

the initial guess $\hat{\boldsymbol{\eta}}(0)$ in the following way:

$$\hat{\boldsymbol{\eta}}(0) = \boldsymbol{\psi}(\hat{\bar{\boldsymbol{s}}}) = [\hat{\bar{\boldsymbol{s}}}^{\mathrm{T}}(\boldsymbol{\psi}_1(\hat{\bar{\boldsymbol{s}}}))^{\mathrm{T}}(\boldsymbol{\psi}_2(\hat{\bar{\boldsymbol{s}}}))^{\mathrm{T}}(\boldsymbol{\psi}_3(\hat{\bar{\boldsymbol{s}}}))^{\mathrm{T}}(\boldsymbol{\psi}_4(\hat{\bar{\boldsymbol{s}}}))^{\mathrm{T}}]^{\mathrm{T}} \quad (85)$$

The simulation results in Section VIII reveal that this initial estimate is precise enough for global convergence.

Remark 6: It can be easily seen from step 10 that the updated value in the $k+1$th iteration is the linear combination of the solution to problem (75) and the estimation result in the kth iteration. Extensive simulation results indicate that as long as w_1 is not close to 1, the final estimation accuracy is not sensitive to the numerical value of w_1. We set $w_1 = w_2 = 0.5$ in the simulation section.

Remark 7: It is impossible to obtain the true weighting matrix $\tilde{\boldsymbol{\Phi}}^{(\mathrm{c})}$, although the algorithm updates this matrix at each iteration step. This is because the calculation of $\tilde{\boldsymbol{\Phi}}^{(\mathrm{c})}$ requires true measurement $\bar{\boldsymbol{r}}^{(\mathrm{c})}$, which is not available in practice. So we have to compute $\tilde{\boldsymbol{\Phi}}^{(\mathrm{c})}$ using $\hat{\bar{\boldsymbol{r}}}^{(\mathrm{c})}$ in place of $\bar{\boldsymbol{r}}^{(\mathrm{c})}$. Fortunately, plentiful simulation results show that the estimation accuracy is relatively insensitive to errors in the weighting matrix and the performance degradation is insignificant due to the approximation of the weighting matrix. This observation is consistent with the findings in [45]–[47].

B. PERFORMANCE ANALYSIS FOR STAGE-1

The aim of this subsection is to provide the theoretical performance analysis for the proposed iterative algorithm in stage-1. First, its convergence property is studied based on the optimality conditions in optimization theory. We prove that if the iterative algorithm converges, then it is able to converge to the optimal solution of the original CWLS problem (74). Next, the MSE expression of the proposed solution is derived by exploiting the first-order perturbation analysis. Moreover, the MSE is proved to achieve the corresponding CRB given in Subsection III.B at moderate error level before the thresholding effect occurs.

1) CONVERGENCE ANALYSIS FOR STAGE-1

Here, the convergence property of the algorithm is investigated. Notice that it is impossible to provide a strict proof as to whether the iteration procedure converges or not, because the original problem (74) is not convex. Therefore, we have to simplify the analysis and prove that if the iterative algorithm converges, then it must converge to the minimizer of problem (74).

The convergence analysis begins with the second-order sufficient condition for the optimal solution to (74). It is formally described as follows:

Lemma 1: Suppose that $\hat{\boldsymbol{\eta}}_{\mathrm{opt}}$, $\{\lambda_{1m}^{(\mathrm{c})}\}_{1\le m\le M}$, $\{\lambda_{2m}^{(\mathrm{c})}\}_{1\le m\le M}$, $\{\lambda_{3n}^{(\mathrm{c})}\}_{1\le n\le N}$ and $\{\lambda_{4n}^{(\mathrm{c})}\}_{1\le n\le N}$ satisfy

$$\begin{aligned}
&(\tilde{\boldsymbol{A}}^{(\mathrm{c})}(\hat{\bar{\boldsymbol{r}}}^{(\mathrm{c})}))^{\mathrm{T}}(\tilde{\boldsymbol{\Phi}}^{(\mathrm{c})})^{-1}(\tilde{\boldsymbol{A}}^{(\mathrm{c})}(\hat{\bar{\boldsymbol{r}}}^{(\mathrm{c})})\hat{\boldsymbol{\eta}}_{\mathrm{opt}} - \tilde{\boldsymbol{b}}^{(\mathrm{c})}(\hat{\bar{\boldsymbol{r}}}^{(\mathrm{c})},\hat{\bar{\boldsymbol{s}}}))\\
&\quad + \sum_{m=1}^{M}\frac{\lambda_{1m}^{(\mathrm{c})}}{2}\left(\boldsymbol{\Omega}_{1m}\hat{\boldsymbol{\eta}}_{\mathrm{opt}} + \frac{1}{2}\boldsymbol{\rho}_{1m}\right)\\
&\quad + \sum_{m=1}^{M}\frac{\lambda_{2m}^{(\mathrm{c})}}{2}\left(\boldsymbol{\Omega}_{2m}\hat{\boldsymbol{\eta}}_{\mathrm{opt}} + \frac{1}{2}\boldsymbol{\rho}_{2m}\right)\\
&\quad + \sum_{n=1}^{N}\frac{\lambda_{3n}^{(\mathrm{c})}}{2}\left(\boldsymbol{\Omega}_{3n}\hat{\boldsymbol{\eta}}_{\mathrm{opt}} + \frac{1}{2}\boldsymbol{\rho}_{3n}\right)\\
&\quad + \sum_{n=1}^{N}\frac{\lambda_{4n}^{(\mathrm{c})}}{2}\left(\boldsymbol{\Omega}_{4n}\hat{\boldsymbol{\eta}}_{\mathrm{opt}} + \frac{1}{2}\boldsymbol{\rho}_{4n}\right)\\
&= \boldsymbol{O}_{(8M+2N)\times 1} \qquad (86)
\end{aligned}$$

$$\begin{cases} \hat{\boldsymbol{\eta}}_{\text{opt}}^{\text{T}}\boldsymbol{\Omega}_{1m}\hat{\boldsymbol{\eta}}_{\text{opt}} + \boldsymbol{\rho}_{1m}^{\text{T}}\hat{\boldsymbol{\eta}}_{\text{opt}} = 0 \\ \hat{\boldsymbol{\eta}}_{\text{opt}}^{\text{T}}\boldsymbol{\Omega}_{2m}\hat{\boldsymbol{\eta}}_{\text{opt}} + \boldsymbol{\rho}_{2m}^{\text{T}}\hat{\boldsymbol{\eta}}_{\text{opt}} = 0 \end{cases} \quad (1 \le m \le M) \tag{87}$$

$$\begin{cases} \hat{\boldsymbol{\eta}}_{\text{opt}}^{\text{T}}\boldsymbol{\Omega}_{3n}\hat{\boldsymbol{\eta}}_{\text{opt}} + \boldsymbol{\rho}_{3n}^{\text{T}}\hat{\boldsymbol{\eta}}_{\text{opt}} = ||\boldsymbol{w}_n||_2^2 \\ \hat{\boldsymbol{\eta}}_{\text{opt}}^{\text{T}}\boldsymbol{\Omega}_{4n}\hat{\boldsymbol{\eta}}_{\text{opt}} + \boldsymbol{\rho}_{4n}^{\text{T}}\hat{\boldsymbol{\eta}}_{\text{opt}} = 2\boldsymbol{w}_n^{\text{T}}\dot{\boldsymbol{w}}_n \end{cases} \quad (1 \le n \le N) \tag{88}$$

Moreover, for any vector $\boldsymbol{y}$ belonging to the null space of $(\boldsymbol{G}^{(\text{c})}(\hat{\boldsymbol{\eta}}_{\text{opt}}))^{\text{T}}$ we have

$$\boldsymbol{y}^{\text{T}}\left(\begin{array}{c}(\tilde{\boldsymbol{A}}^{(\text{c})}(\hat{\bar{\boldsymbol{r}}}^{(\text{c})}))^{\text{T}}(\tilde{\boldsymbol{\Phi}}^{(\text{c})})^{-1}\tilde{\boldsymbol{A}}^{(\text{c})}(\hat{\bar{\boldsymbol{r}}}^{(\text{c})}) + \sum_{m=1}^{M}\frac{\lambda_{1m}^{(\text{c})}}{2}\boldsymbol{\Omega}_{1m} \\ + \sum_{m=1}^{M}\frac{\lambda_{2m}^{(\text{c})}}{2}\boldsymbol{\Omega}_{2m} + \sum_{n=1}^{N}\frac{\lambda_{3n}^{(\text{c})}}{2}\boldsymbol{\Omega}_{3n} + \sum_{n=1}^{N}\frac{\lambda_{4n}^{(\text{c})}}{2}\boldsymbol{\Omega}_{4n}\end{array}\right)\boldsymbol{y} > 0, \tag{89}$$

Then, the vector $\hat{\boldsymbol{\eta}}_{\text{opt}}$ is the strictly optimal solution to the CWLS problem (74).

The proof of Lemma 1 is given in [48]. The scalars $\{\lambda_{1m}^{(\text{c})}\}_{1\le m\le M}$, $\{\lambda_{2m}^{(\text{c})}\}_{1\le m\le M}$, $\{\lambda_{3n}^{(\text{c})}\}_{1\le n\le N}$ and $\{\lambda_{4n}^{(\text{c})}\}_{1\le n\le N}$ are commonly referred to as Lagrange multipliers. Subsequently, we continue describing the first-order necessary condition for the minimizer of problem (75).

Lemma 2: Assuming that the optimal solution to problem (75) is denoted by $\hat{\boldsymbol{\eta}}_{\text{opt}}(k+1)$, there exist $\{\lambda_{1m}^{(\text{c})}(k+1)\}_{1\le m\le M}$, $\{\lambda_{2m}^{(\text{c})}(k+1)\}_{1\le m\le M}$, $\{\lambda_{3n}^{(\text{c})}(k+1)\}_{1\le n\le N}$ and $\{\lambda_{4n}^{(\text{c})}(k+1)\}_{1\le n\le N}$ such that

$$\begin{aligned}&(\tilde{\boldsymbol{A}}^{(\text{c})}(\hat{\bar{\boldsymbol{r}}}^{(\text{c})}))^{\text{T}}(\tilde{\boldsymbol{\Phi}}^{(\text{c})})^{-1}(\tilde{\boldsymbol{A}}^{(\text{c})}(\hat{\bar{\boldsymbol{r}}}^{(\text{c})})\hat{\boldsymbol{\eta}}_{\text{opt}}(k+1) - \tilde{\boldsymbol{b}}^{(\text{c})}(\hat{\bar{\boldsymbol{r}}}^{(\text{c})}, \hat{\bar{\boldsymbol{s}}})) \\ &\quad + \sum_{m=1}^{M}\frac{\lambda_{1m}^{(\text{c})}(k+1)}{2}\left(\boldsymbol{\Omega}_{1m}\hat{\boldsymbol{\eta}}(k) + \frac{1}{2}\boldsymbol{\rho}_{1m}\right) \\ &\quad + \sum_{m=1}^{M}\frac{\lambda_{2m}^{(\text{c})}(k+1)}{2}\left(\boldsymbol{\Omega}_{2m}\hat{\boldsymbol{\eta}}(k) + \frac{1}{2}\boldsymbol{\rho}_{2m}\right) \\ &\quad + \sum_{n=1}^{N}\frac{\lambda_{3n}^{(\text{c})}(k+1)}{2}\left(\boldsymbol{\Omega}_{3n}\hat{\boldsymbol{\eta}}(k) + \frac{1}{2}\boldsymbol{\rho}_{3n}\right) \\ &\quad + \sum_{n=1}^{N}\frac{\lambda_{4n}^{(\text{c})}(k+1)}{2}\left(\boldsymbol{\Omega}_{4n}\hat{\boldsymbol{\eta}}(k) + \frac{1}{2}\boldsymbol{\rho}_{4n}\right) \\ &= \boldsymbol{O}_{(8M+2N)\times 1}\end{aligned} \tag{90}$$

The proof of Lemma 2 can also be found in [48]. Moreover, $\{\lambda_{1m}^{(\text{c})}(k+1)\}_{1\le m\le M}$, $\{\lambda_{2m}^{(\text{c})}(k+1)\}_{1\le m\le M}$, $\{\lambda_{3n}^{(\text{c})}(k+1)\}_{1\le n\le N}$ and $\{\lambda_{4n}^{(\text{c})}(k+1)\}_{1\le n\le N}$ are also called Lagrange multipliers. We are now ready to prove that if the iteration sequence $\{\hat{\boldsymbol{\eta}}_{\text{opt}}(k+1)\}_{0\le k\le+\infty}$ converges, it will converge to $\hat{\boldsymbol{\eta}}_{\text{opt}}$, which is the strictly optimal solution to the CWLS problem (74). For this purpose, three propositions are presented in turn.

Proposition 3: If the sequence $\{\hat{\boldsymbol{\eta}}(k+1)\}_{0\le k\le+\infty}$ converges to $\hat{\boldsymbol{\eta}}_{\text{f}}$, then the sequence $\{\hat{\boldsymbol{\eta}}_{\text{opt}}(k+1)\}_{0\le k\le+\infty}$ also converges to $\hat{\boldsymbol{\eta}}_{\text{f}}$.

Proof: From step 10 in Table 3 we have

$$\begin{aligned}\lim_{k\to+\infty}\hat{\boldsymbol{\eta}}_{\text{opt}}(k+1) &= \frac{1}{w_2}\lim_{k\to+\infty}\hat{\boldsymbol{\eta}}(k+1) - \frac{w_1}{w_2}\lim_{k\to+\infty}\hat{\boldsymbol{\eta}}(k) \\ &= \frac{1-w_1}{w_2}\hat{\boldsymbol{\eta}}_{\text{f}} = \hat{\boldsymbol{\eta}}_{\text{f}}\end{aligned} \tag{91}$$

which completes the proof.

Proposition 4: If the sequence $\{\hat{\boldsymbol{\eta}}(k+1)\}_{0\le k\le+\infty}$ converges, then the sequences $\{\lambda_{1m}^{(\text{c})}(k+1)\}_{1\le m\le M}$, $\{\lambda_{2m}^{(\text{c})}(k+1)\}_{1\le m\le M}$, $\{\lambda_{3n}^{(\text{c})}(k+1)\}_{1\le n\le N}$ and $\{\lambda_{4n}^{(\text{c})}(k+1)\}_{1\le n\le N}$ also converge for arbitrary $1\le m\le M$ and $1\le n\le N$.

The proof of Proposition 4 is provided in Appendix C.

Proposition 5: If the sequence $\{\hat{\boldsymbol{\eta}}(k+1)\}_{0\le k\le+\infty}$ converges to $\hat{\boldsymbol{\eta}}_{\text{f}}$, then $\hat{\boldsymbol{\eta}}_{\text{f}} = \hat{\boldsymbol{\eta}}_{\text{opt}}$ is the strictly optimal solution to the CWLS problem (74).

Appendix D shows the proof of Proposition 5, which reveals that if the proposed iterative algorithm converges, then it can provide the optimal solution for problem (74). It should be noted, however, that there is no guarantee at all that the iterative algorithm always converges. Fortunately, the simulation results in Section VIII demonstrate that in most cases the convergence can be achieved after a few iterations.

2) ESTIMATION MSE FOR STAGE-1

The aim of this subsection is to derive the MSE expression of the proposed solution for stage-1. For this purpose, the first-order perturbation analysis is applied to get the linear relation between the estimation errors and the measurement errors, which consist of $\bar{\boldsymbol{\xi}}$ and $\bar{\boldsymbol{\varepsilon}}^{(\text{c})}$.

Assume that the iterative algorithm described above converges to $\hat{\boldsymbol{\eta}}_{\text{f}}$, which is also the minimizer for (74). According to step 12 in Table 3, the final estimate for sensor locations is given by $\hat{\bar{\boldsymbol{s}}}_{\text{f}} = [\boldsymbol{I}_{6M}\ \boldsymbol{O}_{6M\times(2M+2N)}]\hat{\boldsymbol{\eta}}_{\text{f}}$. Therefore, in order to get the analytical expression for the MSE of $\hat{\bar{\boldsymbol{s}}}_{\text{f}}$, it is necessary to derive the theoretical MSE of $\hat{\boldsymbol{\eta}}_{\text{f}}$ first. Let the estimation error in $\hat{\boldsymbol{\eta}}_{\text{f}}$ be $\Delta\boldsymbol{\eta}_{\text{f}}$. From the theoretical frame of the first-order error analysis, $\Delta\boldsymbol{\eta}_{\text{f}}$ must be the optimal solution of the following constrained optimization problem [28]–[see (92), as shown at the bottom of the next page.]

Assuming the matrix SVD of $\boldsymbol{G}^{(\text{c})}(\boldsymbol{\eta})$ is given by

$$\begin{aligned}\boldsymbol{G}^{(\text{c})}(\boldsymbol{\eta}) &= [\boldsymbol{Q}_{11}^{(\text{c})}\ \boldsymbol{Q}_{12}^{(\text{c})}]\begin{bmatrix}\boldsymbol{\Sigma}_1^{(\text{c})} \\ \boldsymbol{O}_{6M\times(2M+2N)}\end{bmatrix}\boldsymbol{R}_1^{(\text{c})\text{T}} \\ &= \boldsymbol{Q}_{11}^{(\text{c})}\boldsymbol{\Sigma}_1^{(\text{c})}\boldsymbol{R}_1^{(\text{c})\text{T}},\end{aligned} \tag{93}$$

$\Delta\boldsymbol{\eta}_{\text{f}}$ must lie in the range space of $\boldsymbol{Q}_{12}^{(\text{c})}$, which is orthogonal to that of $\boldsymbol{G}^{(\text{c})}(\boldsymbol{\eta})$. As a consequence, we can express $\Delta\boldsymbol{\eta}_{\text{f}}$ as

$$\begin{aligned}\Delta\boldsymbol{\eta}_{\text{f}} = \boldsymbol{Q}_{12}^{(\text{c})}&(\boldsymbol{Q}_{12}^{(\text{c})\text{T}}(\tilde{\boldsymbol{A}}^{(\text{c})}(\bar{\boldsymbol{r}}^{(\text{c})}))^{\text{T}}(\tilde{\boldsymbol{\Phi}}^{(\text{c})})^{-1}\tilde{\boldsymbol{A}}^{(\text{c})}(\bar{\boldsymbol{r}}^{(\text{c})})\boldsymbol{Q}_{12}^{(\text{c})})^{-1} \\ &\times\boldsymbol{Q}_{12}^{(\text{c})\text{T}}(\tilde{\boldsymbol{A}}^{(\text{c})}(\bar{\boldsymbol{r}}^{(\text{c})}))^{\text{T}}(\tilde{\boldsymbol{\Phi}}^{(\text{c})})^{-1}\tilde{\boldsymbol{C}}^{(\text{c})}(\boldsymbol{\eta}, \bar{\boldsymbol{r}}^{(\text{c})})\begin{bmatrix}\bar{\boldsymbol{\varepsilon}}^{(\text{c})} \\ \bar{\boldsymbol{\xi}}\end{bmatrix}\end{aligned} \tag{94}$$

It can be observed from (94) that $\hat{\boldsymbol{\eta}}_{\text{f}}$ is an approximately unbiased estimate of $\boldsymbol{\eta}$ and, moreover, the estimation MSE of $\hat{\boldsymbol{\eta}}_{\text{f}}$ is given by

$$\text{MSE}(\hat{\boldsymbol{\eta}}_{\text{f}}) = \boldsymbol{Q}_{12}^{(\text{c})}(\boldsymbol{Q}_{12}^{(\text{c})\text{T}}\tilde{\boldsymbol{P}}^{(\text{c})}(\bar{\boldsymbol{r}}^{(\text{c})})\boldsymbol{Q}_{12}^{(\text{c})})^{-1}\boldsymbol{Q}_{12}^{(\text{c})\text{T}} \tag{95}$$

where $\tilde{\boldsymbol{P}}^{(\mathrm{c})}(\bar{\boldsymbol{r}}^{(\mathrm{c})}) = (\tilde{\boldsymbol{A}}^{(\mathrm{c})}(\bar{\boldsymbol{r}}^{(\mathrm{c})}))^{\mathrm{T}}(\tilde{\boldsymbol{\Phi}}^{(\mathrm{c})})^{-1}\tilde{\boldsymbol{A}}^{(\mathrm{c})}(\bar{\boldsymbol{r}}^{(\mathrm{c})})$.

Before proceeding, three remarks are concluded in order.

Remark 8: Since $\boldsymbol{Q}_{12}^{(\mathrm{c})\mathrm{T}}\boldsymbol{Q}_{11}^{(\mathrm{c})} = \boldsymbol{O}$, it follows from (93) and (95) that $\mathbf{MSE}(\hat{\boldsymbol{\eta}}_{\mathrm{f}})\boldsymbol{G}^{(\mathrm{c})}(\boldsymbol{\eta}) = \boldsymbol{O}$, which means that $\mathbf{MSE}(\hat{\boldsymbol{\eta}}_{\mathrm{f}})$ is singular or rank deficient. This property results from the equation constraint in (92).

Remark 9: According to (59)-(63), it can be verified that $\boldsymbol{\Psi}(\bar{\boldsymbol{s}})$ is full column rank and the relation $(\boldsymbol{\Psi}(\bar{\boldsymbol{s}}))^{\mathrm{T}}\boldsymbol{G}^{(\mathrm{c})}(\boldsymbol{\eta}) = \boldsymbol{O}$ holds. Moreover, $\boldsymbol{\Psi}(\bar{\boldsymbol{s}})$ and $\boldsymbol{Q}_{12}^{(\mathrm{c})}$ have the same number of columns. Therefore, we have $\mathrm{range}\{\boldsymbol{\Psi}(\bar{\boldsymbol{s}})\} = \mathrm{range}\{\boldsymbol{Q}_{12}^{(\mathrm{c})}\}$.

Remark 10: Combining (71) and (73) yields an alternative expression of $\tilde{\boldsymbol{P}}^{(\mathrm{c})}(\bar{\boldsymbol{r}}^{(\mathrm{c})})$ as follows:

$$\begin{aligned}\tilde{\boldsymbol{P}}^{(\mathrm{c})}(\bar{\boldsymbol{r}}^{(\mathrm{c})}) = {} & (\bar{\boldsymbol{A}}^{(\mathrm{c})}(\bar{\boldsymbol{r}}^{(\mathrm{c})}))^{\mathrm{T}}(\bar{\boldsymbol{C}}^{(\mathrm{c})}(\boldsymbol{\eta},\bar{\boldsymbol{r}}^{(\mathrm{c})}))^{-\mathrm{T}}(\bar{\boldsymbol{E}}_{\mathrm{A}}^{(\mathrm{c})})^{-1} \\ & \times (\bar{\boldsymbol{C}}^{(\mathrm{c})}(\boldsymbol{\eta},\bar{\boldsymbol{r}}^{(\mathrm{c})}))^{-1}\bar{\boldsymbol{A}}^{(\mathrm{c})}(\bar{\boldsymbol{r}}^{(\mathrm{c})}) + \mathrm{blkdiag}[\bar{\boldsymbol{E}}_{\mathrm{B}}^{-1} \ \ \boldsymbol{O}]\end{aligned} \tag{96}$$

It is noteworthy that (96) is useful in the proof of Proposition 6 given below.

Next, we derive the theoretical MSE of the estimate $\hat{\bar{\boldsymbol{s}}}_{\mathrm{f}}$. Assuming that the estimation error in $\hat{\bar{\boldsymbol{s}}}_{\mathrm{f}}$ is defined as $\Delta\bar{\boldsymbol{s}}_{\mathrm{f}}$, it is straightforward to check that $\Delta\bar{\boldsymbol{s}}_{\mathrm{f}} = [\boldsymbol{I}_{6M} \ \boldsymbol{O}_{6M\times(2M+2N)}]\Delta\boldsymbol{\eta}_{\mathrm{f}}$, which immediately gives

$$\begin{aligned}\mathbf{MSE}(\hat{\bar{\boldsymbol{s}}}_{\mathrm{f}}) = {} & [\boldsymbol{I}_{6M} \ \boldsymbol{O}_{6M\times(2M+2N)}]\boldsymbol{Q}_{12}^{(\mathrm{c})} \\ & \times (\boldsymbol{Q}_{12}^{(\mathrm{c})\mathrm{T}}\tilde{\boldsymbol{P}}^{(\mathrm{c})}(\bar{\boldsymbol{r}}^{(\mathrm{c})})\boldsymbol{Q}_{12}^{(\mathrm{c})})^{-1}\boldsymbol{Q}_{12}^{(\mathrm{c})\mathrm{T}}\begin{bmatrix}\boldsymbol{I}_{6M} \\ \boldsymbol{O}_{(2M+2N)\times 6M}\end{bmatrix}\end{aligned} \tag{97}$$

Notice that the solution $\hat{\bar{\boldsymbol{s}}}_{\mathrm{f}}$ is an asymptotically efficient estimate of $\bar{\boldsymbol{s}}$ because it can achieve the associated CRB accuracy under moderate noise level, as shown below.

Proposition 6: Under the first-order approximation, the relation $\mathbf{MSE}(\hat{\bar{\boldsymbol{s}}}_{\mathrm{f}}) = \mathbf{CRB}_{\mathrm{o}}(\bar{\boldsymbol{s}})$ holds.

The proof of Proposition 6 is provided in Appendix E, which reveals that the sensor location estimate obtained in the first stage is asymptotically optimal. The estimator developed in the second stage will exploit the estimation result from stage-1.

C. STAGE-2 OF THE PROPOSED METHOD

In the second phase, we combine the measurement vector $\hat{\bar{\boldsymbol{r}}}$ with the estimate $\hat{\bar{\boldsymbol{s}}}_{\mathrm{f}}$ provided in the first stage to perform multiple-target cooperative positioning. Besides, the sensor location is further refined in comparison with the estimate $\hat{\bar{\boldsymbol{s}}}_{\mathrm{f}}$. Similar to the first stage, an alternative ICWLS algorithm is proposed, which is also asymptotically efficient under Gaussian noise assumption.

1) OPTIMIZATION MODEL FOR MULTIPLE-TARGET COOPERATIVE LOCALIZATION

It is easy to see that the functional forms of $\bar{\boldsymbol{A}}(\cdot,\cdot)$ and $\bar{\boldsymbol{b}}(\cdot,\cdot)$ in (38) are known, but the values of $\bar{\boldsymbol{r}}$ and $\bar{\boldsymbol{s}}$ can not be obtained accurately because only their noisy values (i.e., $\hat{\bar{\boldsymbol{r}}}$ and $\hat{\bar{\boldsymbol{s}}}_{\mathrm{f}}$) are available. To formulate the optimization model for localization, it is necessary to first introduce the following error vector

$$\bar{\boldsymbol{\delta}} = \bar{\boldsymbol{b}}(\hat{\bar{\boldsymbol{r}}},\hat{\bar{\boldsymbol{s}}}_{\mathrm{f}}) - \bar{\boldsymbol{A}}(\hat{\bar{\boldsymbol{r}}},\hat{\bar{\boldsymbol{s}}}_{\mathrm{f}})\bar{\boldsymbol{t}} \tag{98}$$

Applying a first-order Taylor series expansion of $\bar{\boldsymbol{b}}(\hat{\bar{\boldsymbol{r}}},\hat{\bar{\boldsymbol{s}}}_{\mathrm{f}})$ and $\bar{\boldsymbol{A}}(\hat{\bar{\boldsymbol{r}}},\hat{\bar{\boldsymbol{s}}}_{\mathrm{f}})$ around the true values $\bar{\boldsymbol{r}}$ and $\bar{\boldsymbol{s}}$ yields

$$\begin{cases}\bar{\boldsymbol{b}}(\hat{\bar{\boldsymbol{r}}},\hat{\bar{\boldsymbol{s}}}_{\mathrm{f}}) \approx \bar{\boldsymbol{b}}(\bar{\boldsymbol{r}},\bar{\boldsymbol{s}}) + \bar{\boldsymbol{B}}_1(\bar{\boldsymbol{r}},\bar{\boldsymbol{s}})\bar{\boldsymbol{\varepsilon}} + \bar{\boldsymbol{B}}_2(\bar{\boldsymbol{r}},\bar{\boldsymbol{s}})\Delta\bar{\boldsymbol{s}}_{\mathrm{f}} \\ \bar{\boldsymbol{A}}(\hat{\bar{\boldsymbol{r}}},\hat{\bar{\boldsymbol{s}}}_{\mathrm{f}}) \approx \bar{\boldsymbol{A}}(\bar{\boldsymbol{r}},\bar{\boldsymbol{s}}) + \sum_{j=1}^{2D(M-1)}\langle\bar{\boldsymbol{\varepsilon}}\rangle_j\dot{\bar{\boldsymbol{A}}}_{1j}(\bar{\boldsymbol{r}},\bar{\boldsymbol{s}}) \\ \quad + \sum_{j=1}^{6M}\langle\Delta\bar{\boldsymbol{s}}_{\mathrm{f}}\rangle_j\dot{\bar{\boldsymbol{A}}}_{2j}(\bar{\boldsymbol{r}},\bar{\boldsymbol{s}})\end{cases} \tag{99}$$

where

$$\begin{cases}\bar{\boldsymbol{B}}_1(\bar{\boldsymbol{r}},\bar{\boldsymbol{s}}) = \dfrac{\partial\bar{\boldsymbol{b}}(\bar{\boldsymbol{r}},\bar{\boldsymbol{s}})}{\partial\bar{\boldsymbol{r}}^{\mathrm{T}}} \\ = \mathrm{blkdiag}[\boldsymbol{B}_1(\bar{\boldsymbol{r}}_1,\bar{\boldsymbol{s}}) \ \boldsymbol{B}_1(\bar{\boldsymbol{r}}_2,\bar{\boldsymbol{s}}) \ \cdots \ \boldsymbol{B}_1(\bar{\boldsymbol{r}}_D,\bar{\boldsymbol{s}})] \\ \bar{\boldsymbol{B}}_2(\bar{\boldsymbol{r}},\bar{\boldsymbol{s}}) = \dfrac{\partial\bar{\boldsymbol{b}}(\bar{\boldsymbol{r}},\bar{\boldsymbol{s}})}{\partial\bar{\boldsymbol{s}}^{\mathrm{T}}} \\ = [(\boldsymbol{B}_2(\bar{\boldsymbol{r}}_1,\bar{\boldsymbol{s}}))^{\mathrm{T}} \ (\boldsymbol{B}_2(\bar{\boldsymbol{r}}_2,\bar{\boldsymbol{s}}))^{\mathrm{T}} \ \cdots \ (\boldsymbol{B}_2(\bar{\boldsymbol{r}}_D,\bar{\boldsymbol{s}}))^{\mathrm{T}}]^{\mathrm{T}} \\ \dot{\bar{\boldsymbol{A}}}_{1j}(\bar{\boldsymbol{r}},\bar{\boldsymbol{s}}) = \dfrac{\partial\bar{\boldsymbol{A}}(\bar{\boldsymbol{r}},\bar{\boldsymbol{s}})}{\partial\langle\bar{\boldsymbol{r}}\rangle_j} \\ = (\boldsymbol{i}_D^{(d_j)}\boldsymbol{i}_D^{(d_j)\mathrm{T}}) \otimes \dot{\boldsymbol{A}}_{1,j-2(d_j-1)(M-1)}(\bar{\boldsymbol{r}}_{d_j},\bar{\boldsymbol{s}}) \\ \dot{\bar{\boldsymbol{A}}}_{2j}(\bar{\boldsymbol{r}},\bar{\boldsymbol{s}}) = \dfrac{\partial\bar{\boldsymbol{A}}(\bar{\boldsymbol{r}},\bar{\boldsymbol{s}})}{\partial\langle\bar{\boldsymbol{s}}\rangle_j} \\ = \mathrm{blkdiag}[\dot{\boldsymbol{A}}_{2j}(\bar{\boldsymbol{r}}_1,\bar{\boldsymbol{s}}) \ \dot{\boldsymbol{A}}_{2j}(\bar{\boldsymbol{r}}_2,\bar{\boldsymbol{s}}) \ \cdots \ \dot{\boldsymbol{A}}_{2j}(\bar{\boldsymbol{r}}_D,\bar{\boldsymbol{s}})]\end{cases} \tag{100}$$

in which $\boldsymbol{B}_1(\bar{\boldsymbol{r}}_d,\bar{\boldsymbol{s}}) = \frac{\partial\boldsymbol{b}(\bar{\boldsymbol{r}}_d,\bar{\boldsymbol{s}})}{\partial\bar{\boldsymbol{r}}_d^{\mathrm{T}}}$, $\boldsymbol{B}_2(\bar{\boldsymbol{r}}_d,\bar{\boldsymbol{s}}) = \frac{\partial\boldsymbol{b}(\bar{\boldsymbol{r}}_d,\bar{\boldsymbol{s}})}{\partial\bar{\boldsymbol{s}}^{\mathrm{T}}}$, $\dot{\boldsymbol{A}}_{1j}(\bar{\boldsymbol{r}}_d,\bar{\boldsymbol{s}}) = \frac{\partial\boldsymbol{A}(\bar{\boldsymbol{r}}_d,\bar{\boldsymbol{s}})}{\partial\langle\bar{\boldsymbol{r}}_d\rangle_j}$, $\dot{\boldsymbol{A}}_{2j}(\bar{\boldsymbol{r}}_d,\bar{\boldsymbol{s}}) = \frac{\partial\boldsymbol{A}(\bar{\boldsymbol{r}}_d,\bar{\boldsymbol{s}})}{\partial\langle\bar{\boldsymbol{s}}\rangle_j}$ and $d_j = \left\lceil\frac{j}{2(M-1)}\right\rceil$. Putting (99) back into (98) produces

$$\bar{\boldsymbol{\delta}} \approx \bar{\boldsymbol{C}}_1(\bar{\boldsymbol{t}},\bar{\boldsymbol{r}},\bar{\boldsymbol{s}})\bar{\boldsymbol{\varepsilon}} + \bar{\boldsymbol{C}}_2(\bar{\boldsymbol{t}},\bar{\boldsymbol{r}},\bar{\boldsymbol{s}})\Delta\bar{\boldsymbol{s}}_{\mathrm{f}} \tag{101}$$

where

$$\begin{aligned}&\bar{\boldsymbol{C}}_1(\bar{\boldsymbol{t}},\bar{\boldsymbol{r}},\bar{\boldsymbol{s}}) \\ &\quad = \bar{\boldsymbol{B}}_1(\bar{\boldsymbol{r}},\bar{\boldsymbol{s}}) \\ &\qquad - [\dot{\bar{\boldsymbol{A}}}_{11}(\bar{\boldsymbol{r}},\bar{\boldsymbol{s}})\bar{\boldsymbol{t}} \ \dot{\bar{\boldsymbol{A}}}_{12}(\bar{\boldsymbol{r}},\bar{\boldsymbol{s}})\bar{\boldsymbol{t}} \ \cdots \ \dot{\bar{\boldsymbol{A}}}_{1,2D(M-1)}(\bar{\boldsymbol{r}},\bar{\boldsymbol{s}})\bar{\boldsymbol{t}}] \\ &\bar{\boldsymbol{C}}_2(\bar{\boldsymbol{t}},\bar{\boldsymbol{r}},\bar{\boldsymbol{s}}) \\ &\quad = \bar{\boldsymbol{B}}_2(\bar{\boldsymbol{r}},\bar{\boldsymbol{s}})\end{aligned} \tag{102}$$

$$\begin{cases}\min\limits_{\Delta\boldsymbol{\eta}\in R^{(8M+2N)\times 1}} \left(\tilde{\boldsymbol{A}}^{(\mathrm{c})}(\bar{\boldsymbol{r}}^{(\mathrm{c})})\Delta\boldsymbol{\eta} - \tilde{\boldsymbol{C}}^{(\mathrm{c})}(\boldsymbol{\eta},\bar{\boldsymbol{r}}^{(\mathrm{c})})\begin{bmatrix}\bar{\boldsymbol{\varepsilon}}^{(\mathrm{c})} \\ \bar{\boldsymbol{\xi}}\end{bmatrix}\right)^{\mathrm{T}}(\tilde{\boldsymbol{\Phi}}^{(\mathrm{c})})^{-1}\left(\tilde{\boldsymbol{A}}^{(\mathrm{c})}(\bar{\boldsymbol{r}}^{(\mathrm{c})})\Delta\boldsymbol{\eta} - \tilde{\boldsymbol{C}}^{(\mathrm{c})}(\boldsymbol{\eta},\bar{\boldsymbol{r}}^{(\mathrm{c})})\begin{bmatrix}\bar{\boldsymbol{\varepsilon}}^{(\mathrm{c})} \\ \bar{\boldsymbol{\xi}}\end{bmatrix}\right) \\ \text{s.t. } (\boldsymbol{G}^{(\mathrm{c})}(\boldsymbol{\eta}))^{\mathrm{T}}\Delta\boldsymbol{\eta} = \boldsymbol{O}_{(2M+2N)\times 1}\end{cases} \tag{92}$$

$$-[\dot{\bar{A}}_{21}(\bar{r},\bar{s})\bar{t}\ \dot{\bar{A}}_{22}(\bar{r},\bar{s})\bar{t}\ \cdots\ \dot{\bar{A}}_{2,6M}(\bar{r},\bar{s})\bar{t}] \quad (103)$$

It is clear from (101) that $\bar{\delta}$ is approximately Gaussian distributed with zero mean and the covariance matrix

$$\bar{\Phi} = \bar{C}_1(\bar{t},\bar{r},\bar{s})\bar{E}_{\mathrm{A}}(\bar{C}_1(\bar{t},\bar{r},\bar{s}))^{\mathrm{T}} + \bar{C}_2(\bar{t},\bar{r},\bar{s})\cdot\mathbf{MSE}(\hat{\bar{s}}_{\mathrm{f}})\cdot(\bar{C}_2(\bar{t},\bar{r},\bar{s}))^{\mathrm{T}} \quad (104)$$

To delay the noise threshold before performance deviates suddenly from the CRB, the joint estimation of $\bar{u}$ and $\bar{s}$ should be performed [35, 49]. For this purpose, we need to introduce an augmented parameter vector as

$$\tilde{t} = \tilde{h}(\bar{u},\bar{s}) = \begin{bmatrix}\bar{t}\\ \bar{s}\end{bmatrix} = \begin{bmatrix}\bar{h}(\bar{u},\bar{s})\\ \bar{s}\end{bmatrix} \quad (105)$$

Then, from (98) and (104), the criterion function with respect to $\tilde{t}$ can be expressed as

$$J(\tilde{t}) = (\tilde{b}(\hat{\bar{r}},\hat{\bar{s}}_{\mathrm{f}}) - \tilde{A}(\hat{\bar{r}},\hat{\bar{s}}_{\mathrm{f}})\tilde{t})^{\mathrm{T}}\tilde{\Phi}^{-1}(\tilde{b}(\hat{\bar{r}},\hat{\bar{s}}_{\mathrm{f}}) - \tilde{A}(\hat{\bar{r}},\hat{\bar{s}}_{\mathrm{f}})\tilde{t}) \quad (106)$$

where

$$\tilde{b}(\hat{\bar{r}},\hat{\bar{s}}_{\mathrm{f}}) = \begin{bmatrix}\bar{b}(\hat{\bar{r}},\hat{\bar{s}}_{\mathrm{f}})\\ \hat{\bar{s}}_{\mathrm{f}}\end{bmatrix};\quad \tilde{A}(\hat{\bar{r}},\hat{\bar{s}}_{\mathrm{f}}) = \mathrm{blkdiag}[\bar{A}(\hat{\bar{r}},\hat{\bar{s}}_{\mathrm{f}})\ \boldsymbol{I}] \quad (107)$$

Applying the WLS criterion, the weighting matrix $\tilde{\Phi}$ is given in (108), as shown at the bottom of the next page. Besides, it can be verified from (51) that vector $\tilde{t}$ satisfies the constraints

$$\tilde{t}^{\mathrm{T}}\tilde{\Gamma}_{1d}\tilde{t} = 0\ ;\ \tilde{t}^{\mathrm{T}}\tilde{\Gamma}_{2d}\tilde{t} = 0 \quad (1 \le d \le D) \quad (109)$$

where $\tilde{\Gamma}_{1d} = \mathrm{blkdiag}[\bar{\Gamma}_{1d}\ \boldsymbol{O}]$ and $\tilde{\Gamma}_{2d} = \mathrm{blkdiag}[\bar{\Gamma}_{2d}\ \boldsymbol{O}]$.

Combining (106) and (109) yields the following CWLS problem (110), as shown at the bottom of the next page.

Similar to (74), (110) is also a nonconvex problem because the quadratic equality constraints are indefinite. Undoubtedly, the closed-form solution for (110) is analytically intractable; hence we have to solve (110) in an iterative way. In the sequel, an alternative efficient ICWLS algorithm is presented. On the other hand, it is worth noting that the weighting matrix $\tilde{\Phi}$ is related to the unknown vector $\tilde{t}$ and so it should be updated recursively in the proposed procedure.

2) PROPOSED ITERATION ALGORITHM

The numerical technique adopted in Subsection VI.A is also applied here. First, we need to transform problem (110) into a convex programming. To this end, a set of linear equality constraints are employed instead of the homogenous and nonconvex constraints. Specifically, for each quadratic equality constraint in (110), if we replace one of the variable $\tilde{t}$ with its last iteration's estimate, then the non-convex constraints become linear and convex. The resulted programming is a convex approximation of the CWLS problem (110). Mathematically, the approximate problem in the $k+1$th iteration can be formulated [see (111)], as shown at the bottom of the next page.

where $\hat{\tilde{t}}(k)$ is the estimation result in the kth iteration. Similar to problem (75), the closed-form solution for (111) also exists and it can be obtained by means of matrix SVD. We are now ready to show the corresponding result.

Proposition 7: Let $\hat{\bar{t}}(k)$ denote the vector composed of the first $8D$ elements of $\hat{\tilde{t}}(k)$. Defining the matrix

$$\boldsymbol{G}(\hat{\bar{t}}(k)) = [\,\bar{\Gamma}_{11}\hat{\bar{t}}(k)\ \cdots\ \bar{\Gamma}_{1D}\hat{\bar{t}}(k)\ \vdots\ \bar{\Gamma}_{21}\hat{\bar{t}}(k)\ \cdots\ \bar{\Gamma}_{2D}\hat{\bar{t}}(k)\,] \quad (112)$$

and performing matrix SVD on $\boldsymbol{G}(\hat{\bar{t}}(k))$ lead to

$$\boldsymbol{G}(\hat{\bar{t}}(k)) = [\boldsymbol{Q}_1(k)\ \ \boldsymbol{Q}_2(k)]\begin{bmatrix}\boldsymbol{\Sigma}_1(k)\\ \boldsymbol{O}_{6D\times 2D}\end{bmatrix}(\boldsymbol{R}_1(k))^{\mathrm{T}} = \boldsymbol{Q}_1(k)\boldsymbol{\Sigma}_1(k)(\boldsymbol{R}_1(k))^{\mathrm{T}} \quad (113)$$

where $[\boldsymbol{Q}_1(k)\ \ \boldsymbol{Q}_2(k)]$ is an orthogonal matrix; $\boldsymbol{R}_1(k)$ is an orthogonal matrix; $\boldsymbol{\Sigma}_1(k)$ is a diagonal matrix, whose diagonal entries are the singular values of $\boldsymbol{G}(\hat{\bar{t}}(k))$. Besides, let us define $\tilde{\boldsymbol{Q}}_2(k) = \mathrm{blkdiag}[\boldsymbol{Q}_2(k)\ \boldsymbol{I}_{6M\times 6M}]$. Then, the optimal solution for (111) is given by

$$\begin{aligned}\hat{\tilde{t}}_{\mathrm{opt}}(k+1) &= \tilde{\boldsymbol{Q}}_2(k)((\tilde{\boldsymbol{Q}}_2(k))^{\mathrm{T}}(\tilde{A}(\hat{\bar{r}},\hat{\bar{s}}_{\mathrm{f}}))^{\mathrm{T}}\tilde{\Phi}^{-1}\tilde{A}(\hat{\bar{r}},\hat{\bar{s}}_{\mathrm{f}})\tilde{\boldsymbol{Q}}_2(k))^{-1}\\ &\quad\times(\tilde{\boldsymbol{Q}}_2(k))^{\mathrm{T}}(\tilde{A}(\hat{\bar{r}},\hat{\bar{s}}_{\mathrm{f}}))^{\mathrm{T}}\tilde{\Phi}^{-1}\tilde{b}(\hat{\bar{r}},\hat{\bar{s}}_{\mathrm{f}})\end{aligned} \quad (114)$$

The proof of Proposition 7 is similar to that of Proposition 2, so it is omitted due to limited space. Although the solution to problem (111) is an approximation of the optimal solution of the CWLS problem (110), it incorporates $2D$ approximate linear equality constraints to improve the localization accuracy. Intuitively, the optimal solution (114) can be directly used as the $k+1$th iteration's value. But, to avoid the resulted solution sequence switching between two points, we adopt the update strategy in [29] once again. Specifically, the current iteration's value is determined using the linear combination of the solution to problem (111) and the estimation result in the last iteration. Furthermore, the weighting matrix $\tilde{\Phi}$ should also be updated at each iteration step because it is related to $\tilde{t}$.

The second stage of the proposed ICWLS method is formally outlined in Table 4.

At this point, we make three important remarks about the proposed algorithm.

Remark 11: Here, it is also very important to find a proper initial guess for the iterative algorithm. Notice that the unknown vector $\tilde{t}$ is formed by $\bar{t}$ and $\bar{s}$; hence we must choose good starting points for both of them. First, the estimation result in the first stage (i.e., $\hat{\bar{s}}_{\mathrm{f}}$) can be directly considered as the initial value of $\bar{s}$. Second, the common least squares (LS) criterion can be applied to determine the starting point of $\bar{t}$, which can written as

$$\bar{t}(0) = ((\bar{A}(\hat{\bar{r}},\hat{\bar{s}}_{\mathrm{f}}))^{\mathrm{T}}\bar{A}(\hat{\bar{r}},\hat{\bar{s}}_{\mathrm{f}}))^{-1}(\bar{A}(\hat{\bar{r}},\hat{\bar{s}}_{\mathrm{f}}))^{\mathrm{T}}\bar{b}(\hat{\bar{r}},\hat{\bar{s}}_{\mathrm{f}}) \quad (115)$$

Then, the initial estimate of $\tilde{t}$ is given by $\tilde{t}(0) = [(\bar{t}(0))^{\mathrm{T}}\ \hat{\bar{s}}_{\mathrm{f}}^{\mathrm{T}}]^{\mathrm{T}}$. Extensive Monte Carlo simulation tests show that this initial value can yield satisfactory localization accuracy.

Remark 12: As shown in Step 7, the updated value in the $k+1$th iteration is the linear combination of the optimal

solution (114) and the estimation result in the kth iteration. A large number of simulation results show that the localization performance is not sensitive to the numerical value of w_1. In our simulation, w_1 and w_2 are both set to 0.5.

Remark 13: In optimization problem (111), the weighting matrix $\tilde{\boldsymbol{\Phi}}$ is not accurately known because it relies on $\bar{\boldsymbol{t}}$, $\bar{\boldsymbol{s}}$ and $\mathbf{MSE}(\hat{\bar{\boldsymbol{s}}}_{\mathrm{f}})$. It can be seen from Proposition 6 that matrix $\mathbf{MSE}(\hat{\bar{\boldsymbol{s}}}_{\mathrm{f}})$ also depends on $\bar{\boldsymbol{s}}$. Therefore, it is necessary to update $\tilde{\boldsymbol{\Phi}}$ at each iteration step using the current iteration's value. Besides, matrix $\mathbf{MSE}(\hat{\bar{\boldsymbol{s}}}_{\mathrm{f}})$ can be obtained from (97). Theoretical analysis demonstrates that such an approximation of the weighting matrix does not affect the asymptotic properties of the estimator.

D. DISCUSSION ON THE PROPOSED ICWLS ESTIMATOR

As stated above, the proposed ICWLS method comprises two stages: a first stage for refining the sensor locations, and a second stage for multiple-target cooperative localization. At each stage, an efficient iterative algorithm is proposed. Moreover, it can be seen that the two iterative algorithms are developed based on a unified theoretical framework.

It should be pointed out that although the proposed estimator requires iteration, the convergence rate is fast, and moreover, the closed-form solution is available at every iteration. From our simulation results, it can be found that ten iterations are enough to achieve the convergence criterion. In addition, since the weighting matrices are updated recursively, more accurate weighting matrices are obtained, leading to a higher noise threshold than some existing methods before performance breaks away from the CRB.

VII. PERFORMANCE ANALYSIS OF THE PROPOSED ICWLS ESTIMATOR

This section is devoted to the performance analysis of the proposed ICWLS estimator. The theoretical derivation is mainly conducted for the iterative algorithm in stage-2, which provides the final estimation results. Similar to Subsection VI.B, the work also consists of two parts: (1) analysis on convergence property; (2) derivation for estimation MSE. Since the convergence analysis presented here follows the same theoretical framework as in Subsection VI.B, we just describe the main results due to limited space. Besides, the estimation MSE is deduced using the perturbation approach. More importantly, the MSE is proved to asymptotically attain the associated CRB given in Subsection III.A.

A. CONVERGENCE ANALYSIS FOR THE PROPOSED ICWLS ESTIMATOR

Here, the convergence analysis is similar to that in Subsection VI.B. Therefore, we only state the main results without detailed proofs. The objective is to illustrate that as long as the iterative algorithm converges, it must converge to the optimal solution for the CWLS problem (110).

According to the optimality of constrained optimization theory, we first get the following two Lemmas.

Lemma 3: Suppose that $\hat{\tilde{\boldsymbol{t}}}_{\mathrm{opt}}$, $\{\lambda_{1d}\}_{1\le d\le D}$ and $\{\lambda_{2d}\}_{1\le d\le D}$ satisfy

$$(\tilde{\boldsymbol{A}}(\hat{\bar{\boldsymbol{r}}},\hat{\bar{\boldsymbol{s}}}_{\mathrm{f}}))^{\mathrm{T}}\tilde{\boldsymbol{\Phi}}^{-1}(\tilde{\boldsymbol{A}}(\hat{\bar{\boldsymbol{r}}},\hat{\bar{\boldsymbol{s}}}_{\mathrm{f}})\hat{\tilde{\boldsymbol{t}}}_{\mathrm{opt}}-\tilde{\boldsymbol{b}}(\hat{\bar{\boldsymbol{r}}},\hat{\bar{\boldsymbol{s}}}_{\mathrm{f}}))+\sum_{d=1}^{D}\frac{\lambda_{1d}}{2}\tilde{\boldsymbol{\Gamma}}_{1d}\hat{\tilde{\boldsymbol{t}}}_{\mathrm{opt}}+\sum_{d=1}^{D}\frac{\lambda_{2d}}{2}\tilde{\boldsymbol{\Gamma}}_{2d}\hat{\tilde{\boldsymbol{t}}}_{\mathrm{opt}}=\boldsymbol{O}_{(8D+6M)\times 1} \tag{116}$$

$$\hat{\tilde{\boldsymbol{t}}}_{\mathrm{opt}}^{\mathrm{T}}\tilde{\boldsymbol{\Gamma}}_{1d}\hat{\tilde{\boldsymbol{t}}}_{\mathrm{opt}}=0\ ;\quad \hat{\tilde{\boldsymbol{t}}}_{\mathrm{opt}}^{\mathrm{T}}\tilde{\boldsymbol{\Gamma}}_{2d}\hat{\tilde{\boldsymbol{t}}}_{\mathrm{opt}}=0\ (1\le d\le D) \tag{117}$$

Moreover, it is assumed that

$$\boldsymbol{y}^{\mathrm{T}}\left(\begin{array}{c}(\tilde{\boldsymbol{A}}(\hat{\bar{\boldsymbol{r}}},\hat{\bar{\boldsymbol{s}}}_{\mathrm{f}}))^{\mathrm{T}}\tilde{\boldsymbol{\Phi}}^{-1}\tilde{\boldsymbol{A}}(\hat{\bar{\boldsymbol{r}}},\hat{\bar{\boldsymbol{s}}}_{\mathrm{f}})\\ +\sum_{d=1}^{D}\frac{\lambda_{1d}}{2}\tilde{\boldsymbol{\Gamma}}_{1d}+\sum_{d=1}^{D}\frac{\lambda_{2d}}{2}\tilde{\boldsymbol{\Gamma}}_{2d}\end{array}\right)\boldsymbol{y}>0, \tag{118}$$

for any vector $\boldsymbol{y}$ belonging to the null space of $(\tilde{\boldsymbol{G}}(\hat{\tilde{\boldsymbol{t}}}_{\mathrm{opt}}))^{\mathrm{T}}$. Then, vector $\hat{\tilde{\boldsymbol{t}}}_{\mathrm{opt}}$ is the strictly optimal solution to (110).

Lemma 4: Assuming that the optimal solution to (111) is denoted by $\hat{\tilde{\boldsymbol{t}}}_{\mathrm{opt}}(k+1)$, there exist $\{\lambda_{1d}(k+1)\}_{1\le d\le D}$ and $\{\lambda_{2d}(k+1)\}_{1\le d\le D}$ such that

$$(\tilde{\boldsymbol{A}}(\hat{\bar{\boldsymbol{r}}},\hat{\bar{\boldsymbol{s}}}_{\mathrm{f}}))^{\mathrm{T}}\tilde{\boldsymbol{\Phi}}^{-1}(\tilde{\boldsymbol{A}}(\hat{\bar{\boldsymbol{r}}},\hat{\bar{\boldsymbol{s}}}_{\mathrm{f}})\hat{\tilde{\boldsymbol{t}}}_{\mathrm{opt}}(k+1)-\tilde{\boldsymbol{b}}(\hat{\bar{\boldsymbol{r}}},\hat{\bar{\boldsymbol{s}}}_{\mathrm{f}}))+\sum_{d=1}^{D}\frac{\lambda_{1d}(k+1)}{2}\tilde{\boldsymbol{\Gamma}}_{1d}\hat{\tilde{\boldsymbol{t}}}(k)+\sum_{d=1}^{D}\frac{\lambda_{2d}(k+1)}{2}\tilde{\boldsymbol{\Gamma}}_{2d}\hat{\tilde{\boldsymbol{t}}}(k)=\boldsymbol{O}_{(8D+6M)\times 1} \tag{119}$$

$$\tilde{\boldsymbol{\Phi}}=\left[\begin{array}{c|c}\bar{\boldsymbol{C}}_1(\bar{\boldsymbol{t}},\bar{\boldsymbol{r}},\bar{\boldsymbol{s}})\bar{\boldsymbol{E}}_{\mathrm{A}}(\bar{\boldsymbol{C}}_1(\bar{\boldsymbol{t}},\bar{\boldsymbol{r}},\bar{\boldsymbol{s}}))^{\mathrm{T}}+\bar{\boldsymbol{C}}_2(\bar{\boldsymbol{t}},\bar{\boldsymbol{r}},\bar{\boldsymbol{s}})\cdot\mathbf{MSE}(\hat{\bar{\boldsymbol{s}}}_{\mathrm{f}})\cdot(\bar{\boldsymbol{C}}_2(\bar{\boldsymbol{t}},\bar{\boldsymbol{r}},\bar{\boldsymbol{s}}))^{\mathrm{T}} & \bar{\boldsymbol{C}}_2(\bar{\boldsymbol{t}},\bar{\boldsymbol{r}},\bar{\boldsymbol{s}})\cdot\mathbf{MSE}(\hat{\bar{\boldsymbol{s}}}_{\mathrm{f}})\\ \hline \mathbf{MSE}(\hat{\bar{\boldsymbol{s}}}_{\mathrm{f}})\cdot(\bar{\boldsymbol{C}}_2(\bar{\boldsymbol{t}},\bar{\boldsymbol{r}},\bar{\boldsymbol{s}}))^{\mathrm{T}} & \mathbf{MSE}(\hat{\bar{\boldsymbol{s}}}_{\mathrm{f}})\end{array}\right] \tag{108}$$

$$\begin{cases}\min\limits_{\tilde{\boldsymbol{t}}\in R^{(8D+6M)\times 1}} J(\tilde{\boldsymbol{t}})=\min\limits_{\tilde{\boldsymbol{t}}\in R^{(8D+6M)\times 1}}\{(\tilde{\boldsymbol{b}}(\hat{\bar{\boldsymbol{r}}},\hat{\bar{\boldsymbol{s}}}_{\mathrm{f}})-\tilde{\boldsymbol{A}}(\hat{\bar{\boldsymbol{r}}},\hat{\bar{\boldsymbol{s}}}_{\mathrm{f}})\tilde{\boldsymbol{t}})^{\mathrm{T}}\tilde{\boldsymbol{\Phi}}^{-1}(\tilde{\boldsymbol{b}}(\hat{\bar{\boldsymbol{r}}},\hat{\bar{\boldsymbol{s}}}_{\mathrm{f}})-\tilde{\boldsymbol{A}}(\hat{\bar{\boldsymbol{r}}},\hat{\bar{\boldsymbol{s}}}_{\mathrm{f}})\tilde{\boldsymbol{t}})\}\\ \text{s.t. } \tilde{\boldsymbol{t}}^{\mathrm{T}}\tilde{\boldsymbol{\Gamma}}_{1d}\tilde{\boldsymbol{t}}=0\ ;\ \tilde{\boldsymbol{t}}^{\mathrm{T}}\tilde{\boldsymbol{\Gamma}}_{2d}\tilde{\boldsymbol{t}}=0\quad(1\le d\le D)\end{cases} \tag{110}$$

$$\begin{cases}\min\limits_{\tilde{\boldsymbol{t}}\in R^{(8D+6M)\times 1}} J(\tilde{\boldsymbol{t}})=\min\limits_{\tilde{\boldsymbol{t}}\in R^{(8D+6M)\times 1}}\{(\tilde{\boldsymbol{b}}(\hat{\bar{\boldsymbol{r}}},\hat{\bar{\boldsymbol{s}}}_{\mathrm{f}})-\tilde{\boldsymbol{A}}(\hat{\bar{\boldsymbol{r}}},\hat{\bar{\boldsymbol{s}}}_{\mathrm{f}})\tilde{\boldsymbol{t}})^{\mathrm{T}}\tilde{\boldsymbol{\Phi}}^{-1}(\tilde{\boldsymbol{b}}(\hat{\bar{\boldsymbol{r}}},\hat{\bar{\boldsymbol{s}}}_{\mathrm{f}})-\tilde{\boldsymbol{A}}(\hat{\bar{\boldsymbol{r}}},\hat{\bar{\boldsymbol{s}}}_{\mathrm{f}})\tilde{\boldsymbol{t}})\}\\ \text{s.t. } \tilde{\boldsymbol{t}}^{\mathrm{T}}\tilde{\boldsymbol{\Gamma}}_{1d}\hat{\tilde{\boldsymbol{t}}}(k)=0\ ;\ \tilde{\boldsymbol{t}}^{\mathrm{T}}\tilde{\boldsymbol{\Gamma}}_{2d}\hat{\tilde{\boldsymbol{t}}}(k)=0\quad(1\le d\le D)\end{cases} \tag{111}$$

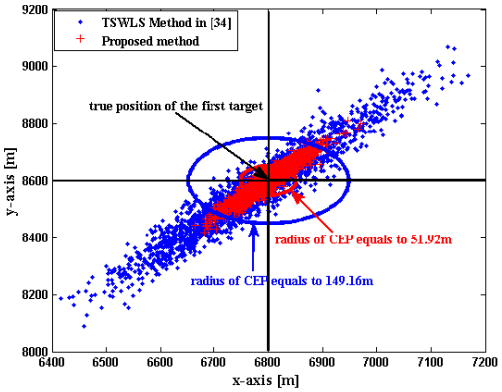

(a). Position estimation results in the x-y plane for the first target.

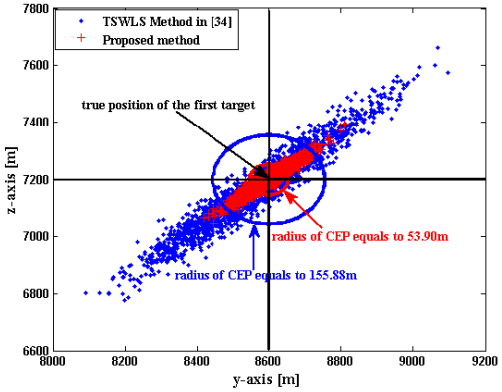

(b). Position estimation results in the y-z plane for the first target.

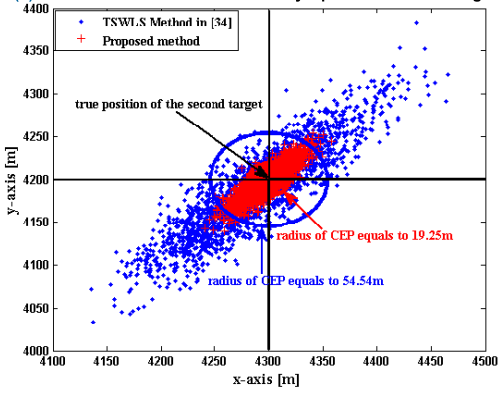

(c). Position estimation results in the x-y plane for the second target.

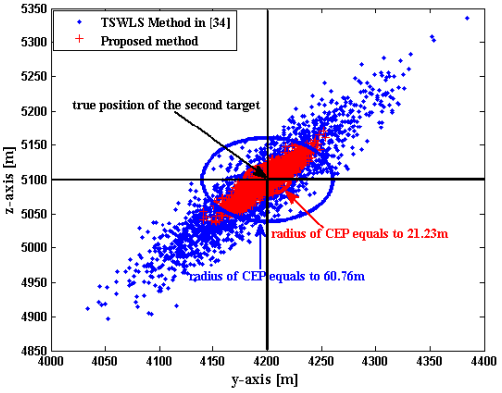

(d). Position estimation results in the y-z plane for the second target.

FIGURE 2. Scatter plots of the target location estimates obtained from the proposed method as well as the method in [34].

Based on Lemmas 3 and 4, we can in turn draw the following results.

TABLE 4. Procedure of the second stage of the proposed ICWLS method.

Step 1: Compute $\mathbf{MSE}(\hat{\tilde{\boldsymbol{s}}}_{\mathrm{f}})$ according to the result in Proposition 6.
Step 2: Define a convergence threshold $\tau > 0$ and choose a good initial value $\hat{\tilde{\boldsymbol{t}}}(0)$.
Step 3: Compute the matrix $\widetilde{\boldsymbol{A}}(\hat{\tilde{\boldsymbol{r}}}, \hat{\tilde{\boldsymbol{s}}}_{\mathrm{f}})$ and the vector $\widetilde{\boldsymbol{b}}(\hat{\tilde{\boldsymbol{r}}}, \hat{\tilde{\boldsymbol{s}}}_{\mathrm{f}})$ using (39) and (107).
Step 4: Set the iteration counter $k := 0$ and compute the weighting matrix $\widetilde{\boldsymbol{\Phi}}$ based on $\mathbf{MSE}(\hat{\tilde{\boldsymbol{s}}}_{\mathrm{f}})$ and (108).
Step 5: Calculate the matrix $\boldsymbol{G}(\hat{\tilde{\boldsymbol{t}}}(k))$ from (112) and perform matrix SVD on $\boldsymbol{G}(\hat{\tilde{\boldsymbol{t}}}(k))$ to generate $\boldsymbol{Q}_2(k)$.
Step 6: Construct the matrix $\widetilde{\boldsymbol{Q}}_2(k) = \mathrm{blkdiag}[\boldsymbol{Q}_2(k)\ \boldsymbol{I}_{6M\times 6M}]$ and compute the vector $\hat{\tilde{\boldsymbol{t}}}_{\mathrm{opt}}(k+1)$ using (114).
Step 7: Calculate $\hat{\tilde{\boldsymbol{t}}}(k+1) = w_1\hat{\tilde{\boldsymbol{t}}}(k) + w_2\hat{\tilde{\boldsymbol{t}}}_{\mathrm{opt}}(k+1)$, where $w_1 > 0$, $w_2 > 0$ and $w_1 + w_2 = 1$. If $\|\hat{\tilde{\boldsymbol{t}}}(k+1) - \hat{\tilde{\boldsymbol{t}}}(k)\|_2 \le \tau$, let $\hat{\tilde{\boldsymbol{t}}}_{\mathrm{s}} = \hat{\tilde{\boldsymbol{t}}}(k+1)$ and go to Step 10; otherwise go to Step 8.
Step 8: Compute $\mathbf{MSE}(\hat{\tilde{\boldsymbol{s}}}_{\mathrm{f}})$ according to the result in Proposition 6.
Step 9: Increment the iteration counter $k := k+1$ and compute the weighting matrix $\widetilde{\boldsymbol{\Phi}}$ based on $\mathbf{MSE}(\hat{\tilde{\boldsymbol{s}}}_{\mathrm{f}})$ and (108) and go to Step 5.
Step 10: Determine the final result by $\begin{bmatrix}\hat{\tilde{\boldsymbol{u}}}_{\mathrm{s}}\\ \hat{\tilde{\boldsymbol{s}}}_{\mathrm{s}}\end{bmatrix} = \left[\begin{array}{c:c}\boldsymbol{I}_D \otimes [\boldsymbol{I}_6\ \boldsymbol{O}_{6\times 2}] & \boldsymbol{I}_D \otimes \boldsymbol{\Xi}\\ \hline \boldsymbol{O}_{6M\times 8D} & \boldsymbol{I}_{6M}\end{array}\right]\hat{\tilde{\boldsymbol{t}}}_{\mathrm{s}}$ and stop the procedure.

Proposition 8: If the sequence $\{\hat{\tilde{\boldsymbol{t}}}(k+1)\}_{0\le k\le+\infty}$ converges to $\hat{\tilde{\boldsymbol{t}}}_{\mathrm{s}}$, then the sequence $\{\hat{\tilde{\boldsymbol{t}}}_{\mathrm{opt}}(k+1)\}_{0\le k\le+\infty}$ also converges to $\hat{\tilde{\boldsymbol{t}}}_{\mathrm{s}}$.

Proposition 9: If the sequence $\{\hat{\tilde{\boldsymbol{t}}}(k+1)\}_{0\le k\le+\infty}$ converges, then the sequences $\{\lambda_{1d}(k+1)\}_{0\le k\le+\infty}$ and $\{\lambda_{2d}(k+1)\}_{0\le k\le+\infty}$ also converge for arbitrary $1 \le d \le D$.

Proposition 10: If the sequence $\{\hat{\tilde{\boldsymbol{t}}}(k+1)\}_{0\le k\le+\infty}$ converges to $\hat{\tilde{\boldsymbol{t}}}_{\mathrm{s}}$, then $\hat{\tilde{\boldsymbol{t}}}_{\mathrm{s}} = \hat{\tilde{\boldsymbol{t}}}_{\mathrm{opt}}$ is the strictly optimal solution to (110).

The proofs of Propositions 8-10 are similar to those of Propositions 3-5, respectively. Proposition 10 shows that if the proposed ICWLS algorithm converges, then it will provide the optimal solution for (110). There is no general approach, however, to ensure that the iterative algorithm must converge. Fortunately, the simulation results in Section VIII reveal that the convergence criterion can be reached within ten iterations in most cases.

B. ESTIMATION MSE FOR THE PROPOSED ICWLS ESTIMATOR

This subsection is devoted to the derivation of the MSE expression for the proposed ICWLS estimator. Moreover, the obtained theoretical MSE is analytically shown to equal the CRB given by (21). The first-order perturbation approach is adopted for this purpose.

Suppose that the proposed ICWLS algorithm in the second stage converges to $\hat{\tilde{\boldsymbol{t}}}_{\mathrm{s}}$, which is also the optimal solution for (110) as shown in Proposition 10. Since the final location estimates for target sources and sensors are obtained by $\begin{bmatrix}\hat{\tilde{\boldsymbol{u}}}_{\mathrm{s}}\\ \hat{\tilde{\boldsymbol{s}}}_{\mathrm{s}}\end{bmatrix} = \left[\begin{array}{c|c}\boldsymbol{I}_D\otimes[\boldsymbol{I}_6\ \boldsymbol{O}_{6\times 2}] & \boldsymbol{I}_D\otimes\boldsymbol{\Xi}\\ \hline \boldsymbol{O}_{6M\times 8D} & \boldsymbol{I}_{6M}\end{array}\right]\hat{\tilde{\boldsymbol{t}}}_{\mathrm{s}}$, we should first deduce the theoretical MSE of $\hat{\tilde{\boldsymbol{t}}}_{\mathrm{s}}$. Let the estimation error in $\hat{\tilde{\boldsymbol{t}}}_{\mathrm{s}}$ be denoted as $\Delta\tilde{\boldsymbol{t}}_{\mathrm{s}}$. In the theoretical frame of the first-order perturbation analysis, $\Delta\tilde{\boldsymbol{t}}_{\mathrm{s}}$ can be approximately expressed as a linear function with respect to the measurement noise $\bar{\boldsymbol{\varepsilon}}$ as well as the estimation error $\Delta\bar{\boldsymbol{s}}_{\mathrm{f}}$ in the first stage. Indeed, by taking the first-order approximation, $\Delta\tilde{\boldsymbol{t}}_{\mathrm{s}}$ is the optimal solution for the following constrained minimization problem [28]:

$$\begin{cases}\min\limits_{\Delta\tilde{\boldsymbol{t}}\in R^{(8D+6M)\times 1}} \left\{\begin{array}{l}\left(\tilde{\boldsymbol{A}}(\bar{\boldsymbol{r}},\bar{\boldsymbol{s}})\Delta\tilde{\boldsymbol{t}}-\bar{\boldsymbol{C}}(\bar{\boldsymbol{t}},\bar{\boldsymbol{r}},\bar{\boldsymbol{s}})\begin{bmatrix}\bar{\boldsymbol{\varepsilon}}\\ \Delta\bar{\boldsymbol{s}}_{\mathrm{f}}\end{bmatrix}\right)^{\mathrm{T}}\tilde{\boldsymbol{\Phi}}^{-1}\\ \quad\times\left(\tilde{\boldsymbol{A}}(\bar{\boldsymbol{r}},\bar{\boldsymbol{s}})\Delta\tilde{\boldsymbol{t}}-\bar{\boldsymbol{C}}(\bar{\boldsymbol{t}},\bar{\boldsymbol{r}},\bar{\boldsymbol{s}})\begin{bmatrix}\bar{\boldsymbol{\varepsilon}}\\ \Delta\bar{\boldsymbol{s}}_{\mathrm{f}}\end{bmatrix}\right)\end{array}\right\}\\ \text{s.t. } (\tilde{\boldsymbol{G}}(\tilde{\boldsymbol{t}}))^{\mathrm{T}}\Delta\tilde{\boldsymbol{t}}=\boldsymbol{O}_{2D\times 1}\end{cases} \tag{120}$$

where $\tilde{\boldsymbol{G}}(\tilde{\boldsymbol{t}}) = [\,\tilde{\boldsymbol{\Gamma}}_{11}\tilde{\boldsymbol{t}}\ \tilde{\boldsymbol{\Gamma}}_{12}\tilde{\boldsymbol{t}}\ \cdots\ \tilde{\boldsymbol{\Gamma}}_{1D}\tilde{\boldsymbol{t}}\ \tilde{\boldsymbol{\Gamma}}_{21}\tilde{\boldsymbol{t}}\ \tilde{\boldsymbol{\Gamma}}_{22}\tilde{\boldsymbol{t}}\ \cdots\ \tilde{\boldsymbol{\Gamma}}_{2D}\tilde{\boldsymbol{t}}\,]$. The matrix SVD of $\tilde{\boldsymbol{G}}(\tilde{\boldsymbol{t}})$ can be described as

$$\begin{aligned}\tilde{\boldsymbol{G}}(\tilde{\boldsymbol{t}}) &= \begin{bmatrix}\boldsymbol{Q}_1 & \boldsymbol{Q}_2 & \boldsymbol{O}_{8D\times 6M}\\ \boldsymbol{O}_{6M\times 2D} & \boldsymbol{O}_{6M\times 6D} & \boldsymbol{I}_{6M\times 6M}\end{bmatrix}\begin{bmatrix}\boldsymbol{\Sigma}_1\\ \boldsymbol{O}_{6D\times 2D}\\ \boldsymbol{O}_{6M\times 2D}\end{bmatrix}\boldsymbol{R}_1\\ &= \begin{bmatrix}\boldsymbol{Q}_1\\ \boldsymbol{O}_{6M\times 2D}\end{bmatrix}\boldsymbol{\Sigma}_1\boldsymbol{R}_1\end{aligned} \tag{121}$$

Due to the fact that $\Delta\tilde{\boldsymbol{t}}_{\mathrm{s}}$ is orthogonal to the range space of $\tilde{\boldsymbol{G}}(\tilde{\boldsymbol{t}})$, it is easy to see that $\Delta\tilde{\boldsymbol{t}}_{\mathrm{s}}$ belongs to the range space of $\tilde{\boldsymbol{Q}}_2 = \mathrm{blkdiag}[\boldsymbol{Q}_2\ \boldsymbol{I}_{6M\times 6M}]$. Therefore, we can express $\Delta\tilde{\boldsymbol{t}}_{\mathrm{s}}$ as

$$\begin{aligned}\Delta\tilde{\boldsymbol{t}}_{\mathrm{s}} = \tilde{\boldsymbol{Q}}_2(\tilde{\boldsymbol{Q}}_2^{\mathrm{T}}(\tilde{\boldsymbol{A}}(\bar{\boldsymbol{r}},\bar{\boldsymbol{s}}))^{\mathrm{T}}\tilde{\boldsymbol{\Phi}}^{-1}\tilde{\boldsymbol{A}}(\bar{\boldsymbol{r}},\bar{\boldsymbol{s}})\tilde{\boldsymbol{Q}}_2)^{-1}\\ \times\tilde{\boldsymbol{Q}}_2^{\mathrm{T}}(\tilde{\boldsymbol{A}}(\bar{\boldsymbol{r}},\bar{\boldsymbol{s}}))^{\mathrm{T}}\tilde{\boldsymbol{\Phi}}^{-1}\bar{\boldsymbol{C}}(\bar{\boldsymbol{t}},\bar{\boldsymbol{r}},\bar{\boldsymbol{s}})\begin{bmatrix}\bar{\boldsymbol{\varepsilon}}\\ \Delta\bar{\boldsymbol{s}}_{\mathrm{f}}\end{bmatrix}\end{aligned} \tag{122}$$

TABLE 5. True positions (in meters) and velocities (in meters/second) of sensors for the first set of simulations.

Sensor no.m	$\boldsymbol{s}_m$			$\dot{\boldsymbol{s}}_m$		
1	2100	1800	1500	16	18	-15
2	1700	1900	-2200	14	10	15
3	2500	-2100	1900	-14	-20	10
4	-1300	1300	2400	-12	10	-18
5	1800	-1900	-1300	-16	20	10
6	-1700	-1800	2000	18	-12	-15
7	-2100	1700	-2400	15	-10	15
8	-2200	-1500	-1600	-14	-12	-16

Since the mean value of $\Delta\tilde{\boldsymbol{t}}_{\mathrm{s}}$ is equal to zero, $\hat{\tilde{\boldsymbol{t}}}_{\mathrm{s}}$ is an approximately unbiased estimate of $\tilde{\boldsymbol{t}}$. From (108) and (122), the estimation MSE of $\hat{\tilde{\boldsymbol{t}}}_{\mathrm{s}}$ is given by

$$\mathbf{MSE}(\hat{\tilde{\boldsymbol{t}}}_{\mathrm{s}}) = \tilde{\boldsymbol{Q}}_2(\tilde{\boldsymbol{Q}}_2^{\mathrm{T}}\tilde{\boldsymbol{P}}(\bar{\boldsymbol{r}},\bar{\boldsymbol{s}})\tilde{\boldsymbol{Q}}_2)^{-1}\tilde{\boldsymbol{Q}}_2^{\mathrm{T}} \tag{123}$$

where $\tilde{\boldsymbol{P}}(\bar{\boldsymbol{r}},\bar{\boldsymbol{s}}) = (\tilde{\boldsymbol{A}}(\bar{\boldsymbol{r}},\bar{\boldsymbol{s}}))^{\mathrm{T}}\tilde{\boldsymbol{\Phi}}^{-1}\tilde{\boldsymbol{A}}(\bar{\boldsymbol{r}},\bar{\boldsymbol{s}})$.

Three remarks are drawn in the sequel.

Remark 14: Since $\tilde{\boldsymbol{Q}}_2^{\mathrm{T}}\tilde{\boldsymbol{G}}(\tilde{\boldsymbol{t}}) = \boldsymbol{O}$, we immediately arrive at $\mathbf{MSE}(\hat{\tilde{\boldsymbol{t}}}_{\mathrm{s}})\tilde{\boldsymbol{G}}(\tilde{\boldsymbol{t}}) = \boldsymbol{O}$, which implies that $\mathbf{MSE}(\hat{\tilde{\boldsymbol{t}}}_{\mathrm{s}})$ is a rank-deficient matrix. The main reason for this is that $\Delta\tilde{\boldsymbol{t}}_{\mathrm{s}}$ must satisfy the equation constraints in (120).

Remark 15: Define matrix $\tilde{\boldsymbol{H}}_1(\bar{\boldsymbol{u}},\bar{\boldsymbol{s}}) = \mathrm{blkdiag}[\tilde{\boldsymbol{H}}_1(\bar{\boldsymbol{u}},\bar{\boldsymbol{s}})\ \boldsymbol{I}_{6M}]$. Combining (52), (54) with the definition of $\tilde{\boldsymbol{G}}(\tilde{\boldsymbol{t}})$ leads to $(\tilde{\boldsymbol{H}}_1(\bar{\boldsymbol{u}},\bar{\boldsymbol{s}}))^{\mathrm{T}}\tilde{\boldsymbol{G}}(\tilde{\boldsymbol{t}}) = \boldsymbol{O}$. Note that the number of columns of $\tilde{\boldsymbol{H}}_1(\bar{\boldsymbol{u}},\bar{\boldsymbol{s}})$ is equal to that of $\tilde{\boldsymbol{Q}}_2$, so it can be verified that $\mathrm{range}\{\tilde{\boldsymbol{H}}_1(\bar{\boldsymbol{u}},\bar{\boldsymbol{s}})\} = \mathrm{range}\{\tilde{\boldsymbol{Q}}_2\}$.

Remark 16: Combining (107) and (108) and applying matrix identities (I) and (II) in Table 2, the detailed expression for matrix $\tilde{\boldsymbol{P}}(\bar{\boldsymbol{r}},\bar{\boldsymbol{s}})$ can be written as shown in (124) [see p. 24].

It is noteworthy that (124) plays an important role in the proof of Proposition 11 described below.

To proceed further, the theoretical MSE of the joint estimate $\begin{bmatrix}\hat{\tilde{\boldsymbol{u}}}_{\mathrm{s}}\\ \hat{\tilde{\boldsymbol{s}}}_{\mathrm{s}}\end{bmatrix}$ is presented. Let its estimation error be $\begin{bmatrix}\Delta\bar{\boldsymbol{u}}_{\mathrm{s}}\\ \Delta\bar{\boldsymbol{s}}_{\mathrm{s}}\end{bmatrix}$. Then, we can get

$$\begin{bmatrix}\Delta\bar{\boldsymbol{u}}_{\mathrm{s}}\\ \Delta\bar{\boldsymbol{s}}_{\mathrm{s}}\end{bmatrix} = \left[\begin{array}{c|c}\boldsymbol{I}_D\otimes[\boldsymbol{I}_6\ \boldsymbol{O}_{6\times 2}] & \boldsymbol{I}_D\otimes\boldsymbol{\Xi}\\ \hline \boldsymbol{O}_{6M\times 8D} & \boldsymbol{I}_{6M}\end{array}\right]\Delta\tilde{\boldsymbol{t}}_{\mathrm{s}} \tag{125}$$

which, combined with (123), yields

$$\begin{aligned}&\mathbf{MSE}\left(\begin{bmatrix}\hat{\tilde{\boldsymbol{u}}}_{\mathrm{s}}\\ \hat{\tilde{\boldsymbol{s}}}_{\mathrm{s}}\end{bmatrix}\right)\\ &= \left[\begin{array}{c|c}\boldsymbol{I}_D\otimes[\boldsymbol{I}_6\ \boldsymbol{O}_{6\times 2}] & \boldsymbol{I}_D\otimes\boldsymbol{\Xi}\\ \hline \boldsymbol{O}_{6M\times 8D} & \boldsymbol{I}_{6M}\end{array}\right]\tilde{\boldsymbol{Q}}_2\\ &\quad\times(\tilde{\boldsymbol{Q}}_2^{\mathrm{T}}\tilde{\boldsymbol{P}}(\bar{\boldsymbol{r}},\bar{\boldsymbol{s}})\tilde{\boldsymbol{Q}}_2)^{-1}\tilde{\boldsymbol{Q}}_2^{\mathrm{T}}\left[\begin{array}{c|c}\boldsymbol{I}_D\otimes\begin{bmatrix}\boldsymbol{I}_6\\ \boldsymbol{O}_{2\times 6}\end{bmatrix} & \boldsymbol{O}_{8D\times 6M}\\ \hline \boldsymbol{I}_D^{\mathrm{T}}\otimes\boldsymbol{\Xi}^{\mathrm{T}} & \boldsymbol{I}_{6M}\end{array}\right]\end{aligned} \tag{126}$$

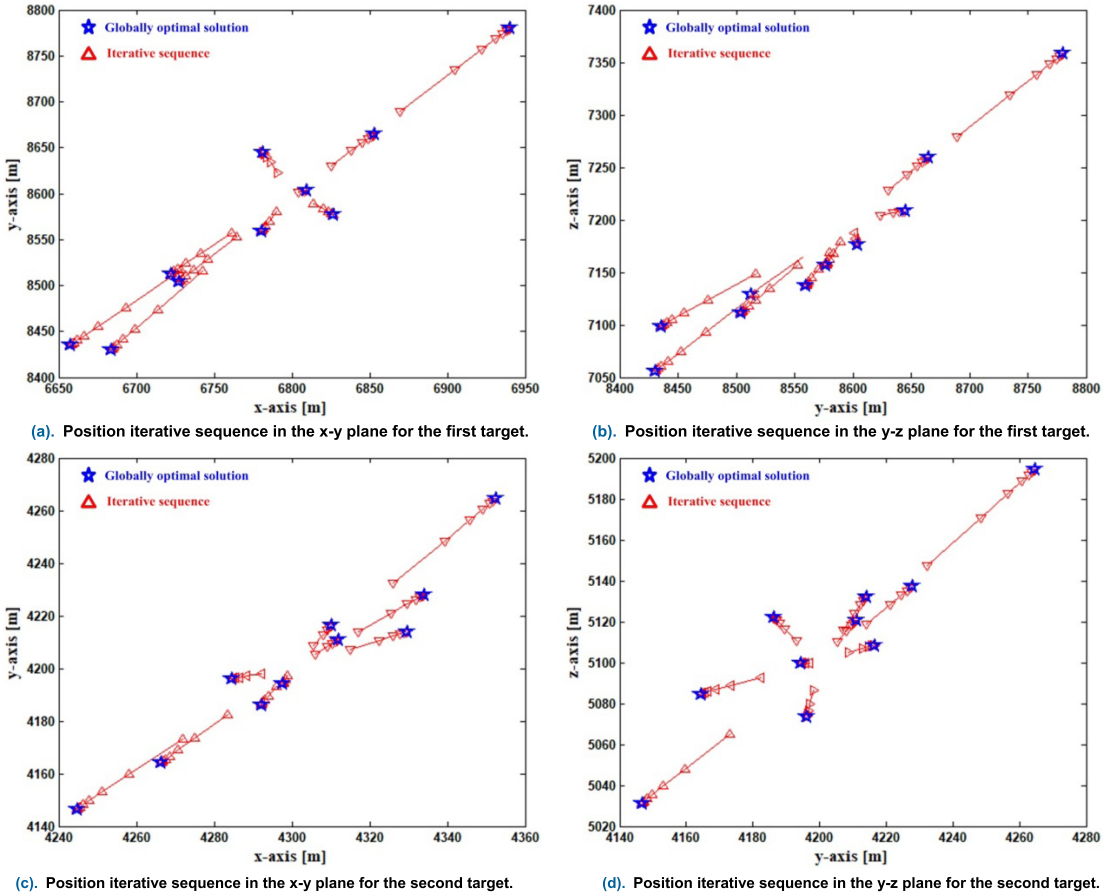

(a). Position iterative sequence in the x-y plane for the first target.

(b). Position iterative sequence in the y-z plane for the first target.

(c). Position iterative sequence in the x-y plane for the second target.

(d). Position iterative sequence in the y-z plane for the second target.

FIGURE 3. Position iterative sequence obtained from the proposed method.

The MSEs of the estimates $\hat{\bar{\boldsymbol{u}}}_{\mathrm{s}}$ and $\hat{\bar{\boldsymbol{s}}}_{\mathrm{s}}$ can be easily obtained from (126). In the sequel, the solution $\begin{bmatrix} \hat{\bar{\boldsymbol{u}}}_{\mathrm{s}} \\ \hat{\bar{\boldsymbol{s}}}_{\mathrm{s}} \end{bmatrix}$ is proved to reach CRB accuracy under moderate noise level.

Proposition 11: Under the first-order approximation, we have

$$\mathbf{MSE}\left(\begin{bmatrix} \hat{\bar{\boldsymbol{u}}}_{\mathrm{s}} \\ \hat{\bar{\boldsymbol{s}}}_{\mathrm{s}} \end{bmatrix}\right) = \mathbf{CRB}\left(\begin{bmatrix} \bar{\boldsymbol{u}} \\ \bar{\boldsymbol{s}} \end{bmatrix}\right) \tag{127}$$

The proof of Proposition 11 is described in Appendix F. The result in Proposition 11 demonstrates that the novel estimator is asymptotically efficient. In Section VIII, some simulations are conducted to support the theoretical development as well as the advantages of the newly proposed method.

VIII. NUMERICAL EXPERIMENT AND RESULT ANALYSIS

In this section, we present a set of Monte Carlo simulations in order to verify the analytical results and evaluate the accuracy of the proposed localization method. The estimation performance is assessed in terms of root-mean-square-error (RMSE) and radius of circular error probability (CEP) [50]. The RMSEs are obtained from the average of 5000 independent runs.

In the first set of experiments, the radius of CEP of the proposed method is compared with that of the TSWLS method in [34], which can locate multiple targets simultaneously but does not utilize the UAV calibration emitters. From this comparison, the performance improvement resulted from the use of the calibration emitters can be clearly observed. Consider a 3-D localization scenario consisting of 8 moving sensors whose true positions and velocities are tabulated in Table 5. These sensors are used to locate 2 moving target sources positioned at $\boldsymbol{u}_1 = [6800\ \ 8600\ \ 7200]^{\mathrm{T}}$ (m) and $\boldsymbol{u}_2 = [4300\ \ 4200\ \ 5100]^{\mathrm{T}}$ (m) with velocities $\dot{\boldsymbol{u}}_1 = [-12\ \ 10\ \ -14]^{\mathrm{T}}$ (m/s) and $\dot{\boldsymbol{u}}_2 = [16\ \ -13\ \ -15]^{\mathrm{T}}$ (m/s). The target sources be stalled on any mobile vehicles, and their TDOAs/FDOAs can be obtained in a disjoint manner. Besides, there exist two UAV calibration emitters, which are positioned at $\boldsymbol{w}_1 = [5000\ \ 6000\ \ 5000]^{\mathrm{T}}$ (m) and $\boldsymbol{w}_2 = [6000\ 4000\ 6000]^{\mathrm{T}}$ (m) with velocities $\dot{\boldsymbol{w}}_1 = [10\ \ -20\ 12]^{\mathrm{T}}$ (m/s) and $\dot{\boldsymbol{w}}_2 = [-15\ \ 16\ \ -18]^{\mathrm{T}}$ (m/s). In generating the simulation results, the TDOA/FDOA measurements from the unknown target sources and calibration emitters are produced via adding to the true values zero mean Gaussian noise with covariance matrices $\boldsymbol{E}_d = \sigma_1^2 \mathrm{blkdiag}[\boldsymbol{T}\ 0.01^2\boldsymbol{T}]$ and $\boldsymbol{E}_n = \sigma_1^2 \mathrm{blkdiag}[\boldsymbol{T}\ 0.01^2\boldsymbol{T}](d\ ,\ n = 1\ ,\ 2)$, where σ_1 is fixed at 5 and $\boldsymbol{T}$ is an $M \times M$ matrix with 1 in the diagonal elements and 0.5 otherwise. The erroneous sensor locations are created in a similar approach, where the covariance matrix of $\bar{\boldsymbol{E}}_{\mathrm{B}}$ is $\sigma_2^2(\boldsymbol{I}_M \otimes \mathrm{blkdiag}[\boldsymbol{I}_3\ 0.01^2\boldsymbol{I}_3])$, and σ_2 is set to 15.

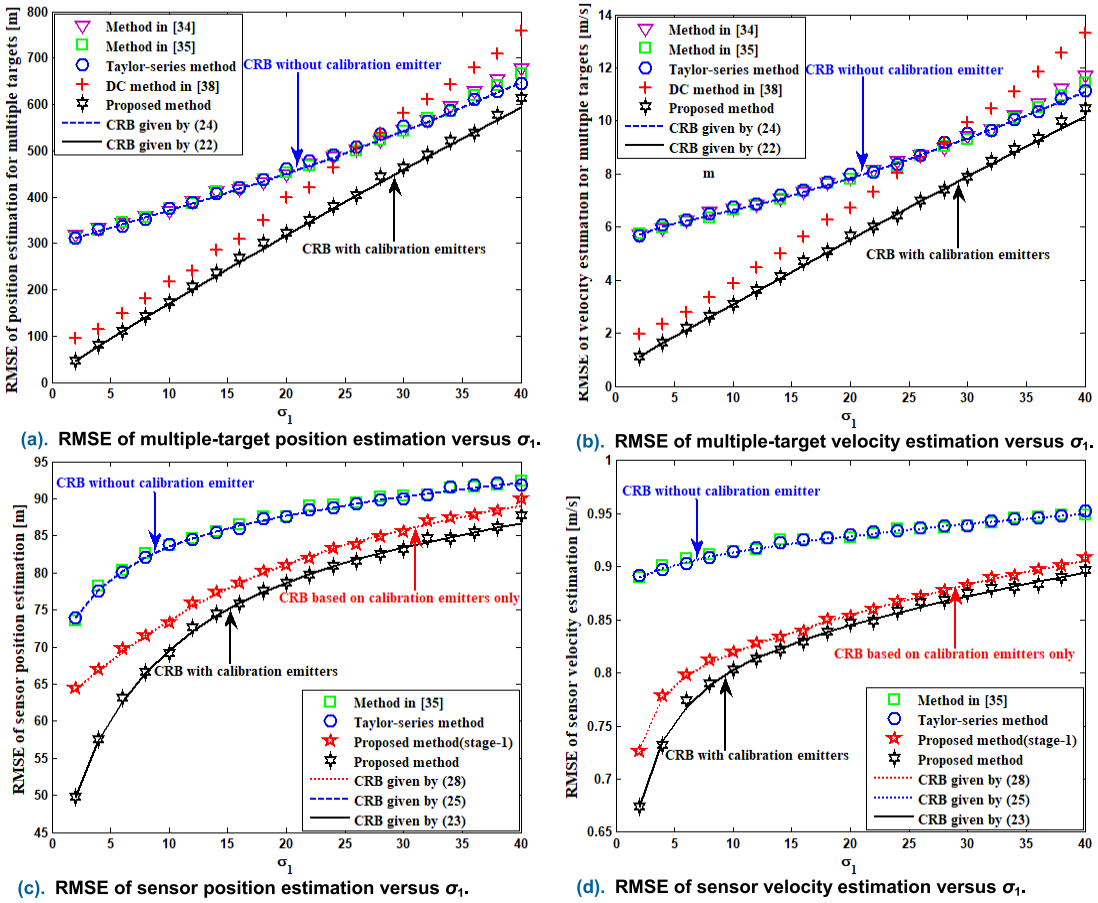

FIGURE 4. RMSE of multiple-target and sensor location estimation versus σ_1.

Figs.2(a)-(d) depict the scatter plots of the target location estimates obtained from the proposed method as well as the TSWLS method in [34] through 2000 independent experiments. The radiuses of CEP for the two localization methods are also provided in these figures. Additionally, the position iterative sequence of the proposed method is plotted in Figs.3(a)-(d), where we perform 10 independent Monte-Carlo runs, each of which has different noise values. Meanwhile, the globally optimal solutions for target positions are also displayed. Note that the optimal solutions can be obtained by a direct grid search and they are generally not equal to the true values due to the presence of measurement errors.

From Figs.2 and 3 we can draw the following conclusions:

(1) From the starting points described in *Remarks 5* and *11*, the new method is able to find the globally optimum solutions. Moreover, the convergence criterion can be reached within 10 iterations in most cases. Therefore, the validity of the convergence analysis presented in Subsections VI.B and VII.A is verified.

(2) The CEP radius of the proposed method is much smaller than that of the TSWLS method in [34]. This finding reveals that the location accuracy could be significantly improved if the measurements from the calibration emitters are fully utilized.

In the second set of simulations, the newly developed method is compared with the TSWLS methods in [34], [35] and the Taylor-series iterative method extended from [51] in terms of estimation RMSE. Since these compared methods do not exploit the calibration emitters, we can accurately assess the performance gain due to the use of the calibration emitters from this comparison. On the other hand, as mentioned in [38], the differential calibration (DC) technique is commonly used in global positioning systems (GPS) to mitigate the effect of uncertainties in satellite position and velocity. This method can be easily extended to the localization scenario studied here. So, it is reasonable to compare our method with the DC technique. The simulation settings are the same as those in the first set of experiments, except that the covariance matrices $\{\boldsymbol{E}_d\}_{1\le d\le 2}$, $\{\boldsymbol{E}_n\}_{1\le n\le 2}$ and $\bar{\boldsymbol{E}}_{\mathrm{B}}$ are changed. First, we choose $\bar{\boldsymbol{E}}_{\mathrm{B}} = 20^2(\boldsymbol{I}_M \otimes \mathrm{blkdiag}[\boldsymbol{I}_3\ 0.01^2\boldsymbol{I}_3])$ and set $\boldsymbol{E}_d = \sigma_1^2\mathrm{blkdiag}[\boldsymbol{T}\ 0.01^2\boldsymbol{T}]$ and $\boldsymbol{E}_n = \sigma_1^2\mathrm{blkdiag}[\boldsymbol{T}\ 0.01^2\boldsymbol{T}](d, n = 1, 2)$, where σ_1 varies from 2 to 40. Figs.4(a)-(d) depict the RMSEs of multiple-target position estimation, multiple-target velocity estimation, sensor position estimation and sensor velocity estimation versus σ_1, respectively. Subsequently, we fix $\boldsymbol{E}_d = 15^2\mathrm{blkdiag}[\boldsymbol{T}\ 0.01^2\boldsymbol{T}]$ and $\boldsymbol{E}_n = 15^2\mathrm{blkdiag}[\boldsymbol{T}\ 0.01^2\boldsymbol{T}](d, n = 1, 2)$, and set $\bar{\boldsymbol{E}}_{\mathrm{B}} = \sigma_2^2(\boldsymbol{I}_M \otimes \mathrm{blkdiag}[\boldsymbol{I}_3\ 0.01^2\boldsymbol{I}_3])$, where σ_2 ranges from 2 to 40. Figs.5(a)-(d) show the RMSEs of multiple-target position

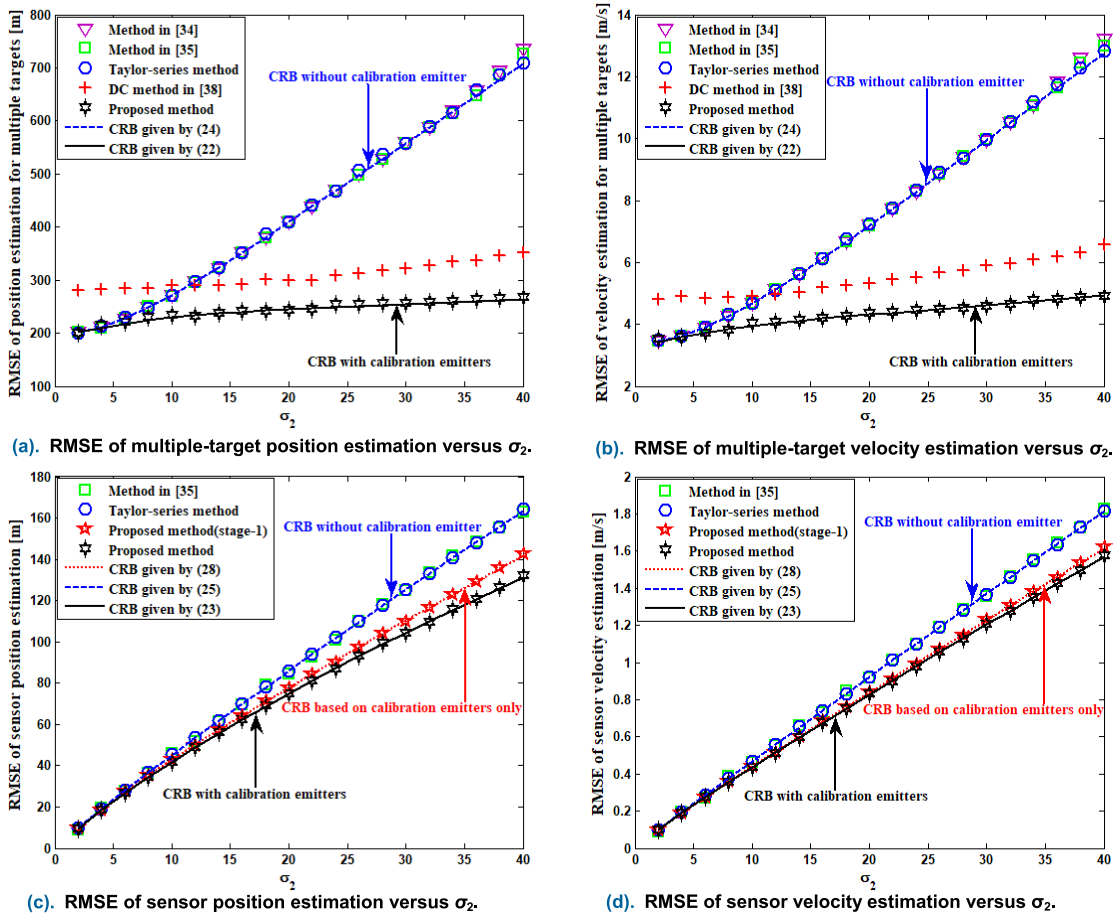

(a). RMSE of multiple-target position estimation versus σ_2.

(b). RMSE of multiple-target velocity estimation versus σ_2.

(c). RMSE of sensor position estimation versus σ_2.

(d). RMSE of sensor velocity estimation versus σ_2.

FIGURE 5. RMSE of multiple-target and sensor location estimation versus σ_2.

estimation, multiple-target velocity estimation, sensor position estimation and sensor velocity estimation as a function of σ_2, respectively.

From Figs.4 and 5 we can draw the following conclusions:

(1) The proposed method is able to reach the corresponding CRB accuracy under a moderate noise level. This is because the new estimator is established based on the WLS criterion, which yields an asymptotically efficient solution under Gaussian model. Note that we prove analytically using first order analysis that the estimation performances in both stage-1 and stage-2 asymptotically attain the relevant CRBs. Hence, the simulation results confirm the theoretical development in this work.

(2) The advantages of the new method over the TSWLS methods in [34], [35] and the Taylor-series iterative method extended from [51] are remarkable. The reason is that none of the compared methods exploits the measurements from the calibration signals. In other words, this significant performance gap mainly comes from the use of the calibration emitters. In addition, both the TSWLS methods and the Taylor-series iterative method can achieve CRB without calibration signal, before the thresholding effect starts to occur.

(3) Our method is superior to the DC technique and, moreover, the RMSE improvement increases as σ_1 increases. Besides, the RMSE of the DC method is larger than the associated CRB because its cost function is not asymptotically efficient. This observation is consistent with the analytical result in [38]. More importantly, the DC approach can not further refine the sensor position and velocity, while the proposed method can.

The third set of simulations is carried out to demonstrate that cooperation positioning for multiple targets can produce considerable performance gain compared to decoupled localization. For this purpose, the localization method presented in [43] is implemented for comparison. Since this method is developed for single-target localization scenario where the TDOA/FDOA measurements from both target source and calibration emitters are used, its performance can be chosen as benchmark to show performance improvement due to joint localization. The simulation scenario has an array of 8 moving sensors and their nominal positions and velocities are the same as in the previous experiments. These sensors are used to locate 3 moving target sources, which are positioned at $\boldsymbol{u}_1 = [7200\ 8400\ 7700]^{\mathrm{T}}$ (m), $\boldsymbol{u}_2 = [6500\ 6400\ 5600]^{\mathrm{T}}$ (m) and $\boldsymbol{u}_3 = [4600\ 4700\ 5400]^{\mathrm{T}}$ (m). Their velocities are set to be $\dot{\boldsymbol{u}}_1 = [14\ -12\ 10]^{\mathrm{T}}$ (m/s), $\dot{\boldsymbol{u}}_2 = [14\ -12\ -15]^{\mathrm{T}}$ (m/s) and

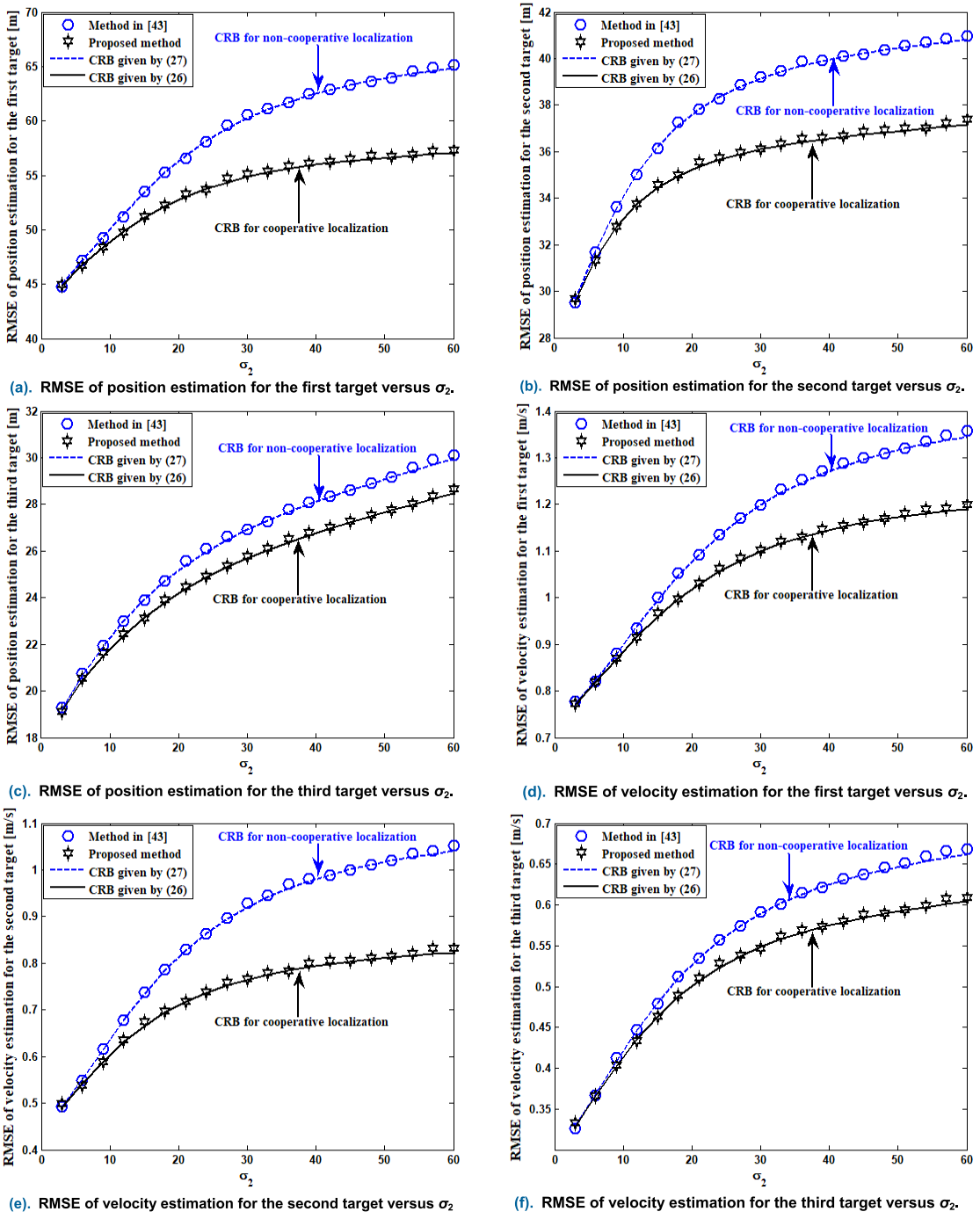

(a). RMSE of position estimation for the first target versus σ_2.

(b). RMSE of position estimation for the second target versus σ_2.

(c). RMSE of position estimation for the third target versus σ_2.

(d). RMSE of velocity estimation for the first target versus σ_2.

(e). RMSE of velocity estimation for the second target versus σ_2

(f). RMSE of velocity estimation for the third target versus σ_2.

FIGURE 6. RMSE of target location estimation versus σ_2 for each target source.

$\dot{\boldsymbol{u}}_3 = [-13\ 16\ 13]^{\mathrm{T}}$ (m/s). Besides, three calibration emitters are deployed near the target source, and they are located at $\boldsymbol{w}_1 = [7000\ 7000\ 8000]^{\mathrm{T}}$ (m), $\boldsymbol{w}_2 = [8000\ 9000\ 6000]^{\mathrm{T}}$ (m) and $\boldsymbol{w}_3 = [9000\ 6000\ 8000]^{\mathrm{T}}$ (m) with velocities $\dot{\boldsymbol{w}}_1 = [-12\ -18\ 14]^{\mathrm{T}}$ (m/s), $\dot{\boldsymbol{w}}_2 = [-16\ 15\ -12]^{\mathrm{T}}$ (m/s) and $\dot{\boldsymbol{w}}_3 = [10\ -14\ 18]^{\mathrm{T}}$ (m/s). Similar to the previous simulations, the TDOA/FDOA measurements from the target sources and calibration emitters are produced by adding to the true values zero-mean Gaussian noise with covariance matrix $\{\boldsymbol{E}_d\}_{1\le d\le 3}$ and $\{\boldsymbol{E}_n\}_{1\le n\le 3}$, respectively. The noisy sensor positions and velocities are created in a similar manner using covariance matrix $\bar{\boldsymbol{E}}_{\mathrm{B}}$. We fix $\boldsymbol{E}_d = 3^2\mathrm{blkdiag}[\boldsymbol{T}\ 0.01^2\boldsymbol{T}]$ and $\boldsymbol{E}_n = 3^2\mathrm{blkdiag}[\boldsymbol{T}\ 0.01^2\boldsymbol{T}](d\ ,\ n = 1\ ,\ 2\ ,\ 3)$, and set $\bar{\boldsymbol{E}}_{\mathrm{B}} = \sigma_2^2(\boldsymbol{I}_M \otimes \mathrm{blkdiag}[\boldsymbol{I}_3\ \ 0.01^2\boldsymbol{I}_3])$, where σ_2 varies from 3 to 60. Figs.6(a)-(f) illustrate the RMSEs of location estimation versus σ_2 for each target source.

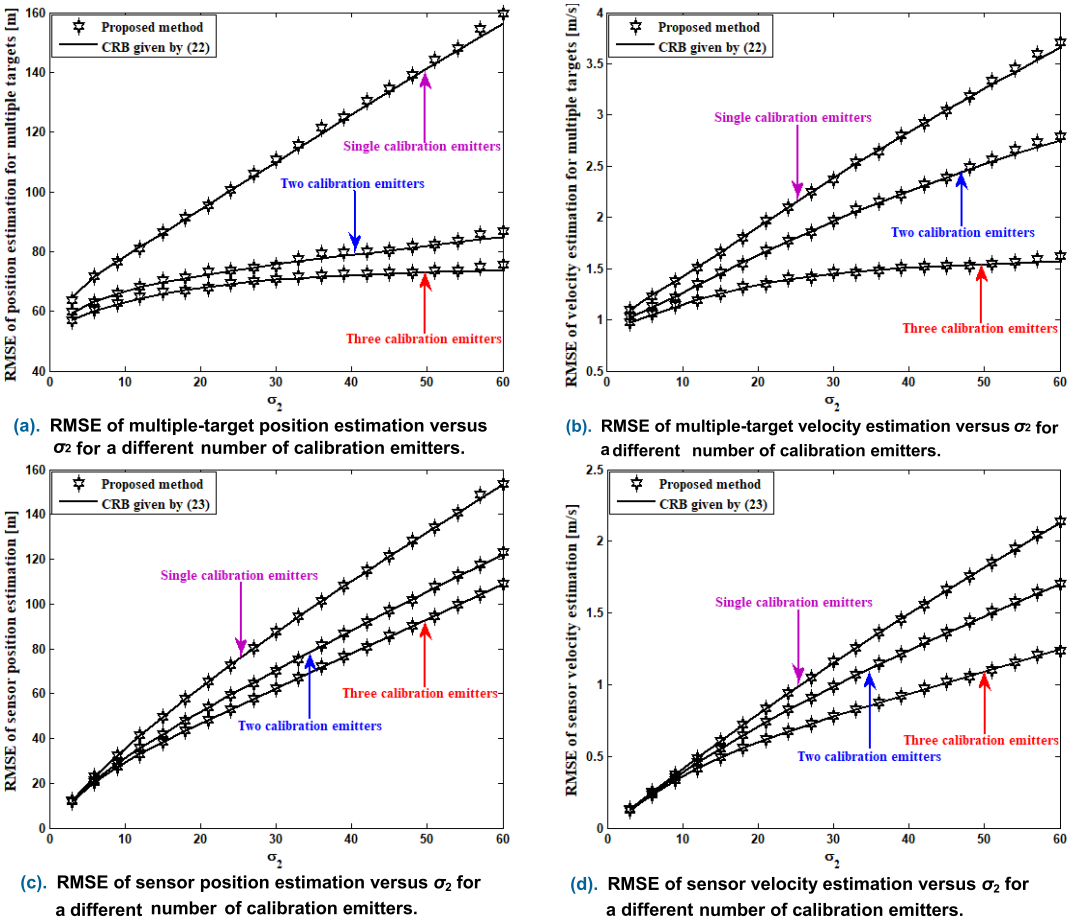

(a). RMSE of multiple-target position estimation versus σ_2 for a different number of calibration emitters.

(b). RMSE of multiple-target velocity estimation versus σ_2 for a different number of calibration emitters.

(c). RMSE of sensor position estimation versus σ_2 for a different number of calibration emitters.

(d). RMSE of sensor velocity estimation versus σ_2 for a different number of calibration emitters.

FIGURE 7. RMSE of target and sensor location estimation versus σ_2 for a different number of calibration emitters.

From Figs.6 we can draw the following conclusions:

(1) The performance improvement in positioning accuracy resulted from cooperative localization is noticeable.
(2) The RMSE gap is more pronounced as σ_2 increases. This is because when σ_2 is large, the uncertainties in sensor position and velocity dominate the performance and then the advantage of cooperative positioning over decoupled localization becomes significant.
(3) The estimation accuracy of the method in [43] is able to attain CRB for non-cooperative localization at moderate noise and error level. This observation confirms the analytical result in [43].

The fourth set of experiments studies the effect of the number of UAV calibration emitters. The simulation parameters are the same as those used to produce Fig.6. We examine the estimation accuracy of the new method for three cases. In the first case, single calibration emitter is used for target localization and it is located at $\boldsymbol{w}_1 = [7000\ 7000\ 8000]^{\mathrm{T}}$ (m) with velocity $\dot{\boldsymbol{w}}_1 = [-12\ \ -18\ \ 14]^{\mathrm{T}}$ (m/s). The second case assumes that there are two calibration emitters, which are positioned at $\boldsymbol{w}_1 = [7000\ \ 7000\ \ 8000]^{\mathrm{T}}$ (m) and $\boldsymbol{w}_2 = [8000\ \ 9000\ \ 6000]^{\mathrm{T}}$ (m) with velocities $\dot{\boldsymbol{w}}_1 = [-12\ \ -18\ \ 14]^{\mathrm{T}}$ (m/s) and $\dot{\boldsymbol{w}}_2 = [-16\ \ 15\ \ -12]^{\mathrm{T}}$ (m/s). In the third case, three calibration emitters are deployed for locating the targets and they are placed at $\boldsymbol{w}_1 = [7000\ 7000\ 8000]^{\mathrm{T}}$ (m), $\boldsymbol{w}_2 = [8000\ 9000\ 6000]^{\mathrm{T}}$ (m) and $\boldsymbol{w}_3 = [9000\ 6000\ 8000]^{\mathrm{T}}$ (m) with velocities $\dot{\boldsymbol{w}}_1 = [-12\ -18\ 14]^{\mathrm{T}}$ (m/s), $\dot{\boldsymbol{w}}_2 = [-16\ 15\ -12]^{\mathrm{T}}$ (m/s) and $\dot{\boldsymbol{w}}_3 = [10\ -14\ 18]^{\mathrm{T}}$ (m/s). We choose $\boldsymbol{E}_d = 3^2\mathrm{blkdiag}[\boldsymbol{T}\ 0.01^2\boldsymbol{T}]$ and $\boldsymbol{E}_n = 3^2\mathrm{blkdiag}[\boldsymbol{T}\ 0.01^2\boldsymbol{T}](d\ ,\ n = 1\ ,\ 2\ ,\ 3)$, and set $\bar{\boldsymbol{E}}_{\mathrm{B}} = \sigma_2^2(\boldsymbol{I}_M \otimes \mathrm{blkdiag}[\boldsymbol{I}_3\ 0.01^2\boldsymbol{I}_3])$, where σ_2 varies from 3 to 60. Figs.7(a)-(d) plot the RMSEs of multiple-target position estimation, multiple-target velocity estimation, sensor position

$$\tilde{\boldsymbol{P}}(\bar{\boldsymbol{r}},\bar{\boldsymbol{s}}) = \left[\begin{array}{c|c} (\bar{\boldsymbol{A}}(\bar{\boldsymbol{r}},\bar{\boldsymbol{s}}))^{\mathrm{T}}(\bar{\boldsymbol{C}}_1(\bar{\boldsymbol{t}},\bar{\boldsymbol{r}},\bar{\boldsymbol{s}}))^{-\mathrm{T}}\bar{\boldsymbol{E}}_{\mathrm{A}}^{-1}(\bar{\boldsymbol{C}}_1(\bar{\boldsymbol{t}},\bar{\boldsymbol{r}},\bar{\boldsymbol{s}}))^{-1}\bar{\boldsymbol{A}}(\bar{\boldsymbol{r}},\bar{\boldsymbol{s}}) & -(\bar{\boldsymbol{A}}(\bar{\boldsymbol{r}},\bar{\boldsymbol{s}}))^{\mathrm{T}}(\bar{\boldsymbol{C}}_1(\bar{\boldsymbol{t}},\bar{\boldsymbol{r}},\bar{\boldsymbol{s}}))^{-\mathrm{T}}\bar{\boldsymbol{E}}_{\mathrm{A}}^{-1}(\bar{\boldsymbol{C}}_1(\bar{\boldsymbol{t}},\bar{\boldsymbol{r}},\bar{\boldsymbol{s}}))^{-1}\bar{\boldsymbol{C}}_2(\bar{\boldsymbol{t}},\bar{\boldsymbol{r}},\bar{\boldsymbol{s}}) \\ \hline -(\bar{\boldsymbol{C}}_2(\bar{\boldsymbol{t}},\bar{\boldsymbol{r}},\bar{\boldsymbol{s}}))^{\mathrm{T}}(\bar{\boldsymbol{C}}_1(\bar{\boldsymbol{t}},\bar{\boldsymbol{r}},\bar{\boldsymbol{s}}))^{-\mathrm{T}}\bar{\boldsymbol{E}}_{\mathrm{A}}^{-1}(\bar{\boldsymbol{C}}_1(\bar{\boldsymbol{t}},\bar{\boldsymbol{r}},\bar{\boldsymbol{s}}))^{-1}\bar{\boldsymbol{A}}(\bar{\boldsymbol{r}},\bar{\boldsymbol{s}}) & \begin{array}{c}(\mathbf{MSE}(\hat{\bar{\boldsymbol{s}}}_{\mathrm{f}}))^{-1} + (\bar{\boldsymbol{C}}_2(\bar{\boldsymbol{t}},\bar{\boldsymbol{r}},\bar{\boldsymbol{s}}))^{\mathrm{T}}(\bar{\boldsymbol{C}}_1(\bar{\boldsymbol{t}},\bar{\boldsymbol{r}},\bar{\boldsymbol{s}}))^{-\mathrm{T}} \\ \times\bar{\boldsymbol{E}}_{\mathrm{A}}^{-1}(\bar{\boldsymbol{C}}_1(\bar{\boldsymbol{t}},\bar{\boldsymbol{r}},\bar{\boldsymbol{s}}))^{-1}\bar{\boldsymbol{C}}_2(\bar{\boldsymbol{t}},\bar{\boldsymbol{r}},\bar{\boldsymbol{s}})\end{array} \end{array}\right] \tag{124}$$

estimation and sensor velocity estimation as a function of σ_2, respectively.

From Figs.7 we can draw the following conclusions:

(1) The proposed estimator is shown to yield the solution reaching the CRB accuracy under moderate noise level. This finding can further support the theoretical development in Section VII.
(2) As expected, the localization accuracy will improve when more calibration signals are available for target localization. Furthermore, the higher the noise level, the greater the performance gain in estimation accuracy resulted from the increase in the number of calibration emitters. However, no matter how many calibration emitters exist, the positioning accuracy will not be higher than the bound for the case of no sensor location errors.

IX. CONCLUSION

This work focuses on the use of UAV calibration emitters for TDOA/FDOA multiple-target positioning in a wireless connected network. The study starts with deriving the CRB for TDOA/FDOA-based target location estimate when some UAV calibration emitters with known locations are available. The insight gained from the CRB reveals that the calibration signals are rather useful in reducing the effects of the uncertainties in sensor position and velocity. Moreover, the cooperative gain is significant when the multiple moving targets are located simultaneously in the presence of calibration emitters, even if the target sources are disjoint. The disjointness may be in time, frequency or both. The paper then proceeds to present a novel ICWLS estimator for multiple-target joint localization based on TDOA/FDOA measurements from both target sources and calibration emitters. The newly proposed method is composed of two stages. Specifically, the first stage refines the sensor locations by using the calibration TDOA/FDOA measurements as well as the statistical characteristic of the noisy sensor locations. The second stage provides the estimate of multiple-target locations by combining the measurements of target signals and the estimated values in the first stage. An efficient ICWLS algorithm is designed at each stage. Both the two algorithms are implemented based on matrix SVD, which is able to find a closed-form solution and update the weighting matrix at every iteration. Performance analysis of the proposed ICWLS estimator is also conducted, which consists of two parts: (1) analysis on convergence property; (2) derivation for estimation MSE. The results demonstrate that the proposed method, if converges, can produce the optimal solution of the formulated nonconvex CWLS problem. Besides, its estimation MSE can achieve CRB with calibration emitters at moderate noise. Simulation results verify the validity of the analytical results in this paper and confirm the superiority of the proposed method over some existing localization methods.

It is worthy to point out that the proposed estimator can be extended to reduce the effects of the clock offsets and frequency deviations on target localization accuracy. In future work, we will focus on this topic.

APPENDIX

A. PROOF OF $CRB(\bar{\boldsymbol{u}}_d) \le CRB_i(\bar{\boldsymbol{u}}_d)$ $(1 \le d \le D)$

First, it is readily checked that

$$\begin{cases} \bar{\boldsymbol{F}}_1(\bar{\boldsymbol{u}}, \bar{\boldsymbol{s}}) \\ = \text{blkdiag}[\boldsymbol{F}_1(\bar{\boldsymbol{u}}_1, \bar{\boldsymbol{s}})\ \boldsymbol{F}_1(\bar{\boldsymbol{u}}_2, \bar{\boldsymbol{s}})\ \cdots\ \boldsymbol{F}_1(\bar{\boldsymbol{u}}_D, \bar{\boldsymbol{s}})] \\ \bar{\boldsymbol{F}}_2(\bar{\boldsymbol{u}}, \bar{\boldsymbol{s}}) \\ = [(\boldsymbol{F}_2(\bar{\boldsymbol{u}}_1, \bar{\boldsymbol{s}}))^{\mathrm{T}}\ (\boldsymbol{F}_2(\bar{\boldsymbol{u}}_2, \bar{\boldsymbol{s}}))^{\mathrm{T}}\ \cdots\ (\boldsymbol{F}_2(\bar{\boldsymbol{u}}_D, \bar{\boldsymbol{s}}))^{\mathrm{T}}]^{\mathrm{T}} \end{cases} \tag{A.1}$$

For convenience, we define the matrix

$$\begin{aligned} \boldsymbol{X} = \bar{\boldsymbol{E}}_{\mathrm{A}} + \bar{\boldsymbol{F}}_2(\bar{\boldsymbol{u}}, \bar{\boldsymbol{s}}) \\ \times (\bar{\boldsymbol{E}}_{\mathrm{B}}^{-1} + (\bar{\boldsymbol{F}}^{(\mathrm{c})}(\bar{\boldsymbol{s}}))^{\mathrm{T}}(\bar{\boldsymbol{E}}_{\mathrm{A}}^{(\mathrm{c})})^{-1}\bar{\boldsymbol{F}}^{(\mathrm{c})}(\bar{\boldsymbol{s}}))^{-1}(\bar{\boldsymbol{F}}_2(\bar{\boldsymbol{u}}, \bar{\boldsymbol{s}}))^{\mathrm{T}}, \end{aligned} \tag{A.2}$$

and partition it into blocks (submatrices) as follows:

$$\boldsymbol{X} = \left[\begin{array}{c:c} \underbrace{\boldsymbol{X}_1}_{2(M-1)\times 2(M-1)} & \underbrace{\boldsymbol{X}_2}_{2(M-1)\times 2(D-1)(M-1)} \\ \hdashline \underbrace{\boldsymbol{X}_2^{\mathrm{T}}}_{2(D-1)(M-1)\times 2(M-1)} & \underbrace{\boldsymbol{X}_3}_{2(D-1)(M-1)\times 2(D-1)(M-1)} \end{array}\right] \tag{A.3}$$

Then, using the second equality in (A.1) yields

$$\begin{aligned} \boldsymbol{X}_1 = \boldsymbol{E}_1 + \boldsymbol{F}_2(\bar{\boldsymbol{u}}_1, \bar{\boldsymbol{s}}) \\ \times (\bar{\boldsymbol{E}}_{\mathrm{B}}^{-1} + (\bar{\boldsymbol{F}}^{(\mathrm{c})}(\bar{\boldsymbol{s}}))^{\mathrm{T}}(\bar{\boldsymbol{E}}_{\mathrm{A}}^{(\mathrm{c})})^{-1}\bar{\boldsymbol{F}}^{(\mathrm{c})}(\bar{\boldsymbol{s}}))^{-1}(\boldsymbol{F}_2(\bar{\boldsymbol{u}}_1, \bar{\boldsymbol{s}}))^{\mathrm{T}} \end{aligned} \tag{A.4}$$

Further, combining matrix identity (I) in Table 2, the first equality in (A.1) and (22) produces (A.5), as shown at the bottom of the next page.

where

$$\begin{cases} \boldsymbol{Y} = (\boldsymbol{X}_1 - \boldsymbol{X}_2\boldsymbol{X}_3^{-1}\boldsymbol{X}_2^{\mathrm{T}})^{-1}\ ;\ \boldsymbol{Z} = (\boldsymbol{X}_3 - \boldsymbol{X}_2^{\mathrm{T}}\boldsymbol{X}_1^{-1}\boldsymbol{X}_2)^{-1} \\ \tilde{\boldsymbol{F}}_{\mathrm{r}}(\bar{\boldsymbol{u}}, \bar{\boldsymbol{s}}) = \text{blkdiag}[\boldsymbol{F}_1(\bar{\boldsymbol{u}}_2, \bar{\boldsymbol{s}})\boldsymbol{F}_1(\bar{\boldsymbol{u}}_3, \bar{\boldsymbol{s}})\cdots\boldsymbol{F}_1(\bar{\boldsymbol{u}}_D, \bar{\boldsymbol{s}})] \end{cases} \tag{A.6}$$

It can be verified from (A.6) that $\boldsymbol{Y}\boldsymbol{X}_2\boldsymbol{X}_3^{-1} = \boldsymbol{X}_1^{-1}\boldsymbol{X}_2\boldsymbol{Z}$. Then, from (A.5) and matrix identity (I) in Table 2, we get

$$\begin{cases} (\mathbf{CRB}(\bar{\boldsymbol{u}}_1))^{-1} = (\boldsymbol{F}_1(\bar{\boldsymbol{u}}_1, \bar{\boldsymbol{s}}))^{\mathrm{T}}\boldsymbol{Y}\boldsymbol{F}_1(\bar{\boldsymbol{u}}_1, \bar{\boldsymbol{s}}) \\ -(\boldsymbol{F}_1(\bar{\boldsymbol{u}}_1, \bar{\boldsymbol{s}}))^{\mathrm{T}}\boldsymbol{X}_1^{-1}\boldsymbol{X}_2\boldsymbol{Z}\tilde{\boldsymbol{F}}_{\mathrm{r}}(\bar{\boldsymbol{u}}, \bar{\boldsymbol{s}}) \\ \times((\tilde{\boldsymbol{F}}_{\mathrm{r}}(\bar{\boldsymbol{u}}, \bar{\boldsymbol{s}}))^{\mathrm{T}}\boldsymbol{Z}\tilde{\boldsymbol{F}}_{\mathrm{r}}(\bar{\boldsymbol{u}}, \bar{\boldsymbol{s}}))^{-1}(\tilde{\boldsymbol{F}}_{\mathrm{r}}(\bar{\boldsymbol{u}}, \bar{\boldsymbol{s}}))^{\mathrm{T}}\boldsymbol{Z}\boldsymbol{X}_2^{\mathrm{T}}\boldsymbol{X}_1^{-1}\boldsymbol{F}_1(\bar{\boldsymbol{u}}_1, \bar{\boldsymbol{s}}) \\ (\mathbf{CRB}(\tilde{\boldsymbol{u}}_{\mathrm{r}}))^{-1} = (\tilde{\boldsymbol{F}}_{\mathrm{r}}(\bar{\boldsymbol{u}}, \bar{\boldsymbol{s}}))^{\mathrm{T}}\boldsymbol{Z}\tilde{\boldsymbol{F}}_{\mathrm{r}}(\bar{\boldsymbol{u}}, \bar{\boldsymbol{s}}) \\ -(\tilde{\boldsymbol{F}}_{\mathrm{r}}(\bar{\boldsymbol{u}}, \bar{\boldsymbol{s}}))^{\mathrm{T}}\boldsymbol{X}_3^{-1}\boldsymbol{X}_2^{\mathrm{T}}\boldsymbol{Y}\boldsymbol{F}_1(\bar{\boldsymbol{u}}_1, \bar{\boldsymbol{s}}) \\ \times((\boldsymbol{F}_1(\bar{\boldsymbol{u}}_1, \bar{\boldsymbol{s}}))^{\mathrm{T}}\boldsymbol{Y}\boldsymbol{F}_1(\bar{\boldsymbol{u}}_1, \bar{\boldsymbol{s}}))^{-1}(\boldsymbol{F}_1(\bar{\boldsymbol{u}}_1, \bar{\boldsymbol{s}}))^{\mathrm{T}}\boldsymbol{Y}\boldsymbol{X}_2\boldsymbol{X}_3^{-1}\tilde{\boldsymbol{F}}_{\mathrm{r}}(\bar{\boldsymbol{u}}, \bar{\boldsymbol{s}}) \end{cases} \tag{A.7}$$

where $\tilde{\boldsymbol{u}}_{\mathrm{r}} = [\bar{\boldsymbol{u}}_2^{\mathrm{T}}\ \bar{\boldsymbol{u}}_3^{\mathrm{T}}\ \cdots\ \bar{\boldsymbol{u}}_D^{\mathrm{T}}]^{\mathrm{T}}$, which does not comprise the first location vector $\boldsymbol{u}_1$.

On the other hand, it readily follows from matrix identity (II) in Table 2 that

$$\begin{cases} \boldsymbol{Y} = \boldsymbol{X}_1^{-1} + \boldsymbol{X}_1^{-1}\boldsymbol{X}_2\boldsymbol{Z}\boldsymbol{X}_2^{\mathrm{T}}\boldsymbol{X}_1^{-1} \\ \boldsymbol{Z} = \boldsymbol{X}_3^{-1} + \boldsymbol{X}_3^{-1}\boldsymbol{X}_2^{\mathrm{T}}\boldsymbol{Y}\boldsymbol{X}_2\boldsymbol{X}_3^{-1} \end{cases} \tag{A.8}$$

Putting (A.8) back into (A.7) produces

$$\begin{cases} (\mathbf{CRB}(\bar{\boldsymbol{u}}_1))^{-1} = (\boldsymbol{F}_1(\bar{\boldsymbol{u}}_1,\bar{\boldsymbol{s}}))^{\mathrm{T}}\boldsymbol{X}_1^{-1}\boldsymbol{F}_1(\bar{\boldsymbol{u}}_1,\bar{\boldsymbol{s}}) \\ +(\boldsymbol{F}_1(\bar{\boldsymbol{u}}_1,\bar{\boldsymbol{s}}))^{\mathrm{T}}\boldsymbol{X}_1^{-1}\boldsymbol{X}_2\boldsymbol{Z}_0\boldsymbol{X}_2^{\mathrm{T}}\boldsymbol{X}_1^{-1}\boldsymbol{F}_1(\bar{\boldsymbol{u}}_1,\bar{\boldsymbol{s}}) \\ (\mathbf{CRB}(\tilde{\boldsymbol{u}}_{\mathrm{r}}))^{-1} = (\tilde{\boldsymbol{F}}_{\mathrm{r}}(\bar{\boldsymbol{u}},\bar{\boldsymbol{s}}))^{\mathrm{T}}\boldsymbol{X}_3^{-1}\tilde{\boldsymbol{F}}_{\mathrm{r}}(\bar{\boldsymbol{u}},\bar{\boldsymbol{s}}) \\ +(\tilde{\boldsymbol{F}}_{\mathrm{r}}(\bar{\boldsymbol{u}},\bar{\boldsymbol{s}}))^{\mathrm{T}}\boldsymbol{X}_3^{-1}\boldsymbol{X}_2^{\mathrm{T}}\boldsymbol{Y}_0\boldsymbol{X}_2\boldsymbol{X}_3^{-1}\tilde{\boldsymbol{F}}_{\mathrm{r}}(\bar{\boldsymbol{u}},\bar{\boldsymbol{s}}) \end{cases} \tag{A.9}$$

where

$$\begin{cases} \boldsymbol{Y}_0 = \boldsymbol{Y} - \boldsymbol{Y}\boldsymbol{F}_1(\bar{\boldsymbol{u}}_1,\bar{\boldsymbol{s}})((\boldsymbol{F}_1(\bar{\boldsymbol{u}}_1,\bar{\boldsymbol{s}}))^{\mathrm{T}}\boldsymbol{Y}\boldsymbol{F}_1(\bar{\boldsymbol{u}}_1,\bar{\boldsymbol{s}}))^{-1} \\ \times(\boldsymbol{F}_1(\bar{\boldsymbol{u}}_1,\bar{\boldsymbol{s}}))^{\mathrm{T}}\boldsymbol{Y} \\ \boldsymbol{Z}_0 = \boldsymbol{Z} - \boldsymbol{Z}\tilde{\boldsymbol{F}}_{\mathrm{r}}(\bar{\boldsymbol{u}},\bar{\boldsymbol{s}})((\tilde{\boldsymbol{F}}_{\mathrm{r}}(\bar{\boldsymbol{u}},\bar{\boldsymbol{s}}))^{\mathrm{T}}\boldsymbol{Z}\tilde{\boldsymbol{F}}_{\mathrm{r}}(\bar{\boldsymbol{u}},\bar{\boldsymbol{s}}))^{-1} \\ \times(\tilde{\boldsymbol{F}}_{\mathrm{r}}(\bar{\boldsymbol{u}},\bar{\boldsymbol{s}}))^{\mathrm{T}}\boldsymbol{Z} \end{cases} \tag{A.10}$$

According to the definition of orthogonal projection matrix, (A.10) can be rewritten as

$$\begin{cases} \boldsymbol{Y}_0 = \boldsymbol{Y}^{1/2}\boldsymbol{\Pi}^{\perp}[\boldsymbol{Y}^{1/2}\boldsymbol{F}_1(\bar{\boldsymbol{u}}_1,\bar{\boldsymbol{s}})]\boldsymbol{Y}^{1/2} \geq \boldsymbol{O} \\ \boldsymbol{Z}_0 = \boldsymbol{Z}^{1/2}\boldsymbol{\Pi}^{\perp}[\boldsymbol{Z}^{1/2}\tilde{\boldsymbol{F}}_{\mathrm{r}}(\bar{\boldsymbol{u}},\bar{\boldsymbol{s}})]\boldsymbol{Z}^{1/2} \geq \boldsymbol{O} \end{cases} \tag{A.11}$$

Substituting (A.11) into the first equality in (A.9) and using (A.4) lead to

$$\begin{aligned} &(\mathbf{CRB}(\bar{\boldsymbol{u}}_1))^{-1} \\ &\geq (\boldsymbol{F}_1(\bar{\boldsymbol{u}}_1,\bar{\boldsymbol{s}}))^{\mathrm{T}}\boldsymbol{X}_1^{-1}\boldsymbol{F}_1(\bar{\boldsymbol{u}}_1,\bar{\boldsymbol{s}}) \\ &= (\boldsymbol{F}_1(\bar{\boldsymbol{u}}_1,\bar{\boldsymbol{s}}))^{\mathrm{T}}\left(\begin{array}{l}\boldsymbol{E}_1 + \boldsymbol{F}_2(\bar{\boldsymbol{u}}_1,\bar{\boldsymbol{s}}) \\ \times\begin{pmatrix}\bar{\boldsymbol{E}}_{\mathrm{B}}^{-1} + (\bar{\boldsymbol{F}}^{(\mathrm{c})}(\bar{\boldsymbol{s}}))^{\mathrm{T}} \\ \times(\bar{\boldsymbol{E}}_{\mathrm{A}}^{(\mathrm{c})})^{-1}\bar{\boldsymbol{F}}^{(\mathrm{c})}(\bar{\boldsymbol{s}})\end{pmatrix}^{-1}(\boldsymbol{F}_2(\bar{\boldsymbol{u}}_1,\bar{\boldsymbol{s}}))^{\mathrm{T}}\end{array}\right)^{-1} \\ &\quad\times\boldsymbol{F}_1(\bar{\boldsymbol{u}}_1,\bar{\boldsymbol{s}}) \\ &= (\mathbf{CRB}_{\mathrm{i}}(\bar{\boldsymbol{u}}_1))^{-1} \end{aligned} \tag{A.12}$$

which implies $\mathbf{CRB}(\bar{\boldsymbol{u}}_1) \leq \mathbf{CRB}_{\mathrm{i}}(\bar{\boldsymbol{u}}_1)$. The derivation described above can be easily extend to prove $\mathbf{CRB}(\bar{\boldsymbol{u}}_d) \leq \mathbf{CRB}_{\mathrm{i}}(\bar{\boldsymbol{u}}_d)$ for $2 \leq d \leq D$, as long as we exchange the order of $\bar{\boldsymbol{u}}_1$ and $\bar{\boldsymbol{u}}_d$ in composite location vector $\bar{\boldsymbol{u}}$. At this point, the proof is completed.

B. PROOF OF PROPOSITION 2

It can be easily checked from (80) that

$$\begin{aligned} (\boldsymbol{G}^{(\mathrm{c})}(\hat{\boldsymbol{\eta}}(k)))^{\mathrm{T}} &= (\boldsymbol{Q}_{11}^{(\mathrm{c})}(k+1)\boldsymbol{\Sigma}_1^{(\mathrm{c})}(k+1)(\boldsymbol{R}_1^{(\mathrm{c})}(k+1))^{\mathrm{T}})^{\mathrm{T}} \\ &= \boldsymbol{R}_1^{(\mathrm{c})}(k+1)\boldsymbol{\Sigma}_1^{(\mathrm{c})}(k+1)(\boldsymbol{Q}_{11}^{(\mathrm{c})}(k+1))^{\mathrm{T}} \end{aligned} \tag{B.1}$$

Combining (B.1) and (82) gives

$$\begin{aligned} &(\boldsymbol{G}^{(\mathrm{c})}(\hat{\boldsymbol{\eta}}(k)))^{\mathrm{T}}\boldsymbol{Q}_{11}^{(\mathrm{c})}(k+1)\boldsymbol{x}_1(k+1) \\ &= \boldsymbol{R}_1^{(\mathrm{c})}(k+1)\boldsymbol{\Sigma}_1^{(\mathrm{c})}(k+1)(\boldsymbol{Q}_{11}^{(\mathrm{c})}(k+1))^{\mathrm{T}}\boldsymbol{Q}_{11}^{(\mathrm{c})}(k+1)\boldsymbol{x}_1(k+1) \\ &= \boldsymbol{R}_1^{(\mathrm{c})}(k+1)\boldsymbol{\Sigma}_1^{(\mathrm{c})}(k+1)\boldsymbol{x}_1(k+1) = \boldsymbol{g}^{(\mathrm{c})}(\hat{\boldsymbol{\eta}}(k)) \end{aligned} \tag{B.2}$$

where the second equality uses the relation $(\boldsymbol{Q}_{11}^{(\mathrm{c})}(k+1))^{\mathrm{T}}\boldsymbol{Q}_{11}^{(\mathrm{c})}(k+1) = \boldsymbol{I}$. From (B.1) and (B.2), it can be seen that the vector $\boldsymbol{Q}_{11}^{(\mathrm{c})}(k+1)\boldsymbol{x}_1(k+1)$ satisfies the equality constraint in (75). As a consequence, we can write the optimal solution of (75) as

$$\hat{\boldsymbol{\eta}}_{\mathrm{opt}}(k+1) = \boldsymbol{Q}_{11}^{(\mathrm{c})}(k+1)\boldsymbol{x}_1(k+1) + \hat{\boldsymbol{\eta}}_{\mathrm{o}}(k+1) \tag{B.3}$$

where $\hat{\boldsymbol{\eta}}_{\mathrm{o}}(k+1)$ fulfils the linear equation $(\boldsymbol{G}^{(\mathrm{c})}(\hat{\boldsymbol{\eta}}(k)))^{\mathrm{T}}\hat{\boldsymbol{\eta}}_{\mathrm{o}}(k+1) = \boldsymbol{O}$ and, moreover, it should minimize the cost function in (75). We are now ready to prove that the vector $\hat{\boldsymbol{\eta}}_{\mathrm{o}}(k+1)$ is equal to $\boldsymbol{Q}_{12}^{(\mathrm{c})}(k+1)\boldsymbol{x}_2(k+1)$.

Since $\hat{\boldsymbol{\eta}}_{\mathrm{o}}(k+1)$ belongs to the null space of $(\boldsymbol{G}^{(\mathrm{c})}(\hat{\boldsymbol{\eta}}(k)))^{\mathrm{T}}$, it can be expressed as

$$\hat{\boldsymbol{\eta}}_{\mathrm{o}}(k+1) = \boldsymbol{Q}_{12}^{(\mathrm{c})}(k+1)\boldsymbol{z}_{\mathrm{o}} \tag{B.4}$$

where $\boldsymbol{z}_{\mathrm{o}} \in R^{6M\times 1}$ needs to be determined. Inserting (B.3) and (B.4) into the objective function in (75) yields

$$\begin{aligned} &J^{(\mathrm{c})}(\hat{\boldsymbol{\eta}}_{\mathrm{opt}}(k+1)) \\ &= (\tilde{\boldsymbol{A}}^{(\mathrm{c})}(\hat{\bar{\boldsymbol{r}}}^{(\mathrm{c})})\hat{\boldsymbol{\eta}}_{\mathrm{opt}}(k+1) - \tilde{\boldsymbol{b}}^{(\mathrm{c})}(\hat{\bar{\boldsymbol{r}}}^{(\mathrm{c})},\hat{\bar{\boldsymbol{s}}}))^{\mathrm{T}}(\tilde{\boldsymbol{\Phi}}^{(\mathrm{c})})^{-1} \\ &\quad\times(\tilde{\boldsymbol{A}}^{(\mathrm{c})}(\hat{\bar{\boldsymbol{r}}}^{(\mathrm{c})})\hat{\boldsymbol{\eta}}_{\mathrm{opt}}(k+1) - \tilde{\boldsymbol{b}}^{(\mathrm{c})}(\hat{\bar{\boldsymbol{r}}}^{(\mathrm{c})},\hat{\bar{\boldsymbol{s}}})) \\ &= ||(\tilde{\boldsymbol{\Phi}}^{(\mathrm{c})})^{-1/2}\tilde{\boldsymbol{A}}^{(\mathrm{c})}(\hat{\bar{\boldsymbol{r}}}^{(\mathrm{c})})\boldsymbol{Q}_{12}^{(\mathrm{c})}(k+1)\boldsymbol{z}_{\mathrm{o}} - (\tilde{\boldsymbol{\Phi}}^{(\mathrm{c})})^{-1/2} \\ &\quad\times(\tilde{\boldsymbol{b}}^{(\mathrm{c})}(\hat{\bar{\boldsymbol{r}}}^{(\mathrm{c})},\hat{\bar{\boldsymbol{s}}}) - \tilde{\boldsymbol{A}}^{(\mathrm{c})}(\hat{\bar{\boldsymbol{r}}}^{(\mathrm{c})})\boldsymbol{Q}_{11}^{(\mathrm{c})}(k+1)\boldsymbol{x}_1(k+1))||_2^2 \end{aligned} \tag{B.5}$$

Substituting (83) into (B.5) leads to (B.6), as shown at the bottom of the next page, which implies that the objective function reaches its minimum value at $\boldsymbol{z}_0 = \boldsymbol{x}_2(k+1)$. Then, combining (B.3) and (B.4) we have

$$\hat{\boldsymbol{\eta}}_{\mathrm{opt}}(k+1) = \boldsymbol{Q}_{11}^{(\mathrm{c})}(k+1)\boldsymbol{x}_1(k+1) + \boldsymbol{Q}_{12}^{(\mathrm{c})}(k+1)\boldsymbol{x}_2(k+1) \tag{B.7}$$

At this point, the proof is ended.

C. PROOF OF PROPOSITION 4

It can be seen from (76), (78) and (90) that (C.2), as shown at the bottom of the next page.

$$\begin{aligned} &(\tilde{\boldsymbol{A}}^{(\mathrm{c})}(\hat{\bar{\boldsymbol{r}}}^{(\mathrm{c})}))^{\mathrm{T}}(\tilde{\boldsymbol{\Phi}}^{(\mathrm{c})})^{-1}\tilde{\boldsymbol{A}}^{(\mathrm{c})}(\hat{\bar{\boldsymbol{r}}}^{(\mathrm{c})})\hat{\boldsymbol{\eta}}_{\mathrm{opt}}(k+1) \\ &= (\tilde{\boldsymbol{A}}^{(\mathrm{c})}(\hat{\bar{\boldsymbol{r}}}^{(\mathrm{c})}))^{\mathrm{T}}(\tilde{\boldsymbol{\Phi}}^{(\mathrm{c})})^{-1}\tilde{\boldsymbol{b}}^{(\mathrm{c})}(\hat{\bar{\boldsymbol{r}}}^{(\mathrm{c})},\hat{\bar{\boldsymbol{s}}}) \\ &\quad - \frac{1}{2}\boldsymbol{G}^{(\mathrm{c})}(\hat{\boldsymbol{\eta}}(k))\boldsymbol{\lambda}^{(\mathrm{c})}(k+1) \\ &\Rightarrow \hat{\boldsymbol{\eta}}_{\mathrm{opt}}(k+1) = ((\tilde{\boldsymbol{A}}^{(\mathrm{c})}(\hat{\bar{\boldsymbol{r}}}^{(\mathrm{c})}))^{\mathrm{T}}(\tilde{\boldsymbol{\Phi}}^{(\mathrm{c})})^{-1}\tilde{\boldsymbol{A}}^{(\mathrm{c})}(\hat{\bar{\boldsymbol{r}}}^{(\mathrm{c})}))^{-1} \\ &\quad\times\begin{pmatrix}(\tilde{\boldsymbol{A}}^{(\mathrm{c})}(\hat{\bar{\boldsymbol{r}}}^{(\mathrm{c})}))^{\mathrm{T}}(\tilde{\boldsymbol{\Phi}}^{(\mathrm{c})})^{-1}\tilde{\boldsymbol{b}}^{(\mathrm{c})}(\hat{\bar{\boldsymbol{r}}}^{(\mathrm{c})},\hat{\bar{\boldsymbol{s}}}) \\ -\frac{1}{2}\boldsymbol{G}^{(\mathrm{c})}(\hat{\boldsymbol{\eta}}(k))\boldsymbol{\lambda}^{(\mathrm{c})}(k+1)\end{pmatrix} \end{aligned} \tag{C.1}$$

$$\mathbf{CRB}(\bar{\boldsymbol{u}}) = \left[\begin{array}{c:c}(\boldsymbol{F}_1(\bar{\boldsymbol{u}}_1,\bar{\boldsymbol{s}}))^{\mathrm{T}}\boldsymbol{Y}\boldsymbol{F}_1(\bar{\boldsymbol{u}}_1,\bar{\boldsymbol{s}}) & -(\boldsymbol{F}_1(\bar{\boldsymbol{u}}_1,\bar{\boldsymbol{s}}))^{\mathrm{T}}\boldsymbol{Y}\boldsymbol{X}_2\boldsymbol{X}_3^{-1}\tilde{\boldsymbol{F}}_{\mathrm{r}}(\bar{\boldsymbol{u}},\bar{\boldsymbol{s}}) \\ \hdashline -(\tilde{\boldsymbol{F}}_{\mathrm{r}}(\bar{\boldsymbol{u}},\bar{\boldsymbol{s}}))^{\mathrm{T}}\boldsymbol{X}_3^{-1}\boldsymbol{X}_2^{\mathrm{T}}\boldsymbol{Y}\boldsymbol{F}_1(\bar{\boldsymbol{u}}_1,\bar{\boldsymbol{s}}) & (\tilde{\boldsymbol{F}}_{\mathrm{r}}(\bar{\boldsymbol{u}},\bar{\boldsymbol{s}}))^{\mathrm{T}}\boldsymbol{Z}\tilde{\boldsymbol{F}}_{\mathrm{r}}(\bar{\boldsymbol{u}},\bar{\boldsymbol{s}})\end{array}\right]^{-1} \tag{A.5}$$

Inserting (C.1) into the equality constraints in (75) and using some algebraic manipulations yield

$$\begin{aligned}&\boldsymbol{\lambda}^{(\mathrm{c})}(k+1)\\&=2((\boldsymbol{G}^{(\mathrm{c})}(\hat{\boldsymbol{\eta}}(k)))^{\mathrm{T}}((\tilde{\boldsymbol{A}}^{(\mathrm{c})}(\hat{\tilde{\boldsymbol{r}}}^{(\mathrm{c})}))^{\mathrm{T}}(\tilde{\boldsymbol{\Phi}}^{(\mathrm{c})})^{-1}\tilde{\boldsymbol{A}}^{(\mathrm{c})}(\hat{\tilde{\boldsymbol{r}}}^{(\mathrm{c})}))^{-1}\\&\quad\times\boldsymbol{G}^{(\mathrm{c})}(\hat{\boldsymbol{\eta}}(k)))^{-1}\times((\boldsymbol{G}^{(\mathrm{c})}(\hat{\boldsymbol{\eta}}(k)))^{\mathrm{T}}((\tilde{\boldsymbol{A}}^{(\mathrm{c})}(\hat{\tilde{\boldsymbol{r}}}^{(\mathrm{c})}))^{\mathrm{T}}(\tilde{\boldsymbol{\Phi}}^{(\mathrm{c})})^{-1}\\&\quad\times\tilde{\boldsymbol{A}}^{(\mathrm{c})}(\hat{\tilde{\boldsymbol{r}}}^{(\mathrm{c})}))^{-1}(\tilde{\boldsymbol{A}}^{(\mathrm{c})}(\hat{\tilde{\boldsymbol{r}}}^{(\mathrm{c})}))^{\mathrm{T}}(\tilde{\boldsymbol{\Phi}}^{(\mathrm{c})})^{-1}\tilde{\boldsymbol{b}}^{(\mathrm{c})}(\hat{\tilde{\boldsymbol{r}}}^{(\mathrm{c})},\hat{\tilde{\boldsymbol{s}}})\\&\quad-\boldsymbol{g}^{(\mathrm{c})}(\hat{\boldsymbol{\eta}}(k)))\end{aligned}\tag{C.3}$$

If $\{\hat{\boldsymbol{\eta}}(k+1)\}_{0\le k\le+\infty}$ converges to $\hat{\boldsymbol{\eta}}_{\mathrm{f}}$, then it can be shown from (76)-(78) that

$$\begin{cases}\boldsymbol{g}^{(\mathrm{c})}(\hat{\boldsymbol{\eta}}_{\mathrm{f}})=\lim\limits_{k\to+\infty}\boldsymbol{g}^{(\mathrm{c})}(\hat{\boldsymbol{\eta}}(k))\\=[(\boldsymbol{g}_1^{(\mathrm{c})}(\hat{\boldsymbol{\eta}}_{\mathrm{f}}))^{\mathrm{T}}(\boldsymbol{g}_2^{(\mathrm{c})}(\hat{\boldsymbol{\eta}}_{\mathrm{f}}))^{\mathrm{T}}(\boldsymbol{g}_3^{(\mathrm{c})}(\hat{\boldsymbol{\eta}}_{\mathrm{f}}))^{\mathrm{T}}(\boldsymbol{g}_4^{(\mathrm{c})}(\hat{\boldsymbol{\eta}}_{\mathrm{f}}))^{\mathrm{T}}]^{\mathrm{T}}\\\boldsymbol{G}^{(\mathrm{c})}(\hat{\boldsymbol{\eta}}_{\mathrm{f}})=\lim\limits_{k\to+\infty}\boldsymbol{G}^{(\mathrm{c})}(\hat{\boldsymbol{\eta}}(k))\\=[\boldsymbol{G}_1^{(\mathrm{c})}(\hat{\boldsymbol{\eta}}_{\mathrm{f}})\,\boldsymbol{G}_2^{(\mathrm{c})}(\hat{\boldsymbol{\eta}}_{\mathrm{f}})\,\boldsymbol{G}_3^{(\mathrm{c})}(\hat{\boldsymbol{\eta}}_{\mathrm{f}})\,\boldsymbol{G}_4^{(\mathrm{c})}(\hat{\boldsymbol{\eta}}_{\mathrm{f}})]\end{cases}\tag{C.4}$$

where

Putting (C.4) into (C.3) leads to

$$\begin{aligned}&\lim_{k\to+\infty}\boldsymbol{\lambda}^{(\mathrm{c})}(k+1)\\&=2((\boldsymbol{G}^{(\mathrm{c})}(\hat{\boldsymbol{\eta}}_{\mathrm{f}}))^{\mathrm{T}}((\tilde{\boldsymbol{A}}^{(\mathrm{c})}(\hat{\tilde{\boldsymbol{r}}}^{(\mathrm{c})}))^{\mathrm{T}}(\tilde{\boldsymbol{\Phi}}^{(\mathrm{c})})^{-1}\tilde{\boldsymbol{A}}^{(\mathrm{c})}(\hat{\tilde{\boldsymbol{r}}}^{(\mathrm{c})}))^{-1}\boldsymbol{G}^{(\mathrm{c})}(\hat{\boldsymbol{\eta}}_{\mathrm{f}}))^{-1}\\&\quad\times((\boldsymbol{G}^{(\mathrm{c})}(\hat{\boldsymbol{\eta}}_{\mathrm{f}}))^{\mathrm{T}}((\tilde{\boldsymbol{A}}^{(\mathrm{c})}(\hat{\tilde{\boldsymbol{r}}}^{(\mathrm{c})}))^{\mathrm{T}}(\tilde{\boldsymbol{\Phi}}^{(\mathrm{c})})^{-1}\\&\quad\times\tilde{\boldsymbol{A}}^{(\mathrm{c})}(\hat{\tilde{\boldsymbol{r}}}^{(\mathrm{c})}))^{-1}(\tilde{\boldsymbol{A}}^{(\mathrm{c})}(\hat{\tilde{\boldsymbol{r}}}^{(\mathrm{c})}))^{\mathrm{T}}(\tilde{\boldsymbol{\Phi}}^{(\mathrm{c})})^{-1}\tilde{\boldsymbol{b}}^{(\mathrm{c})}(\hat{\tilde{\boldsymbol{r}}}^{(\mathrm{c})},\hat{\tilde{\boldsymbol{s}}})-\boldsymbol{g}^{(\mathrm{c})}(\hat{\boldsymbol{\eta}}_{\mathrm{f}}))\end{aligned}\tag{C.7}$$

which implies that the sequences $\{\lambda_{1m}^{(\mathrm{c})}(k+1)\}_{0\le k\le+\infty}$, $\{\lambda_{2m}^{(\mathrm{c})}(k+1)\}_{0\le k\le+\infty}$, $\{\lambda_{3n}^{(\mathrm{c})}(k+1)\}_{0\le k\le+\infty}$ and $\{\lambda_{4n}^{(\mathrm{c})}(k+1)\}_{0\le k\le+\infty}$ converge for arbitrary $1\le m\le M$ and $1\le n\le N$. At this point, the proof is completed.

D. PROOF OF PROPOSITION 5

Since $\{\hat{\boldsymbol{\eta}}(k+1)\}_{0\le k\le+\infty}$ converges, it can be seen from Proposition 4 that the sequences $\{\lambda_{1m}^{(\mathrm{c})}(k+1)\}_{0\le k\le+\infty}$, $\{\lambda_{2m}^{(\mathrm{c})}(k+1)\}_{0\le k\le+\infty}$, $\{\lambda_{3n}^{(\mathrm{c})}(k+1)\}_{0\le k\le+\infty}$ and $\{\lambda_{4n}^{(\mathrm{c})}(k+1)\}_{0\le k\le+\infty}$ also converge for arbitrary $1\le m\le M$ and $1\le n\le N$. Let $\lim\limits_{k\to+\infty}\hat{\boldsymbol{\eta}}(k+1)=\hat{\boldsymbol{\eta}}_{\mathrm{f}}$, $\lim\limits_{k\to+\infty}\lambda_{1m}^{(\mathrm{c})}(k+1)=\lambda_{1m,\mathrm{f}}^{(\mathrm{c})}$, $\lim\limits_{k\to+\infty}\lambda_{2m}^{(\mathrm{c})}(k+1)=\lambda_{2m,\mathrm{f}}^{(\mathrm{c})}$, $\lim\limits_{k\to+\infty}\lambda_{3n}^{(\mathrm{c})}(k+1)=\lambda_{3n,\mathrm{f}}^{(\mathrm{c})}$ and $\lim\limits_{k\to+\infty}\lambda_{4n}^{(\mathrm{c})}(k+1)=\lambda_{4n,\mathrm{f}}^{(\mathrm{c})}$. Using Proposition 3 yields $\lim\limits_{k\to+\infty}\hat{\boldsymbol{\eta}}_{\mathrm{opt}}(k+1)=\lim\limits_{k\to+\infty}\hat{\boldsymbol{\eta}}(k+1)=\hat{\boldsymbol{\eta}}_{\mathrm{f}}$. Then, taking the limit on both sides of (90) produces

$$\begin{aligned}&(\tilde{\boldsymbol{A}}^{(\mathrm{c})}(\hat{\tilde{\boldsymbol{r}}}^{(\mathrm{c})}))^{\mathrm{T}}(\tilde{\boldsymbol{\Phi}}^{(\mathrm{c})})^{-1}(\tilde{\boldsymbol{A}}^{(\mathrm{c})}(\hat{\tilde{\boldsymbol{r}}}^{(\mathrm{c})})\hat{\boldsymbol{\eta}}_{\mathrm{f}}-\tilde{\boldsymbol{b}}^{(\mathrm{c})}(\hat{\tilde{\boldsymbol{r}}}^{(\mathrm{c})},\hat{\tilde{\boldsymbol{s}}}))\\&+\sum_{m=1}^{M}\frac{\lambda_{1m,\mathrm{f}}^{(\mathrm{c})}}{2}\left(\boldsymbol{\Omega}_{1m}\hat{\boldsymbol{\eta}}_{\mathrm{f}}+\frac{1}{2}\boldsymbol{\rho}_{1m}\right)\\&+\sum_{m=1}^{M}\frac{\lambda_{2m,\mathrm{f}}^{(\mathrm{c})}}{2}\left(\boldsymbol{\Omega}_{2m}\hat{\boldsymbol{\eta}}_{\mathrm{f}}+\frac{1}{2}\boldsymbol{\rho}_{2m}\right)\\&+\sum_{n=1}^{N}\frac{\lambda_{3n,\mathrm{f}}^{(\mathrm{c})}}{2}\left(\boldsymbol{\Omega}_{3n}\hat{\boldsymbol{\eta}}_{\mathrm{f}}+\frac{1}{2}\boldsymbol{\rho}_{3n}\right)\\&+\sum_{n=1}^{N}\frac{\lambda_{4n,\mathrm{f}}^{(\mathrm{c})}}{2}\left(\boldsymbol{\Omega}_{4n}\hat{\boldsymbol{\eta}}_{\mathrm{f}}+\frac{1}{2}\boldsymbol{\rho}_{4n}\right)\\&=\boldsymbol{O}_{(8M+2N)\times1}\end{aligned}\tag{D.1}$$

Due to the fact that $\hat{\boldsymbol{\eta}}_{\mathrm{opt}}(k+1)$ is the optimal solution for (75), it can be shown from the equality constraints in (75) that

$$\begin{aligned}&\lim_{k\to+\infty}(\hat{\boldsymbol{\eta}}(k))^{\mathrm{T}}\boldsymbol{\Omega}_{1m}\hat{\boldsymbol{\eta}}_{\mathrm{opt}}(k+1)+\frac{1}{2}\boldsymbol{\rho}_{1m}^{\mathrm{T}}\hat{\boldsymbol{\eta}}_{\mathrm{opt}}(k+1)\\&=\lim_{k\to+\infty}-\frac{1}{2}\boldsymbol{\rho}_{1m}^{\mathrm{T}}\hat{\boldsymbol{\eta}}(k)\\&\Rightarrow\hat{\boldsymbol{\eta}}_{\mathrm{f}}^{\mathrm{T}}\boldsymbol{\Omega}_{1m}\hat{\boldsymbol{\eta}}_{\mathrm{f}}+\boldsymbol{\rho}_{1m}^{\mathrm{T}}\hat{\boldsymbol{\eta}}_{\mathrm{f}}=0\quad(1\le m\le M)\end{aligned}\tag{D.2}$$

$$\begin{aligned}&\lim_{k\to+\infty}(\hat{\boldsymbol{\eta}}(k))^{\mathrm{T}}\boldsymbol{\Omega}_{2m}\hat{\boldsymbol{\eta}}_{\mathrm{opt}}(k+1)+\frac{1}{2}\boldsymbol{\rho}_{2m}^{\mathrm{T}}\hat{\boldsymbol{\eta}}_{\mathrm{opt}}(k+1)\\&=\lim_{k\to+\infty}-\frac{1}{2}\boldsymbol{\rho}_{2m}^{\mathrm{T}}\hat{\boldsymbol{\eta}}(k)\\&\Rightarrow\hat{\boldsymbol{\eta}}_{\mathrm{f}}^{\mathrm{T}}\boldsymbol{\Omega}_{2m}\hat{\boldsymbol{\eta}}_{\mathrm{f}}+\boldsymbol{\rho}_{2m}^{\mathrm{T}}\hat{\boldsymbol{\eta}}_{\mathrm{f}}=0\quad(1\le m\le M)\end{aligned}\tag{D.3}$$

$$\begin{aligned}&\lim_{k\to+\infty}(\hat{\boldsymbol{\eta}}(k))^{\mathrm{T}}\boldsymbol{\Omega}_{3n}\hat{\boldsymbol{\eta}}_{\mathrm{opt}}(k+1)+\frac{1}{2}\boldsymbol{\rho}_{3n}^{\mathrm{T}}\hat{\boldsymbol{\eta}}_{\mathrm{opt}}(k+1)\\&=\lim_{k\to+\infty}||\boldsymbol{w}_n||_2^2-\frac{1}{2}\boldsymbol{\rho}_{3n}^{\mathrm{T}}\hat{\boldsymbol{\eta}}(k)\\&\Rightarrow\hat{\boldsymbol{\eta}}_{\mathrm{f}}^{\mathrm{T}}\boldsymbol{\Omega}_{3n}\hat{\boldsymbol{\eta}}_{\mathrm{f}}+\boldsymbol{\rho}_{3n}^{\mathrm{T}}\hat{\boldsymbol{\eta}}_{\mathrm{f}}=||\boldsymbol{w}_n||_2^2\quad(1\le n\le N)\end{aligned}\tag{D.4}$$

$$\begin{aligned}&\lim_{k\to+\infty}(\hat{\boldsymbol{\eta}}(k))^{\mathrm{T}}\boldsymbol{\Omega}_{4n}\hat{\boldsymbol{\eta}}_{\mathrm{opt}}(k+1)+\frac{1}{2}\boldsymbol{\rho}_{4n}^{\mathrm{T}}\hat{\boldsymbol{\eta}}_{\mathrm{opt}}(k+1)\\&=\lim_{k\to+\infty}2\boldsymbol{w}_n^{\mathrm{T}}\dot{\boldsymbol{w}}_n-\frac{1}{2}\boldsymbol{\rho}_{4n}^{\mathrm{T}}\hat{\boldsymbol{\eta}}(k)\\&\Rightarrow\hat{\boldsymbol{\eta}}_{\mathrm{f}}^{\mathrm{T}}\boldsymbol{\Omega}_{4n}\hat{\boldsymbol{\eta}}_{\mathrm{f}}+\boldsymbol{\rho}_{4n}^{\mathrm{T}}\hat{\boldsymbol{\eta}}_{\mathrm{f}}=2\boldsymbol{w}_n^{\mathrm{T}}\dot{\boldsymbol{w}}_n\quad(1\le n\le N)\end{aligned}\tag{D.5}$$

On the other hand, for any vector $\boldsymbol{y}$ belonging to the null space of $(\boldsymbol{G}^{(\mathrm{c})}(\hat{\boldsymbol{\eta}}_{\mathrm{opt}}))^{\mathrm{T}}$, we can write $\boldsymbol{y}=\boldsymbol{Q}_{12}^{(\mathrm{c})}(\hat{\boldsymbol{\eta}}_{\mathrm{opt}})\boldsymbol{x}$. Moreover, using (C.7) and performing some algebraic manipulations

$$\begin{aligned}&J^{(\mathrm{c})}(\hat{\boldsymbol{\eta}}_{\mathrm{opt}}(k+1))\\&=||\boldsymbol{Q}_{21}^{(\mathrm{c})}(k+1)\boldsymbol{\Sigma}_2^{(\mathrm{c})}(k+1)(\boldsymbol{R}_2^{(\mathrm{c})}(k+1))^{\mathrm{T}}z_{\mathrm{o}}-(\tilde{\boldsymbol{\Phi}}^{(\mathrm{c})})^{-1/2}(\tilde{\boldsymbol{b}}^{(\mathrm{c})}(\hat{\tilde{\boldsymbol{r}}}^{(\mathrm{c})},\hat{\tilde{\boldsymbol{s}}})-\tilde{\boldsymbol{A}}^{(\mathrm{c})}(\hat{\tilde{\boldsymbol{r}}}^{(\mathrm{c})})\boldsymbol{Q}_{11}^{(\mathrm{c})}(k+1)\boldsymbol{x}_1(k+1))||_2^2\\&=\left\|\begin{bmatrix}\boldsymbol{\Sigma}_2^{(\mathrm{c})}(k+1)(\boldsymbol{R}_2^{(\mathrm{c})}(k+1))^{\mathrm{T}}z_{\mathrm{o}}\\\boldsymbol{O}_{2N(M-1)\times1}\end{bmatrix}-\begin{bmatrix}(\boldsymbol{Q}_{21}^{(\mathrm{c})}(k+1))^{\mathrm{T}}(\tilde{\boldsymbol{\Phi}}^{(\mathrm{c})})^{-1/2}(\tilde{\boldsymbol{b}}^{(\mathrm{c})}(\hat{\tilde{\boldsymbol{r}}}^{(\mathrm{c})},\hat{\tilde{\boldsymbol{s}}})-\tilde{\boldsymbol{A}}^{(\mathrm{c})}(\hat{\tilde{\boldsymbol{r}}}^{(\mathrm{c})})\boldsymbol{Q}_{11}^{(\mathrm{c})}(k+1)\boldsymbol{x}_1(k+1))\\(\boldsymbol{Q}_{22}^{(\mathrm{c})}(k+1))^{\mathrm{T}}(\tilde{\boldsymbol{\Phi}}^{(\mathrm{c})})^{-1/2}(\tilde{\boldsymbol{b}}^{(\mathrm{c})}(\hat{\tilde{\boldsymbol{r}}}^{(\mathrm{c})},\hat{\tilde{\boldsymbol{s}}})-\tilde{\boldsymbol{A}}^{(\mathrm{c})}(\hat{\tilde{\boldsymbol{r}}}^{(\mathrm{c})})\boldsymbol{Q}_{11}^{(\mathrm{c})}(k+1)\boldsymbol{x}_1(k+1))\end{bmatrix}\right\|_2^2\end{aligned}\tag{B.6}$$

yield

$$(\boldsymbol{Q}_{12}^{(\mathrm{c})}(\hat{\boldsymbol{\eta}}_{\mathrm{opt}}))^{\mathrm{T}}\begin{pmatrix}(\tilde{\boldsymbol{A}}^{(\mathrm{c})}(\hat{\bar{\boldsymbol{r}}}^{(\mathrm{c})}))^{\mathrm{T}}(\tilde{\boldsymbol{\Phi}}^{(\mathrm{c})})^{-1}\tilde{\boldsymbol{A}}^{(\mathrm{c})}(\hat{\bar{\boldsymbol{r}}}^{(\mathrm{c})})\\ +\sum_{m=1}^{M}\frac{\lambda_{1m,\mathrm{f}}^{(\mathrm{c})}}{2}\boldsymbol{\Omega}_{1m}+\sum_{m=1}^{M}\frac{\lambda_{2m,\mathrm{f}}^{(\mathrm{c})}}{2}\boldsymbol{\Omega}_{2m}\\ +\sum_{n=1}^{N}\frac{\lambda_{3n,\mathrm{f}}^{(\mathrm{c})}}{2}\boldsymbol{\Omega}_{3n}+\sum_{n=1}^{N}\frac{\lambda_{4n,\mathrm{f}}^{(\mathrm{c})}}{2}\boldsymbol{\Omega}_{4n}\end{pmatrix}\boldsymbol{Q}_{12}^{(\mathrm{c})}(\hat{\boldsymbol{\eta}}_{\mathrm{opt}})$$
$$=(\boldsymbol{Q}_{12}^{(\mathrm{c})}(\hat{\boldsymbol{\eta}}_{\mathrm{opt}}))^{\mathrm{T}}(\tilde{\boldsymbol{A}}^{(\mathrm{c})}(\hat{\bar{\boldsymbol{r}}}^{(\mathrm{c})}))^{\mathrm{T}}(\tilde{\boldsymbol{\Phi}}^{(\mathrm{c})})^{-1}\tilde{\boldsymbol{A}}^{(\mathrm{c})}(\hat{\bar{\boldsymbol{r}}}^{(\mathrm{c})})\boldsymbol{Q}_{12}^{(\mathrm{c})}(\hat{\boldsymbol{\eta}}_{\mathrm{opt}})>\boldsymbol{O} \tag{D.6}$$

where the positive definiteness uses the fact that $\boldsymbol{Q}_{12}^{(\mathrm{c})}(\hat{\boldsymbol{\eta}}_{\mathrm{opt}})$ has full column rank. It readily follows from (D.6) that

$$\boldsymbol{y}^{\mathrm{T}}\begin{pmatrix}(\tilde{\boldsymbol{A}}^{(\mathrm{c})}(\hat{\bar{\boldsymbol{r}}}^{(\mathrm{c})}))^{\mathrm{T}}(\tilde{\boldsymbol{\Phi}}^{(\mathrm{c})})^{-1}\tilde{\boldsymbol{A}}^{(\mathrm{c})}(\hat{\bar{\boldsymbol{r}}}^{(\mathrm{c})})\\ +\sum_{m=1}^{M}\frac{\lambda_{1m,\mathrm{f}}^{(\mathrm{c})}}{2}\boldsymbol{\Omega}_{1m}+\sum_{m=1}^{M}\frac{\lambda_{2m,\mathrm{f}}^{(\mathrm{c})}}{2}\boldsymbol{\Omega}_{2m}\\ +\sum_{n=1}^{N}\frac{\lambda_{3n,\mathrm{f}}^{(\mathrm{c})}}{2}\boldsymbol{\Omega}_{3n}+\sum_{n=1}^{N}\frac{\lambda_{4n,\mathrm{f}}^{(\mathrm{c})}}{2}\boldsymbol{\Omega}_{4n}\end{pmatrix}\boldsymbol{y}>0 \tag{D.7}$$

From (D.1), (D.2)-(D.5), (D.7) and Lemma 1 we can conclude that $\hat{\boldsymbol{\eta}}_{\mathrm{f}}=\hat{\boldsymbol{\eta}}_{\mathrm{opt}}$ is the strictly optimal solution to the CWLS problem (74). Hence, the proof is completed.

E. PROOF OF PROPOSITION 6

Since range$\{\boldsymbol{\Psi}(\bar{\boldsymbol{s}})\}=$ range$\{\boldsymbol{Q}_{12}^{(\mathrm{c})}\}$, there exists a nonsingular matrix $\boldsymbol{T}_{\mathrm{A}}\in R^{6M\times 6M}$ such that $\boldsymbol{Q}_{12}^{(\mathrm{c})}=\boldsymbol{\Psi}(\bar{\boldsymbol{s}})\boldsymbol{T}_{\mathrm{A}}$. Putting this into (97) gives

$$\begin{aligned}&\mathbf{MSE}(\hat{\bar{\boldsymbol{s}}}_{\mathrm{f}})\\ &=[\boldsymbol{I}_{6M}\ \ \boldsymbol{O}_{6M\times(2M+2N)}]\boldsymbol{\Psi}(\bar{\boldsymbol{s}})\boldsymbol{T}_{\mathrm{A}}\boldsymbol{T}_{\mathrm{A}}^{-1}\\ &\quad\times((\boldsymbol{\Psi}(\bar{\boldsymbol{s}}))^{\mathrm{T}}\tilde{\boldsymbol{P}}^{(\mathrm{c})}(\bar{\boldsymbol{r}}^{(\mathrm{c})})\boldsymbol{\Psi}(\bar{\boldsymbol{s}}))^{-1}\boldsymbol{T}_{\mathrm{A}}^{-\mathrm{T}}\boldsymbol{T}_{\mathrm{A}}^{\mathrm{T}}\\ &\quad\times(\boldsymbol{\Psi}(\bar{\boldsymbol{s}}))^{\mathrm{T}}\begin{bmatrix}\boldsymbol{I}_{6M}\\ \boldsymbol{O}_{(2M+2N)\times 6M}\end{bmatrix}\\ &=[\boldsymbol{I}_{6M}\ \ \boldsymbol{O}_{6M\times(2M+2N)}]\boldsymbol{\Psi}(\bar{\boldsymbol{s}})((\boldsymbol{\Psi}(\bar{\boldsymbol{s}}))^{\mathrm{T}}\tilde{\boldsymbol{P}}^{(\mathrm{c})}(\bar{\boldsymbol{r}}^{(\mathrm{c})})\boldsymbol{\Psi}(\bar{\boldsymbol{s}}))^{-1}\\ &\quad\times(\boldsymbol{\Psi}(\bar{\boldsymbol{s}}))^{\mathrm{T}}\begin{bmatrix}\boldsymbol{I}_{6M}\\ \boldsymbol{O}_{(2M+2N)\times 6M}\end{bmatrix}\\ &=((\boldsymbol{\Psi}(\bar{\boldsymbol{s}}))^{\mathrm{T}}\tilde{\boldsymbol{P}}^{(\mathrm{c})}(\bar{\boldsymbol{r}}^{(\mathrm{c})})\boldsymbol{\Psi}(\bar{\boldsymbol{s}}))^{-1}\end{aligned} \tag{E.1}$$

where the third equality follows from the relation $(\boldsymbol{\Psi}(\bar{\boldsymbol{s}}))^{\mathrm{T}}\begin{bmatrix}\boldsymbol{I}_{6M}\\ \boldsymbol{O}_{(2M+2N)\times 6M}\end{bmatrix}=\boldsymbol{I}_{6M}$. Substituting (96) into (E.1) produces

$$\begin{aligned}\mathbf{MSE}(\hat{\bar{\boldsymbol{s}}}_{\mathrm{f}})=&((\boldsymbol{\Psi}(\bar{\boldsymbol{s}}))^{\mathrm{T}}(\bar{\boldsymbol{A}}^{(\mathrm{c})}(\bar{\boldsymbol{r}}^{(\mathrm{c})}))^{\mathrm{T}}(\bar{\boldsymbol{C}}^{(\mathrm{c})}(\boldsymbol{\eta},\bar{\boldsymbol{r}}^{(\mathrm{c})}))^{-\mathrm{T}}(\bar{\boldsymbol{E}}_{\mathrm{A}}^{(\mathrm{c})})^{-1}\\ &\times(\bar{\boldsymbol{C}}^{(\mathrm{c})}(\boldsymbol{\eta},\bar{\boldsymbol{r}}^{(\mathrm{c})}))^{-1}\bar{\boldsymbol{A}}^{(\mathrm{c})}(\bar{\boldsymbol{r}}^{(\mathrm{c})})\boldsymbol{\Psi}(\bar{\boldsymbol{s}})+\bar{\boldsymbol{E}}_{\mathrm{B}}^{-1})^{-1}\end{aligned} \tag{E.2}$$

where the second equality follows from the relation

$$(\boldsymbol{\Psi}(\bar{\boldsymbol{s}}))^{\mathrm{T}}\mathrm{blkdiag}[\bar{\boldsymbol{E}}_{\mathrm{B}}^{-1}\ \ \boldsymbol{O}]\boldsymbol{\Psi}(\bar{\boldsymbol{s}})=\bar{\boldsymbol{E}}_{\mathrm{B}}^{-1} \tag{E.3}$$

On the other hand, inserting $\bar{\boldsymbol{r}}^{(\mathrm{c})}=\bar{\boldsymbol{f}}^{(\mathrm{c})}(\bar{\boldsymbol{s}})$ into (49) yields

$$\bar{\boldsymbol{A}}^{(\mathrm{c})}(\bar{\boldsymbol{f}}^{(\mathrm{c})}(\bar{\boldsymbol{s}}))\boldsymbol{\eta}=\bar{\boldsymbol{A}}^{(\mathrm{c})}(\bar{\boldsymbol{f}}^{(\mathrm{c})}(\bar{\boldsymbol{s}}))\boldsymbol{\psi}(\bar{\boldsymbol{s}})=\bar{\boldsymbol{b}}^{(\mathrm{c})}(\bar{\boldsymbol{f}}^{(\mathrm{c})}(\bar{\boldsymbol{s}})) \tag{E.4}$$

Differentiating both sides of (E.4) with respect to $\bar{\boldsymbol{s}}$ leads to

$$\begin{aligned}&\bar{\boldsymbol{B}}^{(\mathrm{c})}(\bar{\boldsymbol{r}}^{(\mathrm{c})})\bar{\boldsymbol{F}}^{(\mathrm{c})}(\bar{\boldsymbol{s}})\\ &=[\dot{\bar{\boldsymbol{A}}}_1^{(\mathrm{c})}(\bar{\boldsymbol{r}}^{(\mathrm{c})})\boldsymbol{\eta}\ \dot{\bar{\boldsymbol{A}}}_2^{(\mathrm{c})}(\bar{\boldsymbol{r}}^{(\mathrm{c})})\boldsymbol{\eta}\ \cdots\ \dot{\bar{\boldsymbol{A}}}_{2N(M-1)}^{(\mathrm{c})}(\bar{\boldsymbol{r}}^{(\mathrm{c})})\boldsymbol{\eta}]\bar{\boldsymbol{F}}^{(\mathrm{c})}(\bar{\boldsymbol{s}})\\ &\quad+\bar{\boldsymbol{A}}^{(\mathrm{c})}(\bar{\boldsymbol{r}}^{(\mathrm{c})})\boldsymbol{\Psi}(\bar{\boldsymbol{s}})\\ &\Rightarrow\bar{\boldsymbol{C}}^{(\mathrm{c})}(\boldsymbol{\eta},\bar{\boldsymbol{r}}^{(\mathrm{c})})\bar{\boldsymbol{F}}^{(\mathrm{c})}(\bar{\boldsymbol{s}})=\bar{\boldsymbol{A}}^{(\mathrm{c})}(\bar{\boldsymbol{r}}^{(\mathrm{c})})\boldsymbol{\Psi}(\bar{\boldsymbol{s}})\Rightarrow\bar{\boldsymbol{F}}^{(\mathrm{c})}(\bar{\boldsymbol{s}})\\ &=(\bar{\boldsymbol{C}}^{(\mathrm{c})}(\boldsymbol{\eta},\bar{\boldsymbol{r}}^{(\mathrm{c})}))^{-1}\bar{\boldsymbol{A}}^{(\mathrm{c})}(\bar{\boldsymbol{r}}^{(\mathrm{c})})\boldsymbol{\Psi}(\bar{\boldsymbol{s}})\end{aligned} \tag{E.5}$$

Combining (E.2) and (E.5), we have

$$\begin{aligned}\mathbf{MSE}(\hat{\bar{\boldsymbol{s}}}_{\mathrm{f}})&=(\bar{\boldsymbol{E}}_{\mathrm{B}}^{-1}+(\bar{\boldsymbol{F}}^{(\mathrm{c})}(\bar{\boldsymbol{s}}))^{\mathrm{T}}(\bar{\boldsymbol{E}}_{\mathrm{A}}^{(\mathrm{c})})^{-1}\bar{\boldsymbol{F}}^{(\mathrm{c})}(\bar{\boldsymbol{s}}))^{-1}\\ &=\mathbf{CRB}_{\mathrm{o}}(\bar{\boldsymbol{s}})\end{aligned} \tag{E.6}$$

which proves the result.

$$\boldsymbol{\lambda}^{(\mathrm{c})}(k+1)=[\,\lambda_{11}^{(\mathrm{c})}(k+1)\ \cdots\ \lambda_{1M}^{(\mathrm{c})}(k+1)\,\vdots\,\lambda_{21}^{(\mathrm{c})}(k+1)\ \cdots\ \lambda_{2M}^{(\mathrm{c})}(k+1)\,\vdots\,\lambda_{31}^{(\mathrm{c})}(k+1)\ \cdots\ \lambda_{3N}^{(\mathrm{c})}(k+1)\,\vdots\,\lambda_{41}^{(\mathrm{c})}(k+1)\ \cdots\ \lambda_{4N}^{(\mathrm{c})}(k+1)\,]^{\mathrm{T}} \tag{C.2}$$

$$\begin{cases}\boldsymbol{g}_1^{(\mathrm{c})}(\hat{\boldsymbol{\eta}}_{\mathrm{f}})=\left[-\frac{1}{2}\boldsymbol{\rho}_{11}^{\mathrm{T}}\hat{\boldsymbol{\eta}}_{\mathrm{f}}\ -\frac{1}{2}\boldsymbol{\rho}_{12}^{\mathrm{T}}\hat{\boldsymbol{\eta}}_{\mathrm{f}}\ \cdots\ -\frac{1}{2}\boldsymbol{\rho}_{1M}^{\mathrm{T}}\hat{\boldsymbol{\eta}}_{\mathrm{f}}\right]^{\mathrm{T}}\\ \boldsymbol{g}_2^{(\mathrm{c})}(\hat{\boldsymbol{\eta}}_{\mathrm{f}})=\left[-\frac{1}{2}\boldsymbol{\rho}_{21}^{\mathrm{T}}\hat{\boldsymbol{\eta}}_{\mathrm{f}}\ -\frac{1}{2}\boldsymbol{\rho}_{22}^{\mathrm{T}}\hat{\boldsymbol{\eta}}_{\mathrm{f}}\ \cdots\ -\frac{1}{2}\boldsymbol{\rho}_{2M}^{\mathrm{T}}\hat{\boldsymbol{\eta}}_{\mathrm{f}}\right]^{\mathrm{T}}\\ \boldsymbol{g}_3^{(\mathrm{c})}(\hat{\boldsymbol{\eta}}_{\mathrm{f}})\\ =\left[||\boldsymbol{w}_1||_2^2-\frac{1}{2}\boldsymbol{\rho}_{31}^{\mathrm{T}}\hat{\boldsymbol{\eta}}_{\mathrm{f}}\ ||\boldsymbol{w}_2||_2^2-\frac{1}{2}\boldsymbol{\rho}_{32}^{\mathrm{T}}\hat{\boldsymbol{\eta}}_{\mathrm{f}}\ \cdots\ ||\boldsymbol{w}_N||_2^2-\frac{1}{2}\boldsymbol{\rho}_{3N}^{\mathrm{T}}\hat{\boldsymbol{\eta}}_{\mathrm{f}}\right]^{\mathrm{T}}\\ \boldsymbol{g}_4^{(\mathrm{c})}(\hat{\boldsymbol{\eta}}_{\mathrm{f}})\\ =\left[2\boldsymbol{w}_1^{\mathrm{T}}\dot{\boldsymbol{w}}_1-\frac{1}{2}\boldsymbol{\rho}_{41}^{\mathrm{T}}\hat{\boldsymbol{\eta}}_{\mathrm{f}}\ 2\boldsymbol{w}_2^{\mathrm{T}}\dot{\boldsymbol{w}}_2-\frac{1}{2}\boldsymbol{\rho}_{42}^{\mathrm{T}}\hat{\boldsymbol{\eta}}_{\mathrm{f}}\ \cdots\ 2\boldsymbol{w}_N^{\mathrm{T}}\dot{\boldsymbol{w}}_N-\frac{1}{2}\boldsymbol{\rho}_{4N}^{\mathrm{T}}\hat{\boldsymbol{\eta}}_{\mathrm{f}}\right]^{\mathrm{T}}\end{cases} \tag{C.5}$$

$$\begin{cases}\boldsymbol{G}_i^{(\mathrm{c})}(\hat{\boldsymbol{\eta}}_{\mathrm{f}})\\ =\left[\boldsymbol{\Omega}_{i1}\hat{\boldsymbol{\eta}}_{\mathrm{f}}+\frac{1}{2}\boldsymbol{\rho}_{i1}\ \boldsymbol{\Omega}_{i2}\hat{\boldsymbol{\eta}}_{\mathrm{f}}+\frac{1}{2}\boldsymbol{\rho}_{i2}\ \cdots\ \boldsymbol{\Omega}_{iM}\hat{\boldsymbol{\eta}}_{\mathrm{f}}+\frac{1}{2}\boldsymbol{\rho}_{iM}\right]\quad(i=1\ ,\ 2)\\ \boldsymbol{G}_j^{(\mathrm{c})}(\hat{\boldsymbol{\eta}}_{\mathrm{f}})\\ =\left[\boldsymbol{\Omega}_{j1}\hat{\boldsymbol{\eta}}_{\mathrm{f}}+\frac{1}{2}\boldsymbol{\rho}_{j1}\ \boldsymbol{\Omega}_{j2}\hat{\boldsymbol{\eta}}_{\mathrm{f}}+\frac{1}{2}\boldsymbol{\rho}_{j2}\ \cdots\ \boldsymbol{\Omega}_{jN}\hat{\boldsymbol{\eta}}_{\mathrm{f}}+\frac{1}{2}\boldsymbol{\rho}_{jN}\right]\quad(j=3\ ,\ 4)\end{cases} \tag{C.6}$$

F. PROOF OF PROPOSITION 11

The proof is comprised of two parts. First, inserting $\bar{\boldsymbol{r}}_d = \boldsymbol{f}(\bar{\boldsymbol{u}}_d, \bar{\boldsymbol{s}})$ into (36) produces

$$\begin{aligned}\boldsymbol{b}(\boldsymbol{f}(\bar{\boldsymbol{u}}_d, \bar{\boldsymbol{s}}), \bar{\boldsymbol{s}}) &= \boldsymbol{A}(\boldsymbol{f}(\bar{\boldsymbol{u}}_d, \bar{\boldsymbol{s}}), \bar{\boldsymbol{s}})\boldsymbol{h}(\bar{\boldsymbol{u}}_d, \bar{\boldsymbol{s}}) \\ &= \boldsymbol{A}(\boldsymbol{f}(\bar{\boldsymbol{u}}_d, \bar{\boldsymbol{s}}), \bar{\boldsymbol{s}})\boldsymbol{t}_d \quad (1 \le d \le D)\end{aligned} \tag{F.1}$$

Differentiating both sides of (F.1) with respect to $\bar{\boldsymbol{u}}_d$ and $\bar{\boldsymbol{s}}$ yields

$$\begin{aligned}&\boldsymbol{B}_1(\bar{\boldsymbol{r}}_d, \bar{\boldsymbol{s}})\boldsymbol{F}_1(\bar{\boldsymbol{u}}_d, \bar{\boldsymbol{s}}) \\ &= [\dot{\boldsymbol{A}}_{11}(\bar{\boldsymbol{r}}_d, \bar{\boldsymbol{s}})\boldsymbol{t}_d\ \dot{\boldsymbol{A}}_{12}(\bar{\boldsymbol{r}}_d, \bar{\boldsymbol{s}})\boldsymbol{t}_d\ \cdots\ \dot{\boldsymbol{A}}_{1,2(M-1)}(\bar{\boldsymbol{r}}_d, \bar{\boldsymbol{s}})\boldsymbol{t}_d] \\ &\quad \times \boldsymbol{F}_1(\bar{\boldsymbol{u}}_d, \bar{\boldsymbol{s}}) + \boldsymbol{A}(\bar{\boldsymbol{r}}_d, \bar{\boldsymbol{s}})\boldsymbol{H}_1(\bar{\boldsymbol{u}}_d, \bar{\boldsymbol{s}}) \\ &\Rightarrow \boldsymbol{F}_1(\bar{\boldsymbol{u}}_d, \bar{\boldsymbol{s}}) \\ &= (\boldsymbol{C}_1(\boldsymbol{t}_d, \bar{\boldsymbol{r}}_d, \bar{\boldsymbol{s}}))^{-1}\boldsymbol{A}(\bar{\boldsymbol{r}}_d, \bar{\boldsymbol{s}})\boldsymbol{H}_1(\bar{\boldsymbol{u}}_d, \bar{\boldsymbol{s}}) \quad (1 \le d \le D) \\ &\boldsymbol{B}_1(\bar{\boldsymbol{r}}_d, \bar{\boldsymbol{s}})\boldsymbol{F}_2(\bar{\boldsymbol{u}}_d, \bar{\boldsymbol{s}}) + \boldsymbol{B}_2(\bar{\boldsymbol{r}}_d, \bar{\boldsymbol{s}}) \\ &= [\dot{\boldsymbol{A}}_{11}(\bar{\boldsymbol{r}}_d, \bar{\boldsymbol{s}})\boldsymbol{t}_d\ \dot{\boldsymbol{A}}_{12}(\bar{\boldsymbol{r}}_d, \bar{\boldsymbol{s}})\boldsymbol{t}_d\ \cdots\ \dot{\boldsymbol{A}}_{1,2(M-1)}(\bar{\boldsymbol{r}}_d, \bar{\boldsymbol{s}})\boldsymbol{t}_d] \\ &\quad \times \boldsymbol{F}_2(\bar{\boldsymbol{u}}_d, \bar{\boldsymbol{s}}) \\ &\quad + [\dot{\boldsymbol{A}}_{21}(\bar{\boldsymbol{r}}_d, \bar{\boldsymbol{s}})\boldsymbol{t}_d\ \dot{\boldsymbol{A}}_{22}(\bar{\boldsymbol{r}}_d, \bar{\boldsymbol{s}})\boldsymbol{t}_d\ \cdots\ \dot{\boldsymbol{A}}_{2,6M}(\bar{\boldsymbol{r}}_d, \bar{\boldsymbol{s}})\boldsymbol{t}_d] \\ &\quad + \boldsymbol{A}(\bar{\boldsymbol{r}}_d, \bar{\boldsymbol{s}})\boldsymbol{H}_2(\bar{\boldsymbol{u}}_d, \bar{\boldsymbol{s}}) \\ &\Rightarrow \boldsymbol{F}_2(\bar{\boldsymbol{u}}_d, \bar{\boldsymbol{s}}) = (\boldsymbol{C}_1(\boldsymbol{t}_d, \bar{\boldsymbol{r}}_d, \bar{\boldsymbol{s}}))^{-1} \\ &\quad \times (\boldsymbol{A}(\bar{\boldsymbol{r}}_d, \bar{\boldsymbol{s}})\boldsymbol{H}_2(\bar{\boldsymbol{u}}_d, \bar{\boldsymbol{s}}) - \boldsymbol{C}_2(\boldsymbol{t}_d, \bar{\boldsymbol{r}}_d, \bar{\boldsymbol{s}})) \quad (1 \le d \le D)\end{aligned} \tag{F.3}$$

where

$$\begin{cases}\boldsymbol{H}_1(\bar{\boldsymbol{u}}_d, \bar{\boldsymbol{s}}) = \dfrac{\partial \boldsymbol{h}(\bar{\boldsymbol{u}}_d, \bar{\boldsymbol{s}})}{\partial \bar{\boldsymbol{u}}_d^{\mathrm{T}}}\ ;\ \boldsymbol{H}_2(\bar{\boldsymbol{u}}_d, \bar{\boldsymbol{s}}) = \dfrac{\partial \boldsymbol{h}(\bar{\boldsymbol{u}}_d, \bar{\boldsymbol{s}})}{\partial \bar{\boldsymbol{s}}^{\mathrm{T}}} \\ \boldsymbol{C}_1(\boldsymbol{t}_d, \bar{\boldsymbol{r}}_d, \bar{\boldsymbol{s}}) = \boldsymbol{B}_1(\bar{\boldsymbol{r}}_d, \bar{\boldsymbol{s}}) \\ -[\dot{\boldsymbol{A}}_{11}(\bar{\boldsymbol{r}}_d, \bar{\boldsymbol{s}})\boldsymbol{t}_d\ \dot{\boldsymbol{A}}_{12}(\bar{\boldsymbol{r}}_d, \bar{\boldsymbol{s}})\boldsymbol{t}_d\ \cdots\ \dot{\boldsymbol{A}}_{1,2(M-1)}(\bar{\boldsymbol{r}}_d, \bar{\boldsymbol{s}})\boldsymbol{t}_d] \\ \boldsymbol{C}_2(\boldsymbol{t}_d, \bar{\boldsymbol{r}}_d, \bar{\boldsymbol{s}}) = \boldsymbol{B}_2(\bar{\boldsymbol{r}}_d, \bar{\boldsymbol{s}}) \\ -[\dot{\boldsymbol{A}}_{21}(\bar{\boldsymbol{r}}_d, \bar{\boldsymbol{s}})\boldsymbol{t}_d\ \dot{\boldsymbol{A}}_{22}(\bar{\boldsymbol{r}}_d, \bar{\boldsymbol{s}})\boldsymbol{t}_d\ \cdots\ \dot{\boldsymbol{A}}_{2,6M}(\bar{\boldsymbol{r}}_d, \bar{\boldsymbol{s}})\boldsymbol{t}_d]\end{cases} \tag{F.4}$$

Putting all the D equations in (F.2) together and writing in matrix form produces (F.5), as shown at the top of the next page.

where $\bar{\boldsymbol{H}}_1(\bar{\boldsymbol{u}}, \bar{\boldsymbol{s}}) = \frac{\partial \bar{\boldsymbol{h}}(\bar{\boldsymbol{u}}, \bar{\boldsymbol{s}})}{\partial \bar{\boldsymbol{u}}^{\mathrm{T}}} = \mathrm{blkdiag}[\boldsymbol{H}_1(\boldsymbol{u}_1, \bar{\boldsymbol{s}})\ \cdots\ \boldsymbol{H}_1(\boldsymbol{u}_D, \bar{\boldsymbol{s}})]$. Analogously, the collection of all the D equations in (F.3) forms (F.6), as shown at the top of the next page.

where $\bar{\boldsymbol{H}}_2(\bar{\boldsymbol{u}}, \bar{\boldsymbol{s}}) = \frac{\partial \bar{\boldsymbol{h}}(\bar{\boldsymbol{u}}, \bar{\boldsymbol{s}})}{\partial \bar{\boldsymbol{s}}^{\mathrm{T}}} = [(\boldsymbol{H}_2(\boldsymbol{u}_1, \bar{\boldsymbol{s}}))^{\mathrm{T}}\ \cdots\ (\boldsymbol{H}_2(\boldsymbol{u}_D, \bar{\boldsymbol{s}}))^{\mathrm{T}}]^{\mathrm{T}}$. Substituting (F.5) and (F.6) into (21) and applying the result in Proposition 6, we can rewritten $\mathbf{CRB}\left(\begin{bmatrix}\bar{\boldsymbol{u}} \\ \bar{\boldsymbol{s}}\end{bmatrix}\right)$ as

$$\mathbf{CRB}\left(\begin{bmatrix}\bar{\boldsymbol{u}} \\ \bar{\boldsymbol{s}}\end{bmatrix}\right) = \begin{bmatrix}\boldsymbol{Z}_1 & \boldsymbol{Z}_2 \\ \boldsymbol{Z}_2^{\mathrm{T}} & \boldsymbol{Z}_3\end{bmatrix}^{-1} \tag{F.7}$$

where

$$\begin{cases}\boldsymbol{Z}_1 = (\bar{\boldsymbol{H}}_1(\bar{\boldsymbol{u}}, \bar{\boldsymbol{s}}))^{\mathrm{T}}(\bar{\boldsymbol{A}}(\bar{\boldsymbol{r}}, \bar{\boldsymbol{s}}))^{\mathrm{T}}(\bar{\boldsymbol{C}}_1(\bar{\boldsymbol{t}}, \bar{\boldsymbol{r}}, \bar{\boldsymbol{s}}))^{-\mathrm{T}}\bar{\boldsymbol{E}}_{\mathrm{A}}^{-1} \\ \qquad \times (\bar{\boldsymbol{C}}_1(\bar{\boldsymbol{t}}, \bar{\boldsymbol{r}}, \bar{\boldsymbol{s}}))^{-1}\bar{\boldsymbol{A}}(\bar{\boldsymbol{r}}, \bar{\boldsymbol{s}})\bar{\boldsymbol{H}}_1(\bar{\boldsymbol{u}}, \bar{\boldsymbol{s}}) \\ \boldsymbol{Z}_2 = (\bar{\boldsymbol{H}}_1(\bar{\boldsymbol{u}}, \bar{\boldsymbol{s}}))^{\mathrm{T}}(\bar{\boldsymbol{A}}(\bar{\boldsymbol{r}}, \bar{\boldsymbol{s}}))^{\mathrm{T}}(\bar{\boldsymbol{C}}_1(\bar{\boldsymbol{t}}, \bar{\boldsymbol{r}}, \bar{\boldsymbol{s}}))^{-\mathrm{T}}\bar{\boldsymbol{E}}_{\mathrm{A}}^{-1} \\ \qquad \times (\bar{\boldsymbol{C}}_1(\bar{\boldsymbol{t}}, \bar{\boldsymbol{r}}, \bar{\boldsymbol{s}}))^{-1}(\bar{\boldsymbol{A}}(\bar{\boldsymbol{r}}, \bar{\boldsymbol{s}})\bar{\boldsymbol{H}}_2(\bar{\boldsymbol{u}}, \bar{\boldsymbol{s}}) - \bar{\boldsymbol{C}}_2(\bar{\boldsymbol{t}}, \bar{\boldsymbol{r}}, \bar{\boldsymbol{s}})) \\ \boldsymbol{Z}_3 = (\bar{\boldsymbol{A}}(\bar{\boldsymbol{r}}, \bar{\boldsymbol{s}})\bar{\boldsymbol{H}}_2(\bar{\boldsymbol{u}}, \bar{\boldsymbol{s}}) - \bar{\boldsymbol{C}}_2(\bar{\boldsymbol{t}}, \bar{\boldsymbol{r}}, \bar{\boldsymbol{s}}))^{\mathrm{T}}(\bar{\boldsymbol{C}}_1(\bar{\boldsymbol{t}}, \bar{\boldsymbol{r}}, \bar{\boldsymbol{s}}))^{-\mathrm{T}} \\ \qquad \times \bar{\boldsymbol{E}}_{\mathrm{A}}^{-1}(\bar{\boldsymbol{C}}_1(\bar{\boldsymbol{t}}, \bar{\boldsymbol{r}}, \bar{\boldsymbol{s}}))^{-1}(\bar{\boldsymbol{A}}(\bar{\boldsymbol{r}}, \bar{\boldsymbol{s}})\bar{\boldsymbol{H}}_2(\bar{\boldsymbol{u}}, \bar{\boldsymbol{s}}) - \bar{\boldsymbol{C}}_2(\bar{\boldsymbol{t}}, \bar{\boldsymbol{r}}, \bar{\boldsymbol{s}})) \\ \qquad + \mathbf{MSE}(\hat{\bar{\boldsymbol{s}}}_{\mathrm{f}})\end{cases} \tag{F.8}$$

Since $\mathrm{range}\{\tilde{\boldsymbol{H}}_1(\bar{\boldsymbol{u}}, \bar{\boldsymbol{s}})\} = \mathrm{range}\{\tilde{\boldsymbol{Q}}_2\}$, there exists a non-singular matrix $\boldsymbol{T}_{\mathrm{B}} \in R^{(6D+6M)\times(6D+6M)}$ such that $\tilde{\boldsymbol{Q}}_2 = \tilde{\boldsymbol{H}}_1(\bar{\boldsymbol{u}}, \bar{\boldsymbol{s}})\boldsymbol{T}_{\mathrm{B}}$. Putting this into (126) leads to

$$\begin{aligned}&\mathbf{MSE}\left(\begin{bmatrix}\hat{\bar{\boldsymbol{u}}}_{\mathrm{s}} \\ \hat{\bar{\boldsymbol{s}}}_{\mathrm{s}}\end{bmatrix}\right) \\ &= \left[\begin{array}{c:c}\boldsymbol{I}_D \otimes [\boldsymbol{I}_6\ \ \boldsymbol{O}_{6\times 2}] & \boldsymbol{I}_D \otimes \boldsymbol{\Xi} \\ \boldsymbol{O}_{6M\times 8D} & \boldsymbol{I}_{6M}\end{array}\right]\tilde{\boldsymbol{H}}_1(\bar{\boldsymbol{u}}, \bar{\boldsymbol{s}}) \\ &\quad \times ((\tilde{\boldsymbol{H}}_1(\bar{\boldsymbol{u}}, \bar{\boldsymbol{s}}))^{\mathrm{T}}\tilde{\boldsymbol{P}}(\bar{\boldsymbol{r}}, \bar{\boldsymbol{s}})\tilde{\boldsymbol{H}}_1(\bar{\boldsymbol{u}}, \bar{\boldsymbol{s}}))^{-1}(\tilde{\boldsymbol{H}}_1(\bar{\boldsymbol{u}}, \bar{\boldsymbol{s}}))^{\mathrm{T}} \\ &\quad \times \left[\begin{array}{c:c}\boldsymbol{I}_D \otimes \begin{bmatrix}\boldsymbol{I}_6 \\ \boldsymbol{O}_{2\times 6}\end{bmatrix} & \boldsymbol{O}_{8D\times 6M} \\ \boldsymbol{I}_D^{\mathrm{T}} \otimes \boldsymbol{\Xi}^{\mathrm{T}} & \boldsymbol{I}_{6M}\end{array}\right]\end{aligned} \tag{F.9}$$

From (53) and the definition of $\tilde{\boldsymbol{H}}_1(\bar{\boldsymbol{u}}, \bar{\boldsymbol{s}})$, we get

$$\begin{aligned}&\left[\begin{array}{c:c}\boldsymbol{I}_D \otimes [\boldsymbol{I}_6\ \ \boldsymbol{O}_{6\times 2}] & \boldsymbol{I}_D \otimes \boldsymbol{\Xi} \\ \boldsymbol{O}_{6M\times 8D} & \boldsymbol{I}_{6M}\end{array}\right]\tilde{\boldsymbol{H}}_1(\bar{\boldsymbol{u}}, \bar{\boldsymbol{s}}) \\ &\qquad = \left[\begin{array}{c:c}\boldsymbol{I}_{6D} & \boldsymbol{I}_D \otimes \boldsymbol{\Xi} \\ \boldsymbol{O}_{6M\times 6D} & \boldsymbol{I}_{6M}\end{array}\right]\end{aligned} \tag{F.10}$$

Inserting (F.10) back into (F.9) yields

$$\begin{aligned}&\mathbf{MSE}\left(\begin{bmatrix}\hat{\bar{\boldsymbol{u}}}_{\mathrm{s}} \\ \hat{\bar{\boldsymbol{s}}}_{\mathrm{s}}\end{bmatrix}\right) \\ &= \left(\left[\begin{array}{c:c}\boldsymbol{I}_{6D} & \boldsymbol{O}_{6D\times 6M} \\ -(\boldsymbol{I}_D^{\mathrm{T}} \otimes \boldsymbol{\Xi}^{\mathrm{T}}) & \boldsymbol{I}_{6M}\end{array}\right]\right. \\ &\quad \left.\times (\tilde{\boldsymbol{H}}_1(\bar{\boldsymbol{u}}, \bar{\boldsymbol{s}}))^{\mathrm{T}}\tilde{\boldsymbol{P}}(\bar{\boldsymbol{r}}, \bar{\boldsymbol{s}})\tilde{\boldsymbol{H}}_1(\bar{\boldsymbol{u}}, \bar{\boldsymbol{s}})\left[\begin{array}{c:c}\boldsymbol{I}_{6D} & -(\boldsymbol{I}_D \otimes \boldsymbol{\Xi}) \\ \boldsymbol{O}_{6M\times 6D} & \boldsymbol{I}_{6M}\end{array}\right]\right)^{-1}\end{aligned} \tag{F.11}$$

On the other hand, it can be proved that

$$\begin{aligned}&\tilde{\boldsymbol{H}}_1(\bar{\boldsymbol{u}}, \bar{\boldsymbol{s}})\left[\begin{array}{c:c}\boldsymbol{I}_{6D} & -(\boldsymbol{I}_D \otimes \boldsymbol{\Xi}) \\ \boldsymbol{O}_{6M\times 6D} & \boldsymbol{I}_{6M}\end{array}\right] \\ &\qquad = \begin{bmatrix}\bar{\boldsymbol{H}}_1(\bar{\boldsymbol{u}}, \bar{\boldsymbol{s}}) & \bar{\boldsymbol{H}}_2(\bar{\boldsymbol{u}}, \bar{\boldsymbol{s}}) \\ \boldsymbol{O}_{6M\times 6D} & \boldsymbol{I}_{6M}\end{bmatrix}\end{aligned} \tag{F.12}$$

which together with (F.11) results in

$$\begin{aligned}&\mathbf{MSE}\left(\begin{bmatrix}\hat{\bar{\boldsymbol{u}}}_{\mathrm{s}} \\ \hat{\bar{\boldsymbol{s}}}_{\mathrm{s}}\end{bmatrix}\right) = \left(\begin{bmatrix}(\bar{\boldsymbol{H}}_1(\bar{\boldsymbol{u}}, \bar{\boldsymbol{s}}))^{\mathrm{T}} & \boldsymbol{O}_{6D\times 6M} \\ (\bar{\boldsymbol{H}}_2(\bar{\boldsymbol{u}}, \bar{\boldsymbol{s}}))^{\mathrm{T}} & \boldsymbol{I}_{6M}\end{bmatrix}\tilde{\boldsymbol{P}}(\bar{\boldsymbol{r}}, \bar{\boldsymbol{s}})\right. \\ &\qquad \left.\times \begin{bmatrix}\bar{\boldsymbol{H}}_1(\bar{\boldsymbol{u}}, \bar{\boldsymbol{s}}) & \bar{\boldsymbol{H}}_2(\bar{\boldsymbol{u}}, \bar{\boldsymbol{s}}) \\ \boldsymbol{O}_{6M\times 6D} & \boldsymbol{I}_{6M}\end{bmatrix}\right)^{-1}\end{aligned} \tag{F.13}$$

$$\begin{aligned}\bar{\boldsymbol{F}}_1(\bar{\boldsymbol{u}},\bar{\boldsymbol{s}}) &= \text{blkdiag}[(\boldsymbol{C}_1(\boldsymbol{t}_1,\bar{\boldsymbol{r}}_1,\bar{\boldsymbol{s}}))^{-1}\ (\boldsymbol{C}_1(\boldsymbol{t}_2,\bar{\boldsymbol{r}}_2,\bar{\boldsymbol{s}}))^{-1}\ \cdots\ (\boldsymbol{C}_1(\boldsymbol{t}_D,\bar{\boldsymbol{r}}_D,\bar{\boldsymbol{s}}))^{-1}] \\ &\quad\times \text{blkdiag}[\boldsymbol{A}(\bar{\boldsymbol{r}}_1,\bar{\boldsymbol{s}})\,\boldsymbol{A}(\bar{\boldsymbol{r}}_2,\bar{\boldsymbol{s}})\ \cdots\ \boldsymbol{A}(\bar{\boldsymbol{r}}_D,\bar{\boldsymbol{s}})] \times \text{blkdiag}[\boldsymbol{H}_1(\bar{\boldsymbol{u}}_1,\bar{\boldsymbol{s}})\,\boldsymbol{H}_1(\bar{\boldsymbol{u}}_2,\bar{\boldsymbol{s}})\ \cdots\ \boldsymbol{H}_1(\bar{\boldsymbol{u}}_D,\bar{\boldsymbol{s}})] \\ &\Rightarrow \bar{\boldsymbol{F}}_1(\bar{\boldsymbol{u}},\bar{\boldsymbol{s}}) = (\bar{\boldsymbol{C}}_1(\bar{\boldsymbol{t}},\bar{\boldsymbol{r}},\bar{\boldsymbol{s}}))^{-1}\bar{\boldsymbol{A}}(\bar{\boldsymbol{r}},\bar{\boldsymbol{s}})\bar{\boldsymbol{H}}_1(\bar{\boldsymbol{u}},\bar{\boldsymbol{s}}) \end{aligned} \tag{F.5}$$

$$\begin{aligned}\bar{\boldsymbol{F}}_2(\bar{\boldsymbol{u}},\bar{\boldsymbol{s}}) &= \text{blkdiag}[(\boldsymbol{C}_1(\boldsymbol{t}_1,\bar{\boldsymbol{r}}_1,\bar{\boldsymbol{s}}))^{-1}\ (\boldsymbol{C}_1(\boldsymbol{t}_2,\bar{\boldsymbol{r}}_2,\bar{\boldsymbol{s}}))^{-1}\ \cdots\ (\boldsymbol{C}_1(\boldsymbol{t}_D,\bar{\boldsymbol{r}}_D,\bar{\boldsymbol{s}}))^{-1}] \\ &\quad\times\left(\text{blkdiag}[\boldsymbol{A}(\bar{\boldsymbol{r}}_1,\bar{\boldsymbol{s}})\,\boldsymbol{A}(\bar{\boldsymbol{r}}_2,\bar{\boldsymbol{s}})\ \cdots\ \boldsymbol{A}(\bar{\boldsymbol{r}}_D,\bar{\boldsymbol{s}})]\begin{bmatrix}\boldsymbol{H}_2(\bar{\boldsymbol{u}}_1,\bar{\boldsymbol{s}})\\ \boldsymbol{H}_2(\bar{\boldsymbol{u}}_2,\bar{\boldsymbol{s}})\\ \vdots\\ \boldsymbol{H}_2(\bar{\boldsymbol{u}}_D,\bar{\boldsymbol{s}})\end{bmatrix} - \begin{bmatrix}\boldsymbol{C}_2(\boldsymbol{t}_1,\bar{\boldsymbol{r}}_1,\bar{\boldsymbol{s}})\\ \boldsymbol{C}_2(\boldsymbol{t}_2,\bar{\boldsymbol{r}}_2,\bar{\boldsymbol{s}})\\ \vdots\\ \boldsymbol{C}_2(\boldsymbol{t}_D,\bar{\boldsymbol{r}}_D,\bar{\boldsymbol{s}})\end{bmatrix}\right) \\ &\Rightarrow \bar{\boldsymbol{F}}_2(\bar{\boldsymbol{u}},\bar{\boldsymbol{s}}) = (\bar{\boldsymbol{C}}_1(\bar{\boldsymbol{t}},\bar{\boldsymbol{r}},\bar{\boldsymbol{s}}))^{-1}(\bar{\boldsymbol{A}}(\bar{\boldsymbol{r}},\bar{\boldsymbol{s}})\bar{\boldsymbol{H}}_2(\bar{\boldsymbol{u}},\bar{\boldsymbol{s}}) - \bar{\boldsymbol{C}}_2(\bar{\boldsymbol{t}},\bar{\boldsymbol{r}},\bar{\boldsymbol{s}})) \end{aligned} \tag{F.6}$$

Inserting (124) into (F.13) gives

$$\mathbf{MSE}\left(\begin{bmatrix}\hat{\bar{\boldsymbol{u}}}_{\mathrm{s}}\\ \hat{\bar{\boldsymbol{s}}}_{\mathrm{s}}\end{bmatrix}\right) = \begin{bmatrix}\boldsymbol{Z}_1 & \boldsymbol{Z}_2\\ \boldsymbol{Z}_2^{\mathrm{T}} & \boldsymbol{Z}_3\end{bmatrix}^{-1} = \mathbf{CRB}\left(\begin{bmatrix}\bar{\boldsymbol{u}}\\ \bar{\boldsymbol{s}}\end{bmatrix}\right) \tag{F.14}$$

Then, the proof is ended.

ACKNOWLEDGMENT

The authors would like to thank all the anonymous reviewers for their valuable comments and suggestions.

REFERENCES

[1] N. Patwari, J. N. Ash, S. Kyperountas, A. O. Hero, R. L. Moses, and N. S. Correal, "Locating the nodes: Cooperative localization in wireless sensor networks," *IEEE Signal Process. Mag.*, vol. 22, no. 4, pp. 54–69, Jul. 2005.

[2] P. Biswas, T.-C. Lian, T.-C. Wang, and Y. Ye, "Semidefinite programming based algorithms for sensor network localization," *ACM Trans. Sens. Netw.*, vol. 2, no. 2, pp. 188–220, 2006.

[3] T. S. Rappaport, J. Reed, and B. D. Woerner, "Position location using wireless communications on highways of the future," *IEEE Commun. Mag.*, vol. 34, no. 10, pp. 33–41, Oct. 1996.

[4] L. Xiao, L. J. Greenstein, and N. B. Mandayam, "Sensor-assisted localization in cellular systems," *IEEE Trans. Wireless Commun.*, vol. 6, no. 12, pp. 4244–4248, Dec. 2007.

[5] Y. Shen and M. Z. Win, "Fundamental limits of wideband localization—Part I: A general framework," *IEEE Trans. Inf. Theory*, vol. 56, no. 10, pp. 4956–4980, Oct. 2010.

[6] J. Liang and D. Liu, "Passive localization of mixed near-field and far-field sources using two-stage MUSIC algorithm," *IEEE Trans. Signal Process.*, vol. 58, no. 1, pp. 108–120, Jan. 2010.

[7] M. Porretta, P. Nepa, G. Manara, and F. Giannetti, "Location, location, location," *IEEE Veh. Technol. Mag.*, vol. 3, no. 2, pp. 20–29, Jun. 2008.

[8] H. Godrich, A. P. Petropulu, and H. V. Poor, "Sensor selection in distributed multiple-radar architectures for localization: A knapsack problem formulation," *IEEE Trans. Signal Process.*, vol. 60, no. 1, pp. 247–260, Jan. 2012.

[9] T. Meng and J. Buck, "Rate distortion bounds on passive sonar performance," *IEEE Trans. Signal Process.*, vol. 58, no. 1, pp. 326–336, Jan. 2010.

[10] X. Cao, J. Chen, Y. Xiao, and Y. Sun, "Building-environment control with wireless sensor and actuator networks: Centralized versus distributed," *IEEE Trans. Ind. Electron.*, vol. 57, no. 11, pp. 3596–3605, Nov. 2010.

[11] M. Z. Win, A. Conti, S. Mazuelas, Y. Shen, W. M. Gifford, D. Dardari, and M. Chiani, "Network localization and navigation via cooperation," *IEEE Commun. Mag.*, vol. 49, no. 5, pp. 56–62, May 2011.

[12] Y. T. Chen, J. Wang, R. L. Xia, Q. Zhang, Z. H. Cao, and K. Yang, "The visual object tracking algorithm research based on adaptive combination kernel," *J. Ambient Intell. Humanized Comput.*, vol. 10, no. 12, pp. 4855–4867, Dec. 2019.

[13] W. Li, Z. Chen, X. Gao, W. Liu, and J. Wang, "Multimodel framework for indoor localization under mobile edge computing environment," *IEEE Internet Things J.*, vol. 6, no. 3, pp. 4844–4853, Jun. 2019.

[14] D. Zhang, T. Yin, G. Yang, M. Xia, L. Li, and X. Sun, "Detecting image seam carving with low scaling ratio using multi-scale spatial and spectral entropies," *J. Vis. Commun. Image Represent.*, vol. 48, pp. 281–291, Oct. 2017.

[15] C. Liu, Y. V. Zakharov, and T. Chen, "Broadband underwater localization of multiple sources using basis pursuit de-noising," *IEEE Trans. Signal Process.*, vol. 60, no. 4, pp. 1708–1717, Apr. 2012.

[16] N. H. Nguyen and K. Doğançay, "Optimal geometry analysis for multistatic TOA localization," *IEEE Trans. Signal Process.*, vol. 64, no. 16, pp. 4180–4193, Aug. 2016.

[17] D. Wang, J. X. Yin, T. Tang, X. Chen, and Z. D. Wu, "Quadratic constrained weighted least-squares method for TDOA source localization in the presence of clock synchronization bias: Analysis and solution," *Digit. Signal Process.*, vol. 82, pp. 237–257, Nov. 2018.

[18] Y. Wang and K. C. Ho, "An asymptotically efficient estimator in closed-form for 3-D AOA localization using a sensor network," *IEEE Trans. Wireless Commun.*, vol. 14, no. 12, pp. 6524–6535, Dec. 2015.

[19] S. Tomic, M. Beko, and R. Dinis, "RSS-based localization in wireless sensor networks using convex relaxation: Noncooperative and cooperative schemes," *IEEE Trans. Veh. Technol.*, vol. 64, no. 5, pp. 2037–2050, May 2015.

[20] K. W. Cheung, H. C. So, W.-K. Ma, and Y. T. Chan, "A constrained least squares approach to mobile positioning: Algorithms and optimality," *EURASIP J. Appl. Signal Process.*, vol. 2006, no. 1, pp. 1–23, Jan. 2006.

[21] K. C. Ho and W. Xu, "An accurate algebraic solution for moving source location using TDOA and FDOA measurements," *IEEE Trans. Signal Process.*, vol. 52, no. 9, pp. 2453–2463, Sep. 2004.

[22] A. Noroozi, A. H. Oveis, S. M. Hosseini, and M. A. Sebt, "Improved algebraic solution for source localization from TDOA and FDOA measurements," *IEEE Wireless Commun. Lett.*, vol. 7, no. 3, pp. 352–355, Jun. 2017.

[23] H. W. Wei, R. Peng, Q. Wan, Z. X. Chen, and S. F. Ye, "Multidimensional scaling analysis for passive moving target localization with TDOA and FDOA measurements," *IEEE Trans. Signal Process.*, vol. 58, no. 3, pp. 1677–1688, Mar. 2010.

[24] W. H. Foy, "Position-location solutions by Taylor-series estimation," *IEEE Trans. Aerosp. Electron. Syst.*, vol. AES-12, no. 2, pp. 187–194, Mar. 1976.

[25] G. Wang, Y. M. Li, and N. Ansari, "A semidefinite relaxation method for source localization using TDOA and FDOA measurements," *IEEE Trans. Veh. Technol.*, vol. 62, no. 2, pp. 853–862, Feb. 2013.

[26] H. Yu, G. Huang, J. Gao, and B. Liu, "An efficient constrained weighted least squares algorithm for moving source location using TDOA and FDOA measurements," *IEEE Trans. Wireless Commun.*, vol. 11, no. 1, pp. 44–47, Jan. 2012.

[27] F. Guo and K. C. Ho, "A quadratic constraint solution method for TDOA and FDOA localization," in *Proc. IEEE Int. Conf. Acoust., Speech Signal Process. (ICASSP)*, Prague, Czech Republic, May 2011, pp. 2588–2591.
[28] K. C. Ho and Y. T. Chan, "Geolocation of a known altitude object from TDOA and FDOA measurements," *IEEE Trans. Aerosp. Electron. Syst.*, vol. 33, no. 3, pp. 770–783, Jul. 1997.
[29] X. Qu, L. Xie, and W. Tan, "Iterative constrained weighted least squares source localization using TDOA and FDOA measurements," *IEEE Trans. Signal Process.*, vol. 65, no. 15, pp. 3990–4003, May 2017.
[30] K. C. Ho, X. Lu, and L. Kovavisaruch, "Source localization using TDOA and FDOA measurements in the presence of receiver location errors: Analysis and solution," *IEEE Trans. Signal Process.*, vol. 55, no. 2, pp. 684–696, Feb. 2007.
[31] X. Lu and K. C. Ho, "Analysis of the degradation in source location accuracy in the presence of sensor location error," in *Proc. IEEE Int. Conf. Acoustic, Speech Signal Process.*, Toulouse, France, May 2006, pp. 14–19.
[32] X. Sun, J. Li, P. Huang, and J. Pang, "Total least-squares solution of active target localization using TDOA and FDOA measurements in WSN," in *Proc. IEEE 22nd Int. Conf. Adv. Inf. Netw. Appl.*, Okinawa, Japan, Mar. 2008, pp. 995–999.
[33] H. Yu, G. Huang, and J. Gao, "Constrained total least-squares localization algorithm using time difference of arrival and frequency difference of arrival measurements with sensor location uncertainties," *LET Radar Sonar Navigat.*, vol. 6, no. 9, pp. 891–899, Dec. 2012.
[34] M. Sun and K. Ho, "An asymptotically efficient estimator for TDOA and FDOA positioning of multiple disjoint sources in the presence of sensor location uncertainties," *IEEE Trans. Signal Process.*, vol. 59, no. 7, pp. 3434–3440, Jul. 2011.
[35] B. J. Hao, Z. Li, J. B. Si, and L. Guan, "Joint source localisation and sensor refinement using time differences of arrival and frequency differences of arrival," *IET Signal Process.*, vol. 8, no. 6, pp. 588–600, 2014.
[36] D. Wang, J. X. Yin, T. Tang, R. R. Liu, and Z. D. Wu, "A two-step weighted least-squares method for joint estimation of source and sensor locations: A general framework," *Chin. J. Aeronaut.*, vol. 32, no. 2, pp. 417–443, 2019.
[37] D. Wang, J. X. Yin, T. Zhang, C. G. Jia, and F. S. Wei, "Iterative constrained weighted least squares estimator for TDOA and FDOA positioning of multiple disjoint sources in the presence of sensor position and velocity uncertainties," *Digital Signal Process.*, vol. 92, no. 9, pp. 179–205, 2019.
[38] K. C. Ho and L. Yang, "On the use of a calibration emitter for source localization in the presence of sensor position uncertainty," *IEEE Trans. Signal Process.*, vol. 56, no. 12, pp. 5758–5772, Dec. 2008.
[39] L. Yang and K. C. Ho, "Alleviating sensor position error in source localization using calibration emitters at inaccurate locations," *IEEE Trans. Signal Process.*, vol. 58, no. 1, pp. 67–83, Jan. 2010.
[40] Z. Ma and K. C. Ho, "A study on the effects of sensor position error and the placement of calibration emitter for source localization," *IEEE Trans. Wireless Commun.*, vol. 13, no. 10, pp. 5440–5452, Oct. 2014.
[41] L. Yang and K. C. Ho, "On using multiple calibration emitters and their geometric effects for removing sensor position errors in TDOA localization," in *Proc. IEEE Int. Conf. Acoust., Speech Signal Process.*, Dallas, TX, USA, Mar. 2010, pp. 2702–2705.
[42] D. Wang, J. X. Yin, X. Chen, C. G. Jia, and F. S. Wei, "On the use of calibration emitters for TDOA source localization in the presence of synchronization clock bias and sensor location errors," *EURASIP J. Adv. Signal Process.*, vol. 37, no. 11, pp. 1–34, 2019.
[43] J. Z. Li, F. C. Guo, and W. L. Jiang, "Source localization and calibration using TDOA and FDOA measurements in the presence of sensor location uncertainty," *Sci. China Inf. Sci.*, vol. 57, no. 4, 2014, Art. no. 042315.
[44] J. Li, F. Guo, L. Yang, W. Jiang, and H. Pang, "On the use of calibration sensors in source localization using TDOA and FDOA measurements," *Digit. Signal Process.*, vol. 27, pp. 33–43, Apr. 2014.
[45] M. Viberg and B. Ottersten, "Sensor array processing based on subspace fitting," *IEEE Trans. Signal Process.*, vol. 39, no. 5, pp. 1110–1121, May 1991.
[46] M. Viberg and A. L. Swindlehurst, "A Bayesian approach to auto-calibration for parametric array signal processing," *IEEE Trans. Signal Process.*, vol. 42, no. 12, pp. 3495–3507, Dec. 1994.
[47] M. Jansson, A. L. Swindlehurst, and B. Ottersten, "Weighted subspace fitting for general array error models," *IEEE Trans. Signal Process.*, vol. 46, no. 9, pp. 2484–2498, Sep. 1998.
[48] D. P. Bertsekas, *Nonlinear Programming*, 2nd ed. Belmont, MA, USA: Athena Scientific, 1999.
[49] M. Sun, L. Yang, and D. K. C. Ho, "Efficient joint source and sensor localization in closed-form," *IEEE Signal Process. Lett.*, vol. 19, no. 7, pp. 399–402, Jul. 2012.
[50] D. J. Torrieri, "Statistical theory of passive location systems," *IEEE Trans. Aerosp. Electron. Syst.*, vol. AES-20, no. 2, pp. 183–198, Mar. 1984.
[51] W. Hao, S. Wei-Min, and G. Hong, "A novel Taylor series method for source and receiver localization using TDOA and FDOA measurements with uncertain receiver positions," in *Proc. IEEE CIE Int. Conf. Radar*, Chengdu, China, Oct. 2011, pp. 1037–1044.

DING WANG received the bachelor's degree from the Department of Communication Engineering, the M.S. degree in military communication, and the Ph.D. degree in communication and system engineering from the Zhengzhou Institute of Information Science and Technology, China, in 2004, 2007, and 2011, respectively. From 2012 to 2015, he was an Assistant Professor with the National Digital Switching System Engineering and Technology Research Center (NDSC) and the Zhengzhou Institute of Information Science and Technology. Since 2016, he has been an Associate Professor at PLA Strategic Support Force Information Engineering University. His research activities are focused on array signal processing and passive location.

PEICHANG ZHANG received the B.Eng. degree (Hons.) in electronic engineering from the University of Central Lancashire, Preston, U.K., in 2009, and the M.Sc. and Ph.D. degrees in wireless communications from the University of Southampton, Southampton, U.K., in 2010 and 2015, respectively. He is currently with the College of Electronics and Information Engineering, Shenzhen University, China. His research interests include antenna selection, coherent and non-coherent detection, iterative detection, and channel estimation.

ZEYU YANG received the B.E. degree from the National Digital Switching System Engineering and Technology Research Center (NDSC), Zhengzhou, China, in 2017. He is currently pursuing the M.S. degree with PLA Strategic Support Force Information Engineering University. His research interests include array signal processing and passive localization.

FUSHAN WEI received the M.S. and Ph.D. degrees in applied mathematics from the Zhengzhou Institute of Information Science and Technology, China, in 2008 and 2011, respectively. He is currently an Associate Professor with the State Key Laboratory of Mathematical Engineering and Advanced Computing, Zhengzhou, China. His research fields include cryptography and information security.

CHENG WANG received the B.S. and Ph.D. degrees from PLA Strategic Support Force Information Engineering University, in 2013 and 2017, respectively. Since July 2017, he has been a Lectuer at PLA Strategic Support Force Information Engineering University. From August 2013 to July 2015, he was a Visiting Student with the Department of Electronic Engineering, Tsinghua University, China. His current research interests include multidimensional signal processing, detection, and estimation theory and adaptive signal processing.